Application of an Ion Exchange Loading Correlation for Nickel Recovery from a Ferrous Containing Solution

by

PARISA SADAT ABBASI JAHROMI

B.Sc., The University of British Columbia, 2011

A THESIS SUBMITTED IN PARTIAL FULFILLMENT OF

THE REQUIREMENTS FOR THE DEGREE OF

MASTER OF APPLIED SCIENCE

in

THE FACULTY OF GRADUATE AND POSTDOCTORAL STUDIES

(Materials Engineering)

THE UNIVERSITY OF BRITISH COLUMBIA

(Vancouver)

April 2014

Abstract

Nickeliferous laterite ore is one of the resources for nickel recovery that can be processed by using commercially-available processes such as High Pressure Acid Leach. Since this is a costly hydrometallurgical process, maximum nickel recovery is required to justify the investment. Recently, the use of ion exchange resins and resin-in-pulp processes have been considered and proposed as methods of primary or secondary metal recovery from nickel laterite leach slurries and leach tailings. The solution produced in the high pressure acid leach treatment of laterite ores contains several impurities. As a result, the presence of high levels of impurities such as the ferrous ion is expected to be present in an actual resin-in-pulp feed slurry. Many of these impurities (including ferrous) initially load onto the resin and are then displaced by the target metal ion (nickel). Thus, it is expected to see a different nickel loading manner in the presence of ferrous ions compared to the loading of nickel in the absence of any impurities (i.e. nickel load onto resin only by displacing hydrogen ions). This emphasizes the significance of testing the desired ion exchange resin under conditions reflective of the expected industrial operating conditions.

This thesis reports on the investigation of the loading rate of nickel onto an iminodiacetic acid ion exchange resin (TP207XL) under the finite solution volume condition in the presence of ferrous in a batch loading system. Initially, the batch loading rate of the ferrous ion onto resin under the infinite solution volume condition was examined. A hybrid correlation model was applied for both ferrous loading and nickel-ferrous displacement loading based on the kinetics experimental datasets. The correlation was found to adequately fit the ferrous loading datasets. According to the obtained fit parameters, it was proven that

the loading rate of the ferrous ions onto the resin is slower than that of copper, nickel and cobalt ions. Furthermore, in the case of ferrous-nickel displacement tests, the experimental fit parameters of the hybrid correlation were used to successfully predict the results of the batch loading experiments by applying the finite difference model.

Preface

This dissertation is original, unpublished, independent work by the author, P Abbasi. The first two publications listed below were products of the efforts of a few people. The main author was Dr. McKevitt, who was under the supervision of Dr. Dreisinger, while Parisa Abbasi conducted experiments in the laboratory and performed experimental data analysis. The third conference paper will be published and presented from research work included in Chapter 4 of the dissertation.

1) McKevitt, B., Abbasi, P. & Dreisinger, D. (2011) *A Comparison of Large Bead Ion Exchange Resins for the Recovery of Base Metals in a Resin-in- (RIP) Circuit*. *Proceedings of the 6th Southern African Base Metals Conference. SAIMM: pp. 337-352.*

2) McKevitt, B., Abbasi, P. & Dreisinger, D. (2011) *The Hybrid Correlation and its Application to a Nickel Resin In Pulp Circuit. The International Ion Exchange Conference (IEX 2012). Queen's College, University of Cambridge, UK.*

3) Abbasi, P., McKevitt, B. & Dreisinger, D. (accepted) *Study of Kinetics of Fe (II) Loading onto Iminodiacetic Ion Exchange Resin. 7th International Symposium of Hydrometallurgy Conference (Hydro 2014). Victoria, BC*. Parts of this manuscript appear in Chapter 4 of the thesis.

Table of Contents

List of Tables

List of Figures

List of Abbreviations

AA	Atomic Absorption
ACS	American Chemical Society
BV	Bed Volumes
CCD	Counter-Current Decantation
CIP	Carbon In Pulp
DI	Deionized
EQ	Equivalents
EDX	Energy Dispersive X-ray Spectroscopy
FSV	Finite Solution Volume
HPAL	High Pressure Acid Leach
ISV	Infinite Solution Volume
IX	Ion Exchange
IDA	Iminodiacetic Acid
LPM	Liter Per Minutes
PPM	Parts Per Million
RIP	Resin In Pulp
RPM	Revolutions Per Minute
SEM	Scanning Electron Microscope
USSR	Union of Soviet Socialist Republics

List of Symbols

a_1	empirical fit parameter for a linear isotherm [-]
a_2	empirical fit parameter for a Freundlich isotherm [-]
[A]	concentration of ion A in the solution [mol A/L]
$[\overline{A}]$	concentration of ion A loaded on ion exchange resin [mol A/L resin]
b	empirically fit Freundlich isotherm exponent [-]
[B]	concentration of ion B in the solution [mol B/L]
$[\overline{B}]$	concentration of ion B loaded on ion exchange resin [mol B/L resin]
d_c	diameter of unreacted core [m]
d_p	resin bead diameter [m]
D_{app}	apparent diffusion coefficient through resin bead in hybrid correlation [m^2/s]
D_s	diffusion coefficient through reacted layer in shrinking core model [m^2/s]
D_f	diffusion coefficient through film [m^2/s]
D_p	diffusion coefficient through resin bead [m^2/s]
F	fractional attainment of equilibrium [-]
[Fe]	concentration of ferrous ion in solution [mol Fe / L]
$[\overline{Fe}]$	concentration of ferrous ion, loaded onto ion exchanger [mol Fe/L Resin]
j	summation counter [-]
[H]	concentration of hydrogen ion in solution [mol H/L]
$[\overline{H}]$	concentration of hydrogen ion, loaded onto ion exchanger [mol H/L Resin]
k_c	constant, shrinking core diffusion control [1/s]
K_e	equilibrium quotient

k_f constant, film diffusion control [1/s]

k_{fwd} kinetic rate constant, forward reaction in pseudo-second order model [1/mol s]

k_g constant, Glucekauf's linear intraparticle diffusion control [1/s]

k_h constant, diffusion control using hybrid correlation [1/s]

k_l constant, linear approach to equilibrium [1/s]

k_{rev} kinetic rate constant, forward reaction in pseudo-second order model [1/mol s]

k_v constant, Vermeulen's approximation to intraparticle diffusion control [1/s]

K selectivity coefficient [-]

L empirical fit parameter to Langmuir isotherm [-]

[M] concentration of divalent ion M in solution [mol M/L]

$[\overline{M}]$ concentration of divalent ion M, loaded onto ion exchanger [mol M/L Resin]

$[M]_{eqb}$ equilibrium concentration of M loaded onto ion exchanger [mol M/L Resin]

$[M]_{max}$ capacity of ion exchanger for divalent ion M [mol M/L Resin]

[Ni] concentration of nickel ion in solution [mol M/L]

$[\overline{Ni}]$ concentration of nickel ion loaded onto ion exchanger [mol Ni/L Resin]

R resin

S_A^B separation factor for ion exchange resin for ion B over ion A [-]

t time [s]

t_r time required under current conditions for resin to achieve the initial loading value [s]

Δt finite differences model time step [s]

Greek Letters:

α	exponent for hybrid correlation [-]
δ	film thickness [m]
η	Glueckauf's shape factor [-]

Acknowledgements

I am grateful to many people whose contributions to this work are required to be acknowledged. First and foremost, I would like to express my sincere gratitude to my supervisor **Dr. Dreisinger** for his guidance, positive attitude and countless instances of useful feedback throughout the entire course of my research. It has been an honor to be one of his students. Appreciation is also extended to **Dr. McKevitt** for her contributions of time, fantastic ideas, and suggestions that made my research interesting and productive. I feel enormously fortunate to have worked with her for two summers as a research assistant during my undergraduate studies and to have her as a support throughout my entire graduate studies. My sincere thanks also goes out to **Dr. Wassink**, who has been always a welcoming presence in the lab and whose valuable discussions were insightful and helpful during my studies.

I acknowledge the financial support from the Natural Sciences and Engineering Research Council of Canada (NSERC). It has been also a great privilege to be a part of the Materials Engineering program as an undergraduate and graduate student at the University of British Columbia. Special thanks to all colleagues and past and present officemates for providing a friendly environment that was always a pleasure to work in.

Finally, I want to dedicate my work to my dearest parents, **Pari and Reza,** and to the best sister in the world **Nakisa** who has been always there for me. Without their endless encouragement, love, and support, completing this thesis would not have been possible. I am deeply grateful to them for each day of my life and my mere expression of thanks does not suffice.

To

My Parents

and

My Sister

1 Introduction

1.1 Background

Nickel is recovered from its ores divided into two types, sulphide and oxide (laterite) ores. Sulphide ores account for the vast majority (approximately 60%) of worldwide nickel production [1]. However, due to the escalating demand of the stainless steel industry and the rapid increase in the world consumption of nickel, sulphide ore reserves have become depleted. As a result, in recent years, there is significant interest in developing economic technologies for the processing of laterite deposits that represent about 70% of the world-land nickel resources [2].

Laterite ores have been discovered globally in many countries including Australia, New Caledonia, Philippines, Indonesia, Cuba and South America [3]. Laterites are near-surface deposits formed by extreme chemical weathering of nickeliferous "ultramafic" rocks containing ferro-magnesium minerals. The weathering or "laterization" process is favored in tropical regions with a warm climate and abundant rainfall. Typically, laterite ores consist of three zones, namely, limonitic, saprolitic and garnieritic [4-9]. The mineralogy varies across these zones. Limonitic laterites primarily contain iron in the form of goethite, which is the principal nickel-bearing mineral in limonite deposits. However, the two other zones are well known for their magnesium silicate mineral content [5, 8-11]. As a result, depending on the chemical composition and the mineralogy of ore minerals, possible and economically feasible metallurgical processing routes can be assigned for the specific nickel laterite ores. Nickeliferous laterite ores are typically extracted using commercially-available processes

classified as both pyrometallurgical and hydrometallurgical. The two conventional pyrometallurgical techniques for nickel recovery are ferronickel smelting and matte smelting. The processing steps commonly include drying, calcination, reduction and electric furnace smelting followed by refining or converting. The final product of such a process is ferronickel or nickel sulphide matte [12-14]. On the other hand, limonitic laterite ores are suitable for hydrometallurgical processes that mainly include ammonia-ammonium carbonate leaching after reductive roasting (Caron process), pressure acid leaching (high pressure acid leaching (HPAL) and atmospheric acid leaching (AL)) [2, 15, 16].

In recent years, according to Ma *et al*. [17], the high-pressure acid leaching of laterite deposits has become the preferred hydrometallurgical alternative in treating nickel limonitic laterite ores. This method has been applied all around the world, particularly in modern industrial Australian projects such as Murrin Murrin, Cawse, and Bulong. In this process, the ore is leached at high temperature (250–270°C) and pressure with sulphuric acid. Subsequently, solid/liquid separation in a series of continuous counter-current decantation thickeners (CCD) and neutralization of excess acid are applied prior to purification and final metal recovery [1, 18, 19]. Since this is a costly process, maximum metal recovery is required. As a result, secondary treatment of washed tailings may increase the extent of nickel recovery by diminishing the soluble losses. This can minimize the environmental impact as well [18]. For more detailed information regarding the chemistry of the HPAL process, the reader is referred to the literature [10].

1.2 Problem Definition

The solution produced in the HPAL treatment of laterite ores contains sulphates of metals such as Al, Mg, Ni, Mn, Zn, Fe, Co, and Cu. In addition, the concentration of these metals in the leach solution varies greatly based on several factors such as acidity of the feed slurry, the ore composition, the leaching time, the temperature and the solid-liquid ratio [19].

The HPAL process is generally followed by a counter current decantation (CCD) process in order to separate the leach liquor from undesired solids. However, this process is slow and inefficient and the capital cost of this part of the plant is very high. Furthermore, a significant loss of leached nickel to the pulp underflow can be encountered through processes such as "solution entrainment, co-precipitation, and sorption processes on the high surface area solids" [20, 21].

Recently, in the case of recovery of base metals from CCD pulp underflow, the use of ion exchange resin and the resin-in-pulp (RIP) process have been considered and proposed as methods of primary or secondary metal recovery from nickel laterite leach operations [11, 21-25]. Thus, in the RIP process, ion exchange has been used as a technique through which metal recovery can be obtained without removing solids from the stream. Previous studies on the application of several forms of resin for the RIP processes proposed that commercially-available chelating resins with the iminodiacetic acid functional group would be most suitable for nickel recovery [11, 26]. Although iminodiacetic acid ion exchange resins have a high affinity for loading nickel, analysis of the loaded resin from the RIP process proved that generally 30-50% of the resin capacity is loaded with nickel and the rest is loaded with several impurities. Typically, analyzing the elution results of the resins

confirmed the fact that large amounts of impurities have been co-loaded along with nickel despite the fact that iminodiacetic acid ion exchange resin is easily eluted by strong sulphuric acid [11, 23, 27]. Iron exists as one of these impurities that can be loaded onto iminodiacetic resins. In the case of nickel recovery, the RIP process generally operates at pH 4 and at this pH iron can be present as ferrous (Fe^{2+}) or ferric (Fe^{3+}). According to Zainol [11] about 70% of the iron in the pulp solution from a typical HPAL operation is present as ferrous. In her work, she emphasized that precipitation processes will not be more than 90% efficient and if the ferric cannot be removed entirely it will be loaded strongly onto resin. In this work, it was shown that iron present as a ferrous ion, which can exist as an impurity in the RIP process, may be loaded onto the resin and thereby suppress the nickel loading and recovery.

1.3 Objectives of the Research

The objective of this research is to investigate the nickel loading behavior onto iminodiacetic acid ion exchange resin in a resin-in-pulp circuit where Fe^{2+} is present as the main solution impurity. Nickel ion extraction onto iminodiacetic acid resins has been studied by McKevitt and others ([19, 23-26, 28]). In order to have a better understanding of the nickel loading behavior from an impure solution in such a resin-in-pulp system, the ferrous loading onto iminodiacetic resin must first be studied. As a result, the objectives of the research are described as follows:

1. To investigate the Fe^{2+} loading process onto iminodiacetic acid ion exchange resin under the infinite solution volume condition (maintaining constant solution composition and pH conditions throughout the loading of ferrous ion for the simplicity of the

kinetics model equations solutions). The study includes the measurement of iron loading under a variety of experimental conditions as well as an attempt to model the loading process using the hybrid correlation advanced by McKevitt [24].

2. To study the Ni^{2+}/Fe^{2+} displacement process on the iminodiacetic ion exchange resin under the non-infinite solution volume condition (allowing the concentration of ions to change as a function of time during the loading experiment). The nickel loading behavior onto resin was investigated under several experimental conditions in the presence of ferrous ions and the loading process was modeled using the hybrid correlation model [24].

2 Literature Review

2.1 Introduction to Ion Exchange and Ion Exchange Fundamentals

For many years, several industrial applications have been developed based on ion exchange technology. In most applications, the ion exchange technique has been mainly used for solution purification purposes performed by eliminating the target dissolved ions by electrostatic sorption into an ion exchange material prepared from a variety of physical materials. Among all the ion exchange applications, water demineralization and water softening are the two most common ones. Most specifically, ion exchange is largely implemented in a wide range of hydrometallurgical applications from large-scale metals extraction processes (eg. uranium and gold) to the refining of valuable metals (gold, silver, platinum) [29]. Note that the uranium industry has been responsible for various advances in ion exchange technology development [30]. Several applications of ion exchange technology in the various fields are summarized in Table 2.1.

More details regarding an ion exchange process and its application can be found in the literature [31]. The next sections include a brief review of basic principles of the ion exchange process, a discussion of the useful capacity of resins and the development of equilibrium isotherms.

Table 2.1: Ion Exchange Applications

Field	Example
Water Treatment	Softening, Demineralization
Food Industry	Manufacturing of Sugar
Chemical Processes	Chromatography, Catalysis
Pharmaceutical Industry	Extraction and Purification of Antibiotics
Mining and Hydrometallurgical Industry	Recovery of Metals Removal of Impurities from Process Streams Treatment of Waste Streams Prior to Disposal

2.1.1 Ion Exchange (IX) Phenomenon

Fundamentally, ion exchange is a stoichiometric reversible reaction involving an exchange of an ion from an aqueous phase (electrolyte solution) with ions of like charge electrostatically bound to the functional group carrying opposite charge [29]. Although the ion exchange process has been traditionally termed as an adsorption process in literature, there are distinct differences between these two sorption processes. For example, according to Inglezakis and Zorpas [32], the adsorption process is physical sorption based on intermolecular attractions between sorption sites (substances with neutral electric charges). However, in the case of ion exchange or electrostatic sorption with opposite charge attraction, the primary force between ions and charged functional groups is the coulombic attractive force. Therefore, the nature of the sorbed species (charged versus uncharged) is completely different in these two processes.

Furthermore, the IX process involves two actions: removal of an ion from solution and the displacement of another ion back into solution, whereas in an adsorption process the species is just being removed from the fluid phase. All of these considerations confirm the fact that the IX process is required to be treated as a more complicated process than simple physical adsorption. Nevertheless, in practical applications and associated literature, these two processes are joined together as sorption for the purpose of a unified treatment. Note that most of the mathematical kinetic models generated for adsorption can be applied with slight modifications for consideration of ion exchange processes.

For the purpose of this work, the ion exchange process is described as a loading process in which a divalent cation, M^{2+}, is loaded onto iminodiacetic ion exchange resin with the concurrent displacement of hydrogen ions attached to the functional group. This loading process is described in Equation 2.1. The symbols used through this work are the same as those used by McKevitt [24]. In Equation 2.1, the concentration of the metal ion of interest in the solution is indicated as [M] whereas its concentration loaded onto resin is described with an overbar symbol $[\overline{M}]$.

$$2\,R\text{-}H + M^{2+} \rightarrow R_2\text{-}M + 2\,H^{+} \qquad [2.1]$$

Since in most engineering models loading rates are introduced as a fractional approach to equilibrium, the equilibrium capacity of resin for the desired metal ion and equilibrium isotherms are two necessary concepts that need to be discussed in the next section.

2.1.2 Equilibrium Loading Capacity

The total stoichiometric capacity of the resin is rarely attained under actual operating conditions such as the resin-in-pulp process. Subsequently, the capacity is defined as equilibrium capacity, which is lower than the total capacity for such a system. This exchange or equilibrium loading capacity of an ion exchange resin is the measurement of the number of desired ions that can be exchanged for the specific amount of the resins in a system in which the equilibrium state can be reached after a certain time [33].

In this work, the equilibrium loading capacity is expressed as $[\overline{M}]_{eqb}$ while the maximum capacity of resin for the specific metal ion is defined as $[\overline{M}]_{max}$, which would be achieved when the total available exchange sites on the resin functional groups are displaced by the desired metal ions from the aqueous phase. Note that the unit of capacity is expressed in mol M/L $_{Resin}$, which is the total moles of a given metal ion that can be removed from solution per unit volume of resin. The equilibrium capacity of the iminodiacetic ion exchange resin was investigated in this work initially for ferrous ion loading and also, most importantly, for nickel ions loading onto the resin previously loaded with ferrous ions. In order to determine the equilibrium capacity it is necessary to generate the equilibrium loading isotherm.

2.1.3 Equilibrium Isotherms

Commonly, the ion exchange loading process is defined as an equilibrium-controlled process. In this research, when the metal ions are displaced with hydrogen ions presented on the ion exchange resin, the equilibrium state can be obtained while the thermodynamic potential of both ions (M^{2+} and H^{+}) in the solution and on the resin phase is equal. An

equilibrium loading generally relates the concentration of the desired ion in the solution to the one in the resin phase.

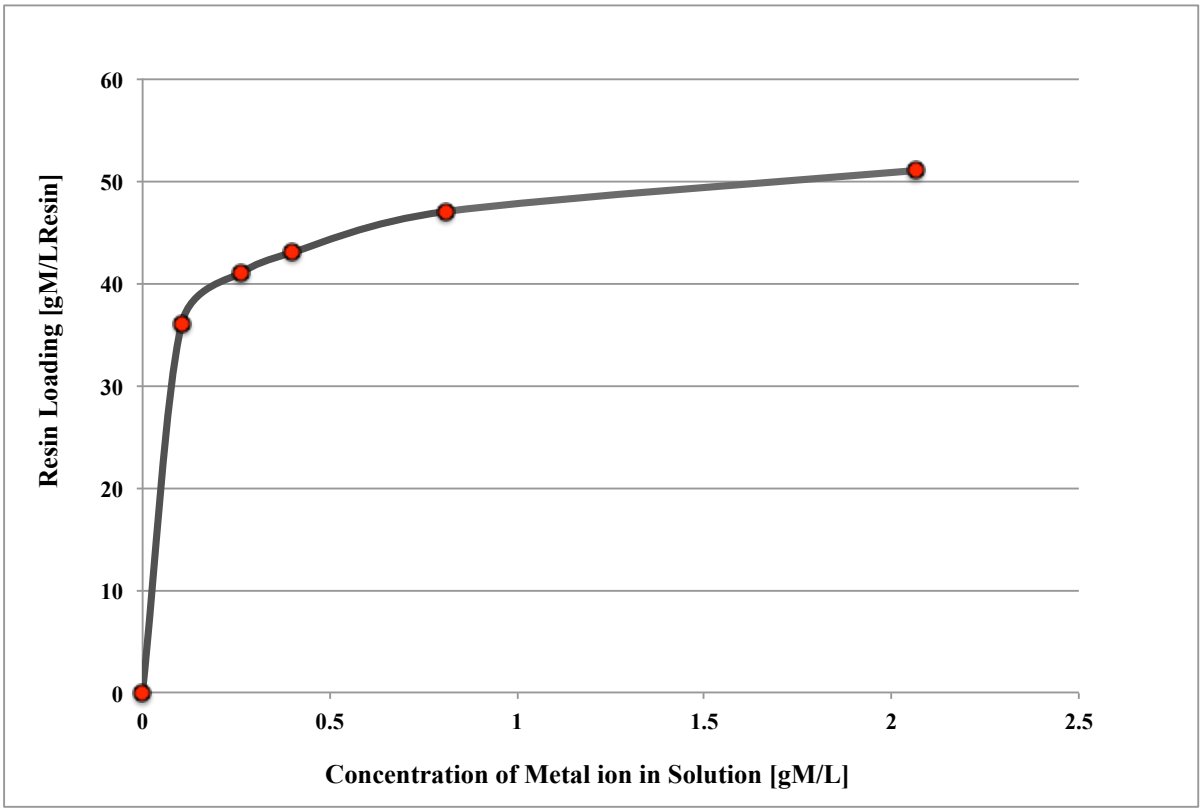

Figure 2.1: A Simple Equilibrium Loading Isotherm for Metal Ion Loading onto Resin

The isotherm graphs are typically plotted with the solution concentration of a metal ion on the X-axis and the concentration on the resin on the Y-axis (Figure 2.1). The adsorption and ion exchange process can be considered as a similar process thus, for ion exchange processes the adsorption isotherm equations could be applied. The study of the isotherm models is not just about description of the relationship between the solution concentration of the specific ion and its related sorption capacity of the resin, it also may help in predicting the loading mechanism of the ion exchange process [34]. In the resin-in-pulp applications for base

metals, several isotherm models have been commonly used to predict the equilibrium distribution and fit the experimental equilibrium datasets. However, the most frequently applied models are Langmuir and Freundlich isotherm models [11, 24, 28, 35-39]. Although these two conventional isotherm models have been known for a long time, they are still the models used to successfully fit a wide range of experimental data. This may relate to the simplicity of their empirical equations and easy estimation of their adjustable parameters [37].

2.1.3.1 Freundlich Isotherm

In 1906, Freundlich developed his empirical adsorption model [40]. The Freundlich isotherm has mostly has been applied with the assumption that the adsorption process takes place on heterogeneous sites having non-uniform energy levels and is not limited to a monolayer [28, 34, 41]. Although the Freundlich equation is simple and easy to use, since no saturated adsorption value (maximum adsorption capacity) has been defined in it, its prediction at both extremes of isotherms has been questioned [24]. The Freundlich equation is simply expressed as:

$$[\overline{\mathrm{M}}]_{\mathrm{eqb}} = a_2[\mathrm{M}]^{\mathrm{b}}_{\mathrm{eqb}} \qquad [2.2]$$

Both a_2 and b are two empirical fit parameters, where the related parameter a_2 represents the adsorption coefficient (i.e. amount of metal adsorbed on the resin) and the constant b is the measure of adsorption intensity. A value of b varies between 0 and 1and, if it gets closer to 0 the adsorption is more likely occurring at heterogeneous sites with non-uniform energy levels

[28, 39, 42]. Furthermore, the linear isotherm is the simplest version of the Freundlich isotherm when the fit parameter b is equal to 1 and the model is simplified to Equation 2.3 described as:

$$[\overline{M}]_{eqb} = a_1[M]_{eqb} \quad [2.3]$$

2.1.3.2 Langmuir Isotherms

Later in 1916, [43] Langmuir described his semi-empirical adsorption equation [2.4] in which he assumed that the adsorption occurs only at homogenous sites having a uniform energy level. As a result, this equation is frequently applied for ion exchange reaction with limitation to the monolayer adsorption in which one active site can only be exchanged with one metal ion [41, 44].

In this model, it is assumed that the resin has a limited loading capacity ($[\overline{M}]_{max}$) and all available exchangeable sites on the resin matrix are identical (i.e. have the same affinity for the desired metal ion) [28, 34, 38, 39, 45, 46] . In the equation, two fit parameters are described as $[\overline{M}]_{max}$ [mol/L_{Resin}] and adsorption equilibrium coefficient, L [L/mol]. $[\overline{M}]_{max}$ is defined as the amount of monolayer of the metal ion loaded onto resin while L is accounted for the measurement of loading intensity.

$$[\overline{M}]_{eqb} = \frac{L[\overline{M}]_{max}[M]_{eqb}}{1 + L[M]_{eqb}} \quad [2.4]$$

2.1.3.3 Mass Action Law

As mentioned, ion exchange reactions are considered stoichiometric and reversible processes in which the desired ions (one in an aqueous phase and the other bound to the resin) are exchanged until the equilibrium state is achieved. The equilibrium isotherm of such a system can be described by the application of the law of mass action rather than using the Freundlich and Langmuir isotherms that appear to be misapplied for ionic interactions regarding the ion exchangers [31]. Application of the law of mass action assumes that, for the ions in the resin phase, the activities cannot be determined precisely as a result, an apparent exchange constant K_e is calculated. For the ion exchange reaction described in Equation 2.5 where ion B in an aqueous phase is exchanged with ion A attached to the resin functional group, the related K_e is derived based on the law of mass action as described in Equation 2.6.

$$R\text{-}A^+ + B^+ \rightarrow R\text{-}B^+ + A^+ \qquad [2.5]$$

$$K_e = \frac{[\overline{B}^+][A^+]}{[\overline{A}^+][B^+]} \qquad [2.6]$$

K_e is termed "the equilibrium quotient" since it is not an actual thermodynamic equilibrium constant. According to Dorfner, to be able to determine the K_e analytically in practical applications, the activity coefficients of both ions in the resin and the solution phase are neglected and, instead the concentration of ions are used to calculate the equilibrium quotient [31]. This equilibrium quotient varies based on characteristics of ion exchangers and the composition and properties of the electrolytes. Therefore, different equilibrium quotients

such as the "selectivity coefficient" and "separation factor" are acquired for various ions involved in an ion exchange reaction.

2.1.3.3.1 Selectivity Coefficient

The concept of selectivity coefficient is derived from a thermodynamic equilibrium constant of the ion exchange reaction where the equation is expressed using the molar concentration of species with a unit activity coefficient [47]. However, the selectivity coefficient varies from one system to another [48]. The selectivity coefficient for the reaction 2.5 is given by Equation 2.7.

$$K_A^B = \frac{[\overline{B}].[A]}{[\overline{A}].[B]} \qquad [2.7]$$

The selectivity coefficient can determine the affinity of the resin for ion B over ion A. As a result, for K>1, the resin prefers ion B and for K< 1, it prefers ion A. In the case of K equal to 1, the ion exchanger has no preference for ion A or ion B.

In this study, the selectivity coefficient for the loading of divalent metal ions by iminodiacetic acid ion exchange resin when pH is maintained to be constant can be expressed by Equation 2.8 [49]. In this work, ideally, K is independent of the ratio of [M] to [H] however, in real applications this is not true, since the activity coefficients of metal ions on the resins differ in a complex manner with resin composition. Since species in the solution (M^{2+}) and the species attached to the resin functional group (H^{+}) have unequal charge, the distribution relates to the solution concentration. Thus, if solution dilution increases, as one

can expect from the Mass Action Law, the ion of the higher charge (M^{2+}) is more strongly loaded onto the resin [50]. As a result, constant K as a selectivity coefficient will be introduced and calculated experimentally by fitting the mass action law to experimental datasets. By considering that two protons are exchanged with one metal ion, the selectivity coefficient equation is shown below.

$$K = \frac{[H]^2[\overline{M}]}{[M][\overline{H}]^2} \qquad [2.8]$$

2.1.3.3.2 Separation Factor

The preference of a resin for one of the ions involved in an ion exchange reaction is typically described by "separation factor". According to Helfferich [51],"this quantity is particularly convenient for practical applications while the selectivity coefficient is more convenient for theoretical studies". The factor is calculated based on the composition of both ions in the resin phase and the solution and described in Equation 2.9.

$$S_A^B = \frac{[\overline{B}][A]}{[\overline{A}][B]} \qquad [2.9]$$

Generally, for a separation factor larger than unity, the resin takes up ion B more strongly. On the other hand, for a separation factor less than unity, the resin prefers ion A over ion B. This factor is typically not a constant value and thereby depends on several factors such as concentration of solution and temperature [51]. According to Dorfner [31], "under the

important restriction that the selectivity coefficient is different from the separation factor only in the case of the uptake of ions of different valences".

2.2 Ion Exchange Resins

Ion exchange resins are categorized as either anion exchangers possessing negatively-charged mobile ions or cation exchangers with positively-charged exchangeable ions. They both are typically engineered from organic polymers. The ion exchange resin properties vary according to the attached functional groups supported by the hydrocarbon structural networks. Essentially, the physical properties of the ion exchange resin are controlled by the polymeric matrix and its structure while the chemical performance (capacity and selectivity) of the resin is largely determined by the types of functional groups contained [52]. Resins can be generally considered as strong or weak acid cation exchange resins or strong or weak base anion exchange resins. In addition, chelating resins are a special sub-group of the cation exchange resin grouping. The properties of chelating resins will be discussed in the next section.

2.2.1 Chelating Ion Exchange Resins

Chelating ion exchange resins typically are identified as cation exchange resins with coordinating copolymer matrix containing covalently-bounded hydrocarbon chains attached to the specific chelating functional group, which donates sulphur, nitrogen or oxygen atoms. These donor atoms act as Lewis bases and they form complexes directly with Lewis acids such as metal ions. One of the main reasons for the high affinity of the resin towards the

desired metal ions (M2+) is the coordinating-type interaction between the metal ion loaded and the resin structure. The most commonly applied chelating resins with oxygen and nitrogen donor atoms in the industry are resins possessing iminodiacetate, carboxylate and phosphonate functional groups as described graphically in Figure 2.2 [53] .

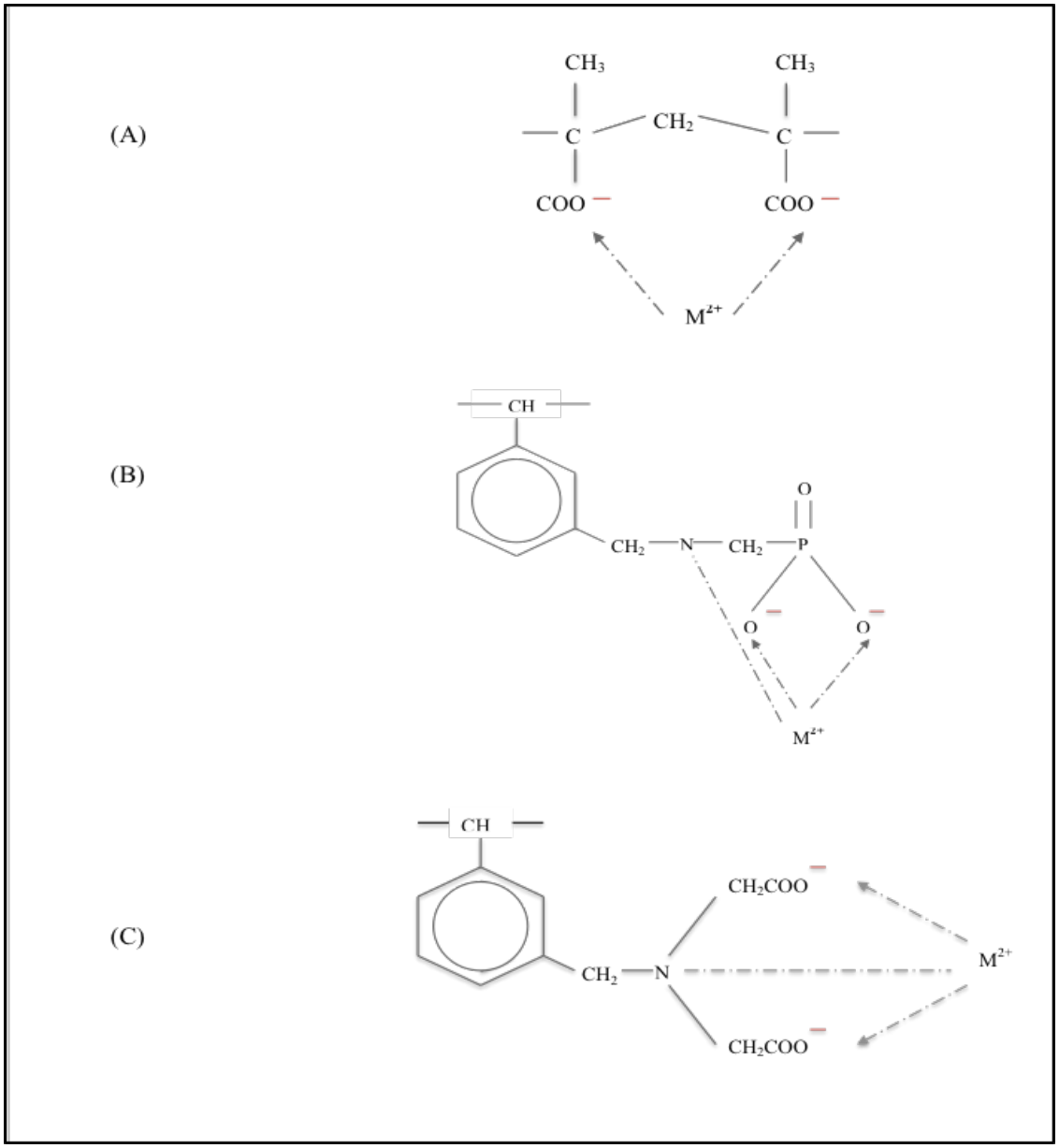

Figure 2.2: Chelating Functional Groups: (A) Carboxylate (B) Phosphonate (C) Iminodiacetate

Further selectivity for the base metals is attainable by changing the acidity of the solution in which the ion exchange reaction occurs [54] . In contrast to the conventional resins used for water treatment (eg. strong acid resins), these resins establish greater selectivity for base metal ions [44]. Zainol [11] explains this high selectivity of resin in terms of how metal ions are loaded onto chelating resins. She quoted the loading process as a combination of ionic interaction and coordination that results in having greater selectivity for some ions compared to conventional resins. These resins can contain exchangeable H^+ cations that give the resins the ability to behave as insoluble, but very reactive acids. Cation exchange resins with phosphonic acid functional groups can be used in slightly acidic solutions and have been found to be selective for ions such as copper, zinc and cadmium compared to nickel. Weakly-acidic resins with carboxylic acid groups provide high loading capacity but their application is restricted due to poor selectivity over alkaline earth metals. However, among these several chelating resins, iminodiacetic resins are proven and known to be very selective exchangers for nickel recovery. If only common divalent non-ferrous metal cations are selected, then, among those cations, the selectivity of this type of resin ranks nickel second after copper. Comparative selectivity orders of these three types of resins are described in Table 2.2 [11].

Table 2.2: Selectivity Orders of the Iminodiacetic Acid Chelating Resins Compared to Carboxylic and Phosphonic Acid Resins [11]

Chelating Resin Type	Selectivity Order
Carboxylic	$Cu^{2+} > Pb^{2+} > Zn^{2+} > Cd^{2+} > Ni^{2+} > Ca^{2+}$
Phosphonic	$Cu^{2+} > Zn^{2+} > Cd^{2+} > Mn^{2+} > Co^{2+} > Ni^{2+} > Ca^{2+}$
Iminodiacetic	$Cr^{3+} > In^{3+} > Fe^{3+} > Al^{3+} > Hg^{2+} > UO_2^{2+} > Cu^{2+} > Pb^{2+} > Ni^{2+} > Cd^{2+} > Zn^{2+} > Co^{2+} > Fe^{2+} > Mn^{2+} > Ca^{2+} > Mg^{2+}$

2.2.1.1 Iminodiacetic Acid (IDA) Chelating Resins

Iminodiacetic acid type of resin has been commercially used since the late 1950's. Figure 2.3 (a) illustrates the iminodiacetic acid ion exchange resin (IDA). The resin consists of the functional group containing two carboxylic groups and one amino group. In addition, Figure (b) shows that the chelate structure formed when a divalent metal cation is loaded onto the hydrogen form of the resin [11].

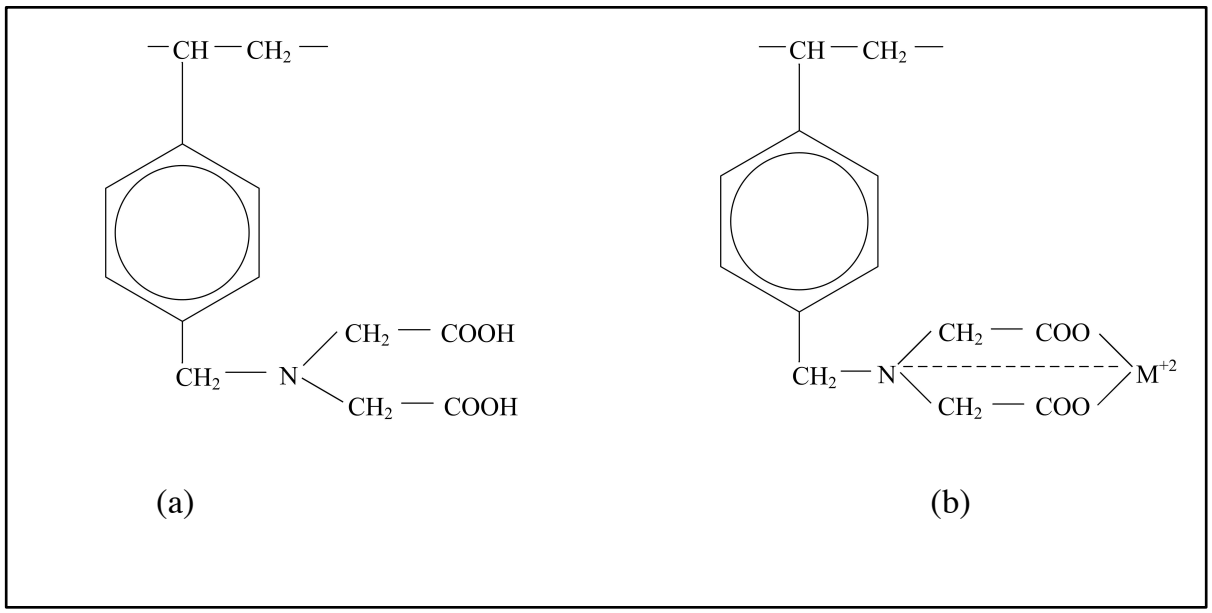

Figure 2.3: (a) Chemical Structure of Iminodiacetic Acid, (b) Chelate Structure of Iminodiacetic Resin with Divalent Cation [11]

As illustrated in Figure 2.4, as the pH increases the iminodiacetic functional group of the resin tends to lose its hydrogen ions. The authors of these works [11, 31, 55] confirmed the fact that resin is fully protonated at pH below 2 and, as the pH reaches 4, the first proton is released. At pH 12.3, the resin will completely lose all the hydrogen ions. As a result, in terms of the industrial use of the iminodiacetic ion exchange resin, the resin will be inefficient in low pH (pH 1 – 2) solutions. Since most divalent metal cations are relatively insoluble at pH higher than 5, this weakly acidic nature theoretically limits the use of the resin in hydrometallurgical operations. On the other hand, this type of resin is more applicable than conventional cation exchange resins in slightly acidic (pH 4 to 5) media due to strong bounding with numerous metal ions combined with its macroporous structure creates high resistance to osmotic shock, fast kinetics, and high mechanical strength. Elution of adsorbed metals from the iminodiacetic resin process can be accomplished by decreasing the pH using dilute acid [11].

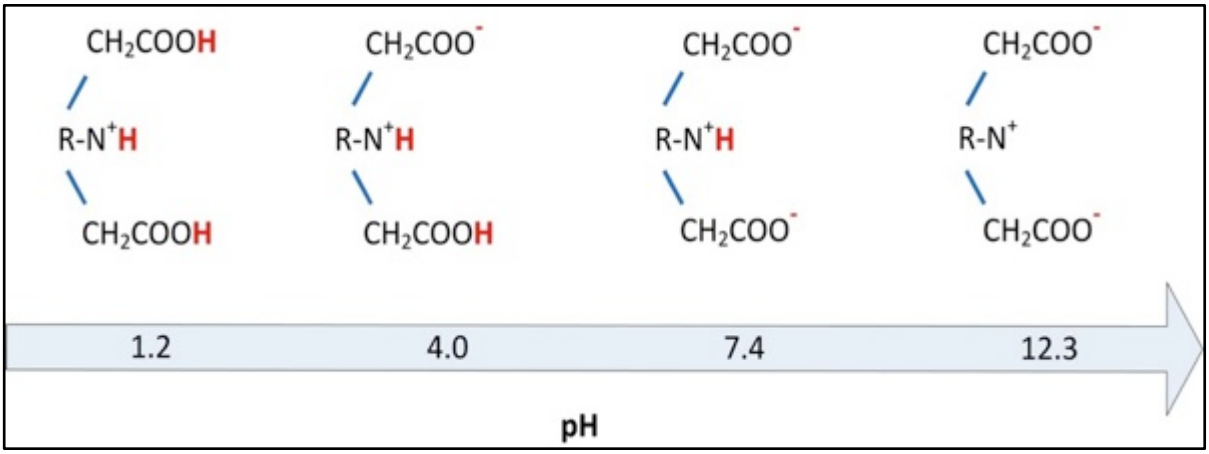

Figure 2.4: Iminodiacetic Functional Group at Different pH Values [31]

2.2.2 Available Iminodiacetic Ion Exchange Resins

Iminodiacetic ion exchange resins have been widely used for removal of heavy metal ions from wastewater or aqueous solutions. Extensive studies have been performed in these areas [56-61] . In these studies, the chelating resins possessing iminodiacetic acid (IDA) functional groups namely, Purolite S930, Chelex 100, Lewatit TP 207 and Amberlite IRC 748R were typically applied owing to their high selectivity and low manufacturing cost [56, 57, 59, 61]. Korngold *et a*l. [59, 61] used Purolite S930 resin as a cation exchanger in their study to remove Cu^{2+}, Ni^{2+}, Co^{2+}, and Cd^{2+} from tap water that contained small quantities of salts of carboxylic acids. Moreover, according to Gode and Pehlivan [56] , Chelex-100 and Lewatit TP 207 have numerous features (such as abundant, inexpensive) that make them suitable media for the removal of dissolved metal contaminants.

Commercially-available iminodiacetic ion exchange resins have also been investigated for their suitability in terms of the loading of nickel in resin-in-pulp (RIP) applications applied

for the treatment of pressure acid leaching tailing for nickel ore laterites (The resin-in-pulp process will be discussed in section 2.3). In the resin-in-pulp processes, the selectivity of the resin for nickel over other metals existing in laterite leach solutions is one of the principal concerns. As such, significant research has been undertaken to establish the resin most appropriate to nickel resin-in-pulp [19, 22, 23, 25, 28].

Following the Mandes and Martin's studies [19, 25], it was presented that Amberlite IRC 748R is the most suitable IDA resin in the nickel recovery process from HPAL pulps. Furthermore, Zainol and Nicol [22, 28] studied the loading behavior of Ni along with Co, Mg, and Mn at various pH values using several types of iminodiacetic resins. They reported that Lewatit TP207 MonoPlus resin was found to be the most promising resin in terms of loading capacity coupled with its uniform bead size for nickel loading in resin-in-pulp applications.

2.2.2.1 Lewatit MonoPlus TP207XL

The majority of studies on resin-in-pulp developments have been undertaken using Lewatit MonoPlus TP207XL (henceforward it is identified as TP207XL) IDA resin for nickel recovery [20, 26, 27]. Littlejohn and Vaughan performed wide-ranging studies on TP207XL resin [20, 27]. They characterized the properties of six ion exchange resins with different functional groups and they reported that TP207XL was confirmed to have a higher operational capacity for Ni among other commercially-available resins [27]. In the previous research study by the authors of this work [26], various large bead iminodiacetic ion exchange resins (Ambersep XE818, Lewatit MonoPlus TP207XL, Purolite S930+/4888)

have been evaluated for nickel recovery. These large resin beads are generated specially for the base metals resin-in-pulp processes where the resins are required to be separated from the solids in the pulp slurry. Although loading rates decrease as resin bead sizes increase, in RIP applications large bead resins are favored because it is easier to screen these from the solids. For various resin size fractions, the loading rate and capacity were determined using synthetic nickel sulphate solution at pH 4.The TP207XL resin with size fraction of 710 – 850 micron was found to have the fastest loading rate. However, it presented a somewhat lower capacity compared with the Purolite S930+ and the Lewatit TP207 resins.

2.3 Resin In Pulp Process

In 1953, the Union of Soviet Socialist Republics (USSR) introduced the resin-in-pulp technology as a "non-filtrational sorptive-extractive" method to the hydrometallurgical industries for the recovery of uranium [62]. RIP process implementation became a favorable method by eliminating the solid/liquid separation step following leaching in addition to combining the recovery and purification stages that results in the reducing of capital and operating costs. The RIP process can result in high metal recovery, especially when the solid slurry is hard to settle or filter. However, in the Western world, RIP applications have been largely ignored due to the perceived high operating costs related to several factors, one of which was resin loss during operation. One of the primary reasons for the degradation of resin may be osmotic shock occurring due to chemical and physical environmental changes [63]. In addition, according to Zainol [11], one of the causes for the lack of the RIP process in Western industries can be the fact that resins are more costly compared to activated carbon

used in the Carbon In Pulp process (CIP), which is a similar process to RIP and is widely applied for recovery of gold from cyanide leach slurries.

2.3.1 Definition of Resin In Pulp

In the early periods of development of the RIP operation, this process was generally indicated to be any process in which resins would be used in the solution that had not been fully separated from solids. Traditionally, ion exchange between resins and solution could be accomplished by various methods such as batch operation, column operation (fixed or fluidized bed), and continuous systems. However, today the ion exchange process can be clearly classified into four types: fixed bed, moving packed bed, fluidized bed, and resin-in-pulp, according to McKevitt [24].

Generally, the RIP system is operated based on counter current contact between the resin-and the leach slurry, using either a continuous (cascade) or semi-continuous (carousel) operating style. For the purpose of this work, the three-stage cascade operation will be considered and discussed in detail here. For the three-stage cascade operation as illustrated in Figure 2.5, the feed slurry always pumps through the tank in the same manner (from tank 1 to tank 3) and exits the cascade circuit as slurry tailings from tank 3. On the other hand, resin is transferred from tank 3 going towards tank 1 in which the feed concentration of the desired metal ion is high.

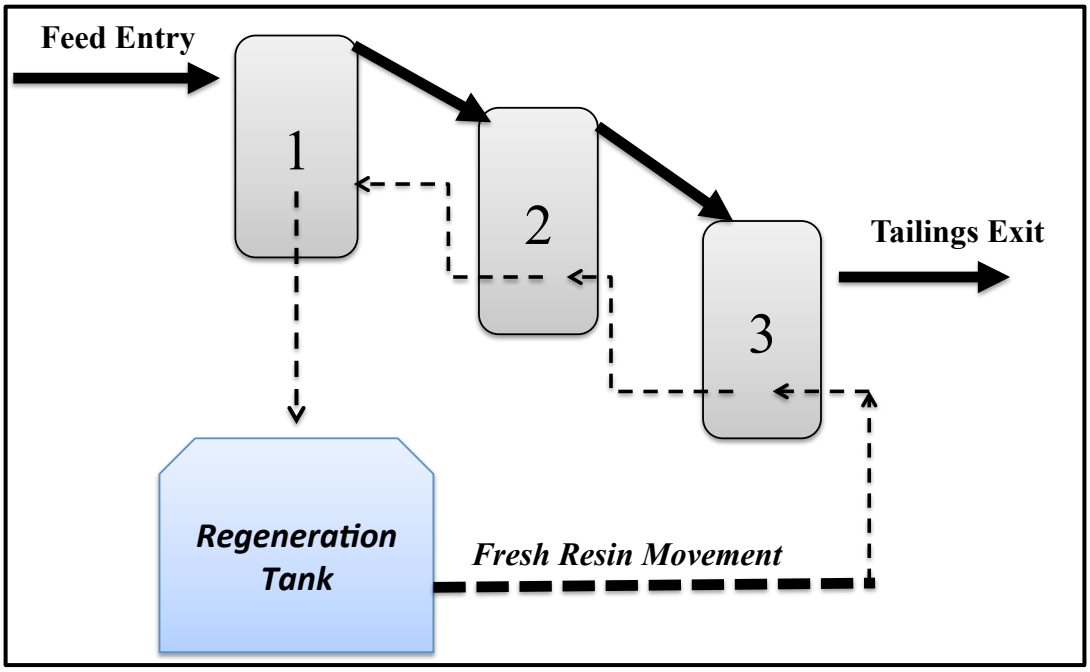

Figure 2.5: Three-Stage Cascade Operation Strategy [24]

2.3.2 Resin In Pulp Applications for Nickel Recovery

In the case of the recovery of nickel through the use of ion exchange resin-in-pulp loading from HPAL tailings, several studies have been performed previously [11, 23, 24, 28, 64-67]. For example, in 2003, Nicol and Zainol [67] performed laboratory experiments and designed a continuous six-stage pilot mini-plant to improve the efficiency of the RIP processes for nickel and cobalt recoveries. Following in 2005 for nickel and cobalt loading performance, Zainol [11] developed an introductory model that was applied to define the operation parameters for a five counter-current stages RIP mini-plant that resulted in high recovery of nickel and cobalt at the end. Most recently, McKevitt [24] also established a mathematical model (correlation), which explains loading behavior of base metal ions onto iminodiacetic ion exchange resins. After verification of her model, she applied it to simulate the implementation of the full-scale base metal RIP circuit under various operation conditions.

Although there is no significant industrial growth for base metal RIP operations McKevitt and Dreisinger reviewed the literature [68] related to RIP developments for gold and uranium.

2.4 Kinetics of Ion Exchange

In terms of the kinetics study of the ion exchange reaction, one objective can be the investigation of how the system moves towards an equilibrium state. As a result, the chemical rates of the exchanging of ions in the desired ion exchange system can be studied. This can be accomplished by determining a rate-limiting step for the ion exchange process that is the required step ahead of applying any engineering models to the kinetic experimental datasets.

2.4.1 Rate Limiting Step

Determining a rate-limiting step for the ion exchange process is required ahead of applying any engineering models. In formulating the mathematical engineering model, a resin bead is considered as a spherical particle surrounded by an exterior solution with the desired ion concentration. The heterogeneous ion exchange process that occurs between the resin (solid phase) and ion in solution (liquid phase) is controlled by one or more of the following steps when the metal ion in the solution is displaced by the hydrogen ion previously loaded onto resin functional group. Figure 2.6 is the modified version of the figure provided by Wołowicz and Hubicki [44]. The steps in the exchange process are:

(1) diffusion of M^{2+} through the aqueous film (Nernst film) surrounding the particle (film diffusion);

(2) diffusion of M^{2+} through the resin bead (particle diffusion);

(3) chemical reaction within the resin bead between the metal ion and hydrogen ion attached to the functional group present in the resin matrix (ion exchange reaction);

(4) diffusion of the displaced H^+ from the resin matrix (particle diffusion);

(5) diffusion of the displaced H^+ from the resin particles to the solution (film diffusion) [44] .

Steps (4) and (5) are the reverse processes of steps (2) and (1), correspondingly.

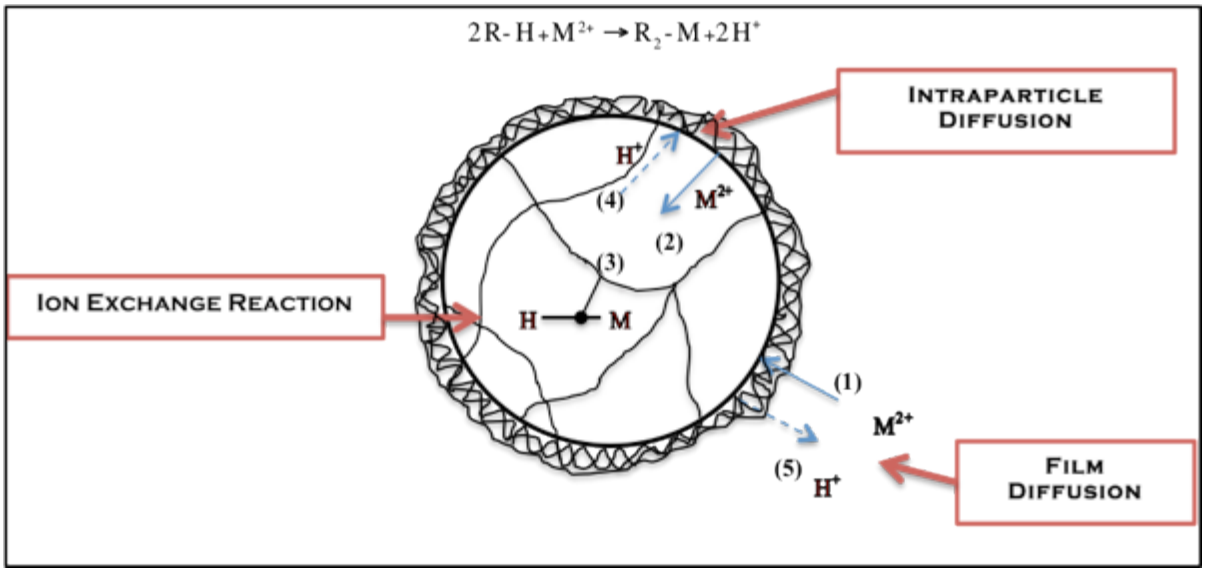

Figure 2.6: Rate Determining Step in Ion Exchange (schematic); 1,5 – Film diffusion; 2,4 – Particle diffusion; 3 – Chemical reaction [44]

Therefore, film diffusion, intraparticle diffusion and ion exchange processes are the only three possible rate-limiting steps. Mostly, the rate at which the ion exchange process progresses is a function of physical and chemical factors such as: resin particle size, the

agitation speed, the solution concentration, temperature, and the degree of resin cross linking [69].

Fleming and Nicol [70] studied the rate of the ion exchange process for uranium recovery and they stated that the process was predominantly controlled by the film diffusion regime when resins having small particle size, high capacity, and low degree of cross linking are introduced to the inadequately-agitated dilute solutions. Inversely, particle diffusion regime can prevail when highly cross-linked low-capacity resins of large bead size are contacted with sufficiently-agitated concentrated solutions. Generally speaking, for the ion exchange process it would be expected that the initial loading is controlled by film diffusion and the later stages by intraparticle diffusion or chemical reaction. In terms of agitation effect, McKevitt [24] concluded that, in the case of nickel recovery using iminodiacetic ion exchange resins in a batch system when film diffusion was rate limiting, if the agitation rate increases, it can result in increasing the loading rate. However, she noted that this can occur over an exact range and thereby giving is an upper limit for the agitation effect in the film diffusion-controlled ion exchange process. Furthermore, she concluded that if the process is being performed under the intraparticle-diffusional-control-regime, the increase in the agitation rate has no significant effect.

Until now, ion exchange loading rates have mostly been modeled by either fully empirical rate equations or more fundamental diffusional mechanisms. While the fundamental models describe the ion exchange loading process as scientifically as possible, the empirical (engineering) models sufficiently describe system performance. Earlier studies have presented the typical validity of such diffusional mechanisms [69, 71-76]. In most of these

studies, Fick's law was applied to explain the diffusional processes. However, the Nernst-Planck equation was applied, which also considers the effect of the electric potential in the diffusion process [75]. According to the Nernst-Planck flux equations, it was revealed that diffusion "gives rise to an electric potential gradient which acts on the diffusing ions and results in a variable inter-diffusion coefficient and quite different rate laws" [76].

Broad ranges of studies have been performed for kinetics of chelating ion exchangers. Yoshida *et al*. [76, 77] modeled the kinetics of the loading rate of metallic ions such as Cu^{2+} by a chelate resin by applying the Nernst-Plank equation to the flux of ions in the resin matrix. In addition, Fernandez and Diaz [78] studied the applicability of the Nernst-Plank equation to fit experimental results verified using the sodium form of the iminodiacetic ion exchange resin. However, the complexity of the kinetic description and differential equations with no analytical solutions of the Nernst-Planck model has resulted in the extensive application of simpler empirical or semi- empirical models in the design and operation of the ion exchange process.

Generally, engineering models (empirical or semi-empirical) are generated to describe the loading process of the ion exchange system. Recently, McKevitt [24] developed the hybrid correlation to model the loading of divalent metal ions such as copper, nickel and cobalt onto iminodiacetic ion exchange resins. As a result, this model has been selected for the purpose of this study, which involves the measurement of ferrous and nickel loading onto an iminodiacetic ion exchange resin under a variety of experimental conditions.

2.5 Hybrid Correlation Model Developed by McKevitt

McKevitt developed the hybrid correlation in order to model the loading of the base metal ions in an RIP circuit. The detailed information regarding this model is available in the literature [24]. This section explains more generally how this model was initially generated.

2.5.1 Qualitative Evaluation of the Rate-Limiting Step(s) for Loading of a Divalent Metal Ion onto Iminodiacetic Ion Exchange Resins

McKevitt and Dreisinger evaluated the rate-limiting steps qualitatively by running several loading experiments with copper, cobalt, and nickel onto the TP207 iminodiacetic ion exchange resin [49]. They developed the model first by determining and understanding the rate-limiting step(s) of the ion exchange reaction given in Equation 2.1. The possible rate-limiting regimes described in section [2.4.1] were film diffusion, intraparticle diffusion and ion exchange reaction. In order to determine the rate-limiting step, various parameters described in Table 2.3 were evaluated.

As mentioned, the loading rate is faster for smaller resin bead sizes that also resulted in having the much higher final loading values. The concept that smaller resin beads have higher loading capacity due to containing a greater concentration of the functional groups, confirms the fact that the diffusion process can be predominantly governed by intraparticle diffusion regimes. Furthermore, interruption tests also illustrated that the diffusion is limited to intraparticle diffusion. In the test, the resin beads were removed from the test solution

mid-way during an experiment. The resin beads were left apart for a length of time and afterward the beads reintroduced to the test solution. Intraparticle diffusion was mainly controlled the rate of the system when a discontinuity is observed in the loading rate curve.

Most importantly, it was shown that since the selectivity of the iminodiacetic ion exchange resin varies for the various metal ions according to the complex formation rate, the ion exchange reaction could also be the rate-limiting step for the process. According to those experimental results, they [49] concluded that the process was controlled by the film diffusion regime in the beginning stage of the process and followed by some combination of intraparticle diffusion and ion exchange reaction.

Table 2.3: Various Factors That Can Have Effects on the Ion Exchange Loading Rate Provided by McKevitt [24]

Increasing Parameter	**Film Diffusion**	**Intraparticle Diffusion (Vermeulen)**	**Shrinking Core Intraparticle Diffusion**	**Exchange Process**
Resin Bead Diameter: d_p	Rate $\propto d_p$	Rate $\propto d_p^2$	Rate $\propto d_p^2$	No Effect
Bulk Solution Concentration [M]	Increases	No Effect	Increases	Increases
Agitation Rate	Increases to a point	No Effect	No Effect	No Effect
Interruption Test	No Effect	Discontinuity	Discontinuity	No Effect
Rate of Complex Formation	No Effect	No Effect	No Effect	Increases

2.5.2 Evaluation of Existing Engineering Loading Models

Evaluation of the rate-limiting step resulted in confirming the fact that the system rate was mainly controlled by some combination of intraparticle diffusion and ion exchange reaction. To develop an adequate kinetic model for such a system four conventional engineering models (linear approach to equilibrium, Vermeulen approximation, Shrinking Core model, and second order reaction), summarized in Table 2.4 were fitted to the data for the loading of nickel onto the iminodiacetic ion exchange resin (TP207MP) [49].

However, to develop the proper kinetic model for the loading rate of the system, McKevitt and Dreisinger [49] quantified the film diffusion part using a linear approach to the equilibrium model separately from the combination of the intraparticle and ion exchange rate limited regime.

The linear approach to the equilibrium model has been widely used for modeling the ion loading onto resins due to the simplicity of its application. The model presented by Helfferich [73] as the "linear driving force model" assumed that the rate is "proportional to the distance the system is from equilibrium" at any given time. For both film diffusion and intraparticle, the rate model can be defined in the table. The constant k is related to the diffusion coefficient (D) and the resin bead particle size (d_P) for both cases of diffusion. However, in the case of film diffusion the k_f is based on film thickness as well as the concentration of ions in the solution and on the resin matrix. For intraparticle diffusion, Glueckauf [49, 79] has introduced the shape factor η (>1/2) parameter in the k equation

Table 2.4: Four Conventional Engineering Models Applied for the Ion exchange Rate Modeling

Engineering Models	Rate Equation	Solution of Rate Equation	Rate Constant
Linear Approach to Equilibrium	$\frac{d}{dt}[\overline{M}] = k_1([\overline{M}]_{eqb} - [\overline{M}])$	$F = \frac{[\overline{M}]}{[\overline{M}]_{eqb}} = 1 - \exp(-k_1 t)$	$k_f = \frac{6 D_f [M]}{d_p \delta [\overline{M}]}$ $k_g = \frac{D_p}{\eta d_p^2}$
Second Order Rate Model (Thomas Model)	$\frac{d[\overline{M}]}{[dt]} = k_{fwd}[M][\overline{H}] - k_{rev}[H][\overline{M}$	----------	k_{fwd} and k_{rev}
Vermeulen's approximation	$\frac{d}{dt}[\overline{M}] = \frac{2 k_V([\overline{M}]_{eqb}^2 [\overline{M}]^2)}{[\overline{M}]}$	$F = \sqrt{1 - \exp(-4 k_V t)}$	$k_v = \frac{\pi^2 D_p}{d_p^2}$
Shrinking Core Model	$\frac{dF}{dt} = \frac{k_c d_c}{2(d_p - d_c)}$	$F = 1 - \left[\frac{1}{2} + \sin\left(\frac{\sin^{-1}(1 - 2 k_c t)}{3}\right)\right]$	$k_c = \frac{24 D_s [\overline{M}]}{d_p^2 [\overline{M}]_{max}}$

According to McKevitt and Dreisinger [49], the linear approach to the equilibrium model could not sufficiently describe the full data set since, as the nickel concentration increased in the system the model did not properly fit the datasets. The second order rate model (Thomas model) also was fitted to the datasets. Among several kinetics models that consider the ion

exchange process as a chemical reaction, the Thomas model is the most famous in which the ion exchange process is studied as a second order reversible reaction [80] . In this model, the reaction rate can be determined based on the concentration of the divalent metal ions in solution and the one loaded onto resin. For a binary system, the rate equation and two related empirical rate constants are described in the table. This rate law is valid where the ion exchange process is more likely controlled by the ion exchange reaction only, not by any other diffusion processes in the solution or in the resin bead [49]. The Thomas model fit pretty well for each specific data set however, the model overpredicted loading at high concentration and underpredicted loading at low concentration when applied over the various range of solution concentrations.

Vermeulen's approximation and Shrinking Core model were also fitted to the nickel loading datasets. Since the hybrid correlation model was constructed based on these two models, they are described separately in detail in the next sections.

2.5.2.1 Vermeulen's Approximation

Vermeulen’s approximation equation is another selected model that has been applied to describe the kinetics of the ion exchange process when it is controlled by intraparticle diffusion. Several studies performed on the solid ion exchanger (Zeolite) led to this model first using Fick's second law with the assumption of a constant shape of the particle and a constant value of the diffusion coefficient [81, 82]. The model, which expresses the metal ion concentration in the zeolite with time, is described as below [83]:

$$\frac{\partial[\overline{M}]}{\partial t} = D\left[\frac{\partial^2[\overline{M}]}{dr^2} + \frac{2}{r}\frac{\partial[\overline{M}]}{dr}\right] \quad [2.10]$$

If the assumption is made that the concentration of M ions is constant and the volume of the solution is much higher than the volume of resin using batch system then equation [2.10] can be expressed as:

$$F = 1 - \frac{6}{\pi^2}\sum_{j=1}^{\infty}\frac{1}{j^2}\exp\left(\frac{Dt\pi^2 j^2}{r^2}\right) \quad [2.11]$$

Vermeulen simplified Equation 2.11 by developing an approximation typically referred to as Vermeulen's quadratic approach to equilibrium, which is written in differential form assuming no initial loading in Equation 2.12 [84]. The solution to the approximation is expressed in Equations 2.13-2.15. Equation 2.13 calculates the time it would take to load a resin to any given metal loading, $[\overline{M}]$, while Equation 2.14 calculates the fractional attainment of equilibrium (F). It is required to mention that the rate constant k_v is independent of solution concentration for the Vermeulen approximation case [24].

$$\frac{d}{dt}[\overline{M}] = \frac{2k_V([\overline{M}]_{eq\bar{b}}^2[\overline{M}]^2)}{[\overline{M}]} \quad [2.12]$$

$$t = \frac{-1}{4k_V}\ln\left(\frac{[\overline{M}]_{eq\bar{b}}^2[\overline{M}]^2}{[\overline{M}]_{eqb}^2}\right) \quad [2.13]$$

$$F = \sqrt{1 - \exp(-4k_V t)} \quad [2.14]$$

$$k_v = \frac{\pi^2 D_p}{d_p^2} \qquad [2.15]$$

2.5.2.2 Shrinking Core Model

The shrinking core model also known as the "unreacted core model" describes the presence of a sharp moving boundary within the spherical resin bead between the reacted outer shell and the unreacted inner core as illustrated in Figure 2.7. Several researchers [11, 78, 85] applied this model successfully to describe the loading behavior of divalent metal ions onto iminodiacetic ion exchange resin.

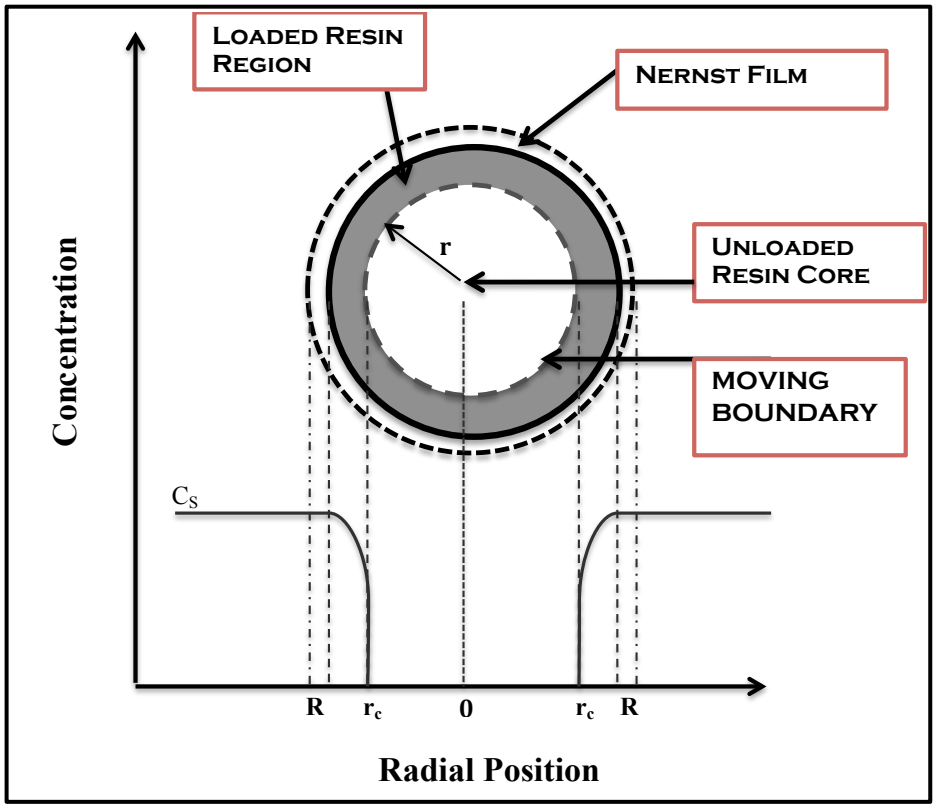

Figure 2.7: Schematic Representation of the Shell Progressive Mechanism in a Spherical Ion Exchange Bead [86]

One of the hypotheses considered by the model is that the loading of a divalent metal ion occurs as a very fast chemical reaction controlled by the diffusion of the metal ion through the reacted region of the resin bead [86]. Assuming constant solution volume condition and constant diffusion coefficients, the Shrinking Core model and its solution can be written as Equations 2.16- 2.19 [87]. In contrast to Vermeulen approximation rate constant (k_v), k_c is a function of solution concentration.

$$\frac{dF}{dt} = \frac{k_c d_c}{2(d_p - d_c)} \qquad [2.16]$$

$$t = \frac{1 - 3(1 - F)^{2/3} + 2(1 - F)}{k_c} \qquad [2.17]$$

$$F = 1 - \left[\frac{1}{2} + \sin\left(\frac{\sin^{-1}(1 - 2k_c t)}{3}\right)\right] \qquad [2.18]$$

$$k_c = \frac{24 D_s [\overline{M}]}{d_p^2 [\overline{M}]max} \qquad [2.19]$$

After applying Vermeulen's approximation and the Shrinking Core model to the nickel loading datasets, it was concluded that the best-fitted, effective intraparticle diffusion coefficient (D_p for Vermeulen model and D_s for shrinking core model) varied from test to test for both models, suggesting that none of them could adequately describe the effect of solution concentration for nickel loading. However, both models could make an excellent starting point for modeling of nickel loading even when the diffusion coefficient varied. It was additionally noted that when an attempt was made to fit the full set of test results using only a single effective diffusion coefficient, the Vermeulen underpredicted and the shrinking

core model overpredicted the effect of solution concentration [83]. Development of a hybrid correlation model based on these two engineering rate equations is described in the next section.

2.5.3 Development of Hybrid Correlation for Intraparticle Diffusion

After running those rate-limiting investigation experiments and applying several conventional engineering models to the system it was concluded that none of them could adequately explain the system over the full range of metal ion concentrations in solution [49]. As a result, they proposed "a new two-parameter hybrid correlation" [88].

The idea of this new correlation came from the fact that the system dependency on concentration is somewhere between $[Ni]^0$ according to the Vermeulen model and $[Ni]^1$ according to Shrinking Core model. Since both models fit the data fairly well for the first stage of the loading curve it was considered that if there is any correlation between two constants (k_c and k_s), it could minimize the error between the two models. They stated that the error was minimized when $k_v = 0.677\ k_c$ which results in the approximation of the Shrinking Core model by a Vermeulen expression. To combine the Vermeulen model and the Vermeulen approximation to the Shrinking Core model into a single hybrid correlation, a second empirical fit parameter, α, besides the apparent diffusivity (D_{app}), was defined for the system.

This empirical fit alpha (α) provides good understanding of the metal ion loading profile within the resin bead. Regarding the metal loading profile, when alpha can be considered as

a measurement of sharpness of the boundary present between the loaded and unloaded part of the resin bead. When alpha approaches to zero, the hybrid correlation reduces to Vermeulen's approximation to intraparticle diffusion whereas for alpha equals to one, the correlation becomes an approximation to the Shrinking Core model. The equations describing the hybrid correlation are defined in Equation 2.20 where Equation 2.21 (F) is the mathematical solution for it. In addition, Equation 2.22 also defines a new rate constant, k_h (1/s), introduced by the hybrid correlation [88]. The step-by-step derivation of the hybrid model is explained in Appendix C.

$$\frac{d}{dt}[\overline{M}] = \frac{2k_h([\overline{M}]_{eqb} - [\overline{M}]^2)}{[\overline{\overline{M}}]} \qquad [2.20]$$

$$F = \sqrt{1 - \exp(-4k_h t)} \qquad [2.21]$$

$$k_h = \frac{\pi^2 D_{app}}{d_P^2}\left(\frac{16[M]}{\pi^2[\overline{\overline{M}}]_{max}}\right)^{\alpha} \qquad [2.22]$$

In this thesis, the application of an ion exchange correlation (hybrid model) for ferrous loading onto resin under infinite solution volume condition and nickel loading behavior under finite solution volume condition was examined. In order to meet these two objectives of this study, two sets of experiments were conducted. The details regarding the related experimental procedures are described in the next chapter.

3 Experimental Procedures

Two experimental methods were used for studying the loading of nickel. The first one used the infinite solution volume condition for ferrous loading and the second one used the finite solution volume condition for nickel-ferrous displacement loading. Both experimental methods are described right after the section (3.1) that describes the materials used in both loading experiments.

3.1 Material

In this study, all the experiments were carried out using one of the recently manufactured iminodiacetic ion exchange resins (Lanxess Lewatit Monoplus TP207XL) to investigate the loading behavior of ferrous and nickel ions. This polymeric resin is used for ion exchange experiments in either the hydrogen or sodium form. For the objective of this work, the as-received resin was converted to the hydrogen form following the manufacturer's recommended procedure. The hydrogen form and chelate structure of this iminodiacetic ion exchange resin has already been illustrated in Figure 2.3. Prior to use, the resin was wet-screened to remove the -710 and +850 microns fractions to give resin of 710-850 microns. This resin was selected for the purpose of this research, since according to the previous study it has a narrow size distribution for a large bead resin, which is desired in the RIP application by providing for easy screening of the resin from solids. In addition, this resin showed the fastest loading rate for this size fraction compared to other commercially available resins.

Table 3.1 summarizes the resin (TP207XL) operational capacity reported by McKevitt [24] and Littlejohn and Vaughan [27] for the same resin bead particle size of 710 - 850 microns at pH 4. As described in this table, the capacity for this resin is rated between 2.0 - 2.36 (eq/L). The resin capacity unit of eq/L is the number of equivalents of exchangeable ions per unit volume of resin. Note that in this work, all resin volumes are in terms of the wet-settled bulk volume of the resin in hydrogen form.

Table 3.1: Operational Capacity Reported for TP207XL

Resin	Resin Bead Size (µm)	Capacity at pH 4 (eq/L)	Reference
TP207XL (Lot # CHC5034)	710 - 815	2.01	[24]
TP207XL (Lot # CHC50019)	710 - 815	2.36	[24]
TP207XL	710 - 815	2.13	[27]

Note that a synthetic solution was prepared for each experiment from ferrous and nickel sulphate salts with various target concentrations ranging from 100 to 10,000 ppm using American Chemical Society (ACS) grade reagents.

3.2 Method Development for Batch System

The original methodology was developed previously by McKevitt to study the loading behavior of metal ions such as copper nickel and cobalt [24]. This method was performed for ferrous loading batch tests from the solution in a reactor equipped with an overhead stirrer, which simulates the RIP environment. The hybrid correlation model for ferrous loading onto resin was validated at a constant solution pH=4 under infinite solution volume conditions (ISV) where the composition of the solution remains constant with time. This was performed in order to simplify solving differential equations regarding the hybrid model. In addition, pH 4 was maintained for the entire time of the experiment by means of the pH-stat method modified by McKevitt [24]. A constant pH in the test solutions is obtained in the standard pH-stat method that utilizes a pH electrode and controller for adding alkali hydroxide (base). The rate of base addition can be used to calculate rate of metal ion loading onto the resin. In order to select the best alkali hydroxides for minimizing the co-loading of alkali onto resin, McKevitt performed several experiments using different alkali hydroxides (Li, K and Na). Consequently, she confirmed that sodium hydroxide would be used with minimal interference in the experiments when the nickel is kept constant in the solution. Furthermore, in this study, the solution composition was maintained constant with time by continuously adding ferrous sulphate from a stock solution into the experimental solution. The rate of addition of ferrous sulphate solution was controlled in proportion to the loading of ferrous (as represented by the consumption of sodium hydroxide in the test).

For the second objective of the research (study of nickel-ferrous displacement loading) the same approach was taken. The only difference between two approaches is that nickel-ferrous

displacement experiments have been performed under finite solution volume conditions (FSV) where the concentrations of ions in solution were not maintained constant through each experiment. As a result, there was no need of nickel and ferrous sulphate stock addition and experiments were just performed under constant pH conditions at pH 4.

3.3 Experimental Procedures for Ferrous and Nickel-Ferrous Loading onto TP207XL

Ferrous loading experiments were performed in a batch system in which the synthetic solution reached equilibrium after a certain time by mixing the solution with resins under sufficient agitation. The procedure is described as follows:

- For each experiment, 495 mL of deionized water was added to the test vessel equipped with overhead stirrer impeller and placed in a water bath with the temperature fixed at 30°C. To provide good suspension of the resin in the test solution, 300-RPM speed of overhead stirrer (cole parmer) was provided throughout the test.
- The test solution was deaerated for approximately 20 to 30 minutes with 1 LPM nitrogen gas sparging. This results in limiting any chance of ferrous oxidation reaction by the time that the ferrous sulphate amount was added to the solution to make up the specific desired concentration. The nitrogen gas sparging was employed through the entire each experiment.
- Ferrous sulphate salt with various target concentrations ranging from 100 to 10,000 ppm then added to the test solution.

- A pH probe with temperature compensation calibrated using pH buffers 7 and 4 ahead of the time to equilibrate 5 mL resin samples at pH 4. To perform that, the resins were added to 50 ml beaker with 15 ml deionized water pH of which was adjusted to 4 by adding dilute sulphuric acid or sodium hydroxide drops.
- The 5mL pH-equilibrated resin samples also were deaerated with nitrogen gas sparging for 15 minutes.
- Depending on the desired ferrous sulphate solution concentration in the test vessel, a related stock solution was made up. The ferrous sulphate stock solution concentration was calculated and prepared in a way that the concentration of ferrous sulphate in solution in the test vessel stayed constant for the duration of each experiment.
- Sodium hydroxide stock solution of 0.25 M was prepared and its specific gravity was measured more than 5 times by weighing of 10.00 ± 0.02 mL of stock solution. Then, the average value of specific gravity was applied in mass balance analysis part of the experimental results.
- The two stock containers weights (as illustrated in Figure 3.1) measured before and after each experiment were placed on two separate balances (Sartorius TE4101 scales).
- The balances were connected to a computer in which Windmill software was installed to connect to the balances and record the weight on the scales every 15 seconds for the duration of each test.

A photograph of the experimental equipment used for the loading tests is illustrated in Figure 3.1.

In the case of nickel-ferrous displacement experimental procedure, some slight modifications have been applied to the described procedure for ferrous loading. However, the overall detailed procedure is similar. First of all, the synthetic solution contained approximately 10,000-ppm iron added as ferrous sulphate salt. Nickel as nickel sulphate was also added in variable concentrations at the beginning of the test. Furthermore, since these experiments were performed under non-infinite solution volume conditions, there was no need to make stock solutions 78 of nickel or ferrous sulphate, i.e. the nickel and ferrous solution concentrations were allowed to change with time as the nickel-ferrous displacement reaction progressed. Most importantly, the 5 ml resin sample added to the test solution was previously loaded from a solution containing ~10,000 ppm iron added as ferrous sulphate at pH 4 (pH 4 was maintained for the entire time of the experiment by means of the pH-stat) under the infinite solution volume condition. A copy of a blank test sheet for ferrous loading and also nickel-ferrous displacement tests in addition to more detailed photographs of each experimental setup are provided in Appendix A and B.

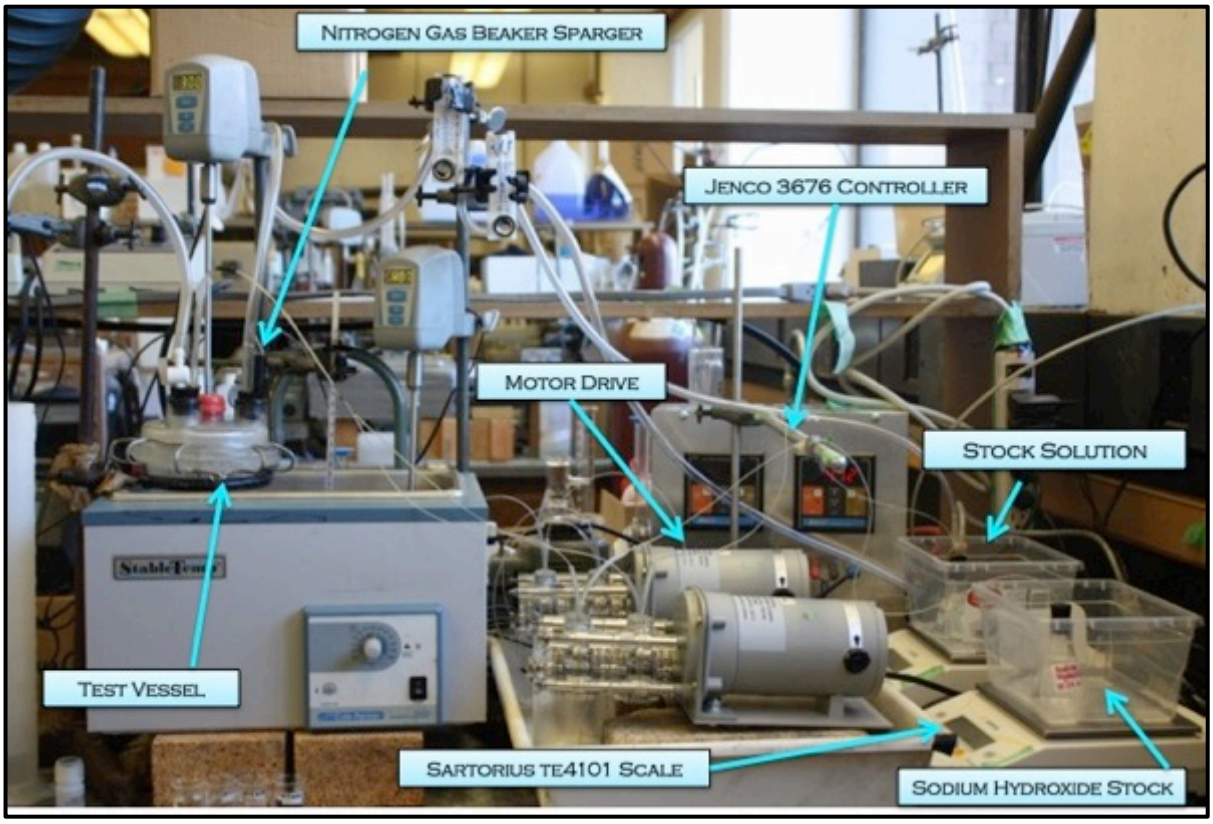

Figure 3.1: Batch Loading Study Experimental Equipment

3.3.1 Batch Loading Procedure

The loading procedure is described individually for ferrous loading and then for nickel-iron displacement loading in this section.

3.3.1.1 Ferrous Loading under Infinite Solution Volume Condition

The loading behavior of ferrous ions onto TP207XL was studied using a batch equilibration technique. The loading process began by adding 5 mL of resin into the previously prepared feed solution with the desired concentration of ferrous (100 to 10,000 ppm). Note that the pH

of the test solution was already adjusted to 4 through the addition of few drops of dilute sulphuric acid or sodium hydroxide depending on its initial pH. The resin was transferred using 10 mL pipette with "upside-down" manner where pipette bulb placed over the tip to minimize the amount of water that was added to the test beaker at the time of transferring the resins. It was attempted to transfer the whole resin sample into the test vessel containing ferrous sulphate solution at the same time.

In order to maintain the constant ferrous sulphate concentration and pH 4 in the test solution for the entire time of the experiment a Jenco 3676 controller was used. This pH-controller device was attached to a single motor drive with two mounted Masterflex L/S 13 pumpheads (as marked in Figure 3.1). The controller maintained the pH of the solution in a way that if the pH dropped below 3.9, the controller would turn on a motor drive to deliver the stock solution of sodium hydroxide and ferrous sulphate via separate pump heads. The motor would turn off once the solution pH reached 4.1. In this way, the ferrous sulphate depletion (by iron loading on the resin) would be compensated by addition of ferrous sulphate stock solution, in proportion to the addition of sodium hydroxide.

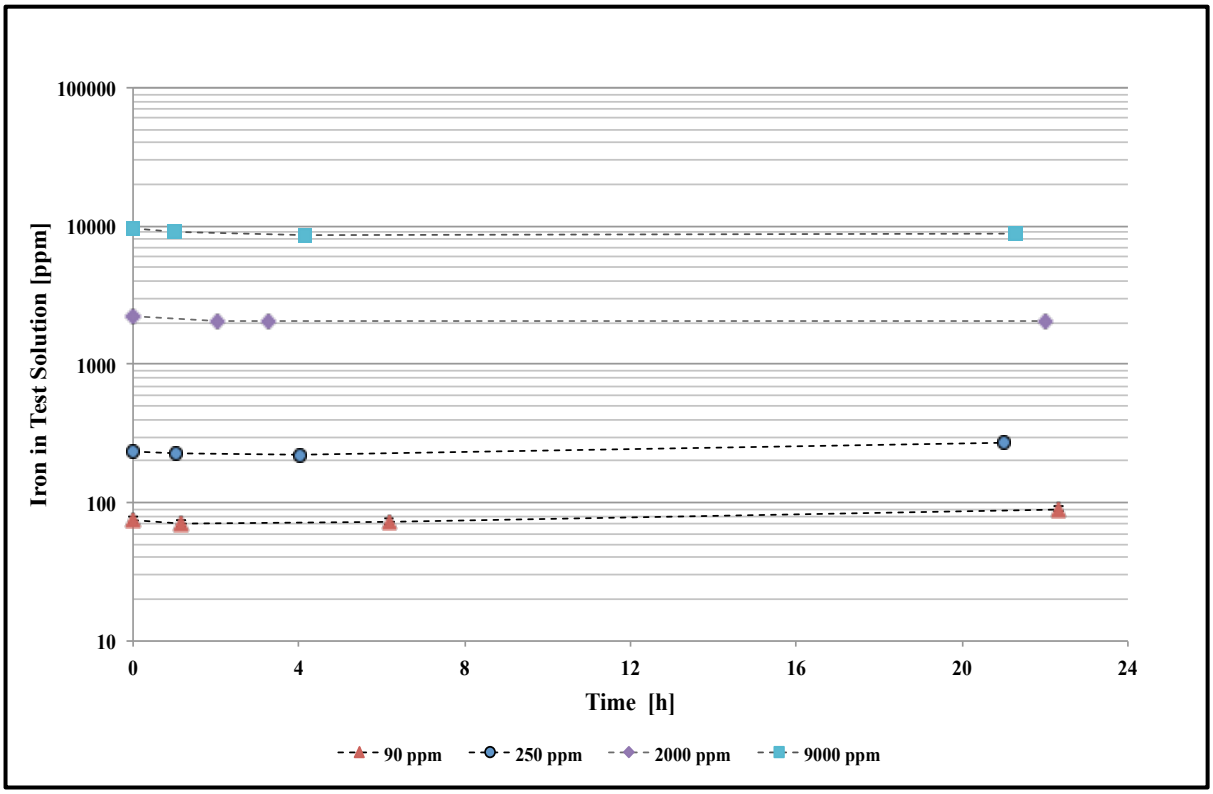

Figure 3.2 : Ferrous Concentrations over Duration of Selected Loading Tests *(Constant Ferrous Concentration, pH 4, 30^0C)*

Since all the experiments were performed under ISV conditions, it was necessary to confirm that the target solution concentration for ferrous was achieved throughout the test. Thus, samples were collected after approximately 1, 4, and 20 hours. Although obtaining constant solution composition for all the tests was quite hard to achieve some experiments results run at 90, 250, 2,000 and 5,000-ppm iron showed that nearly constant ferrous concentrations were obtained for the duration of the tests (Figure 3.2). The tests were completed after about 20 hours, which typically provided adequate time for the ion exchange reaction to reach equilibrium. After equilibration, resin and test solution were separated by filtration.

3.3.1.2 Nickel-Ferrous Displacement Loading under Finite Solution Volume Conditions

The second part of the experimental procedure was performing the Ni^{2+}/Fe^{2+} displacement experiments. To achieve that objective, it was necessary to have the resin loaded as much as possible with ferrous sulphate initially. As a result, the 5 mL resin samples for displacement tests initially were loaded with very high concentrations of ferrous (~10,000) under infinite solution volume conditions. Then the resin in the ferrous form was introduced to the test solution containing the desired nickel sulphate concentration and also a background concentration of ferrous close to 10,000 ppm. Accordingly, for example, if the resin was primarily loaded to approximately 10,000-ppm ferrous sulphate solution test, the displacement test solution would contain about 10,000-ppm ferrous sulphate as well as the 1,000-ppm nickel sulphate amount. Similar to the ferrous loading experiment, here one still needed to maintain a constant pH of 4 in the test vessel. However, since these displacement tests were performed under finite solution volume conditions (i.e. the concentration ferrous and nickel sulphate in solution were not kept constant) there was no need of nickel or ferrous sulphate stock addition to the test vessel. As illustrated in Figure 3.3, for the experiment starting with nearly 9,000 ppm iron as ferrous sulphate and 2,500 nickel as nickel sulphate, due to removal of nickel ions from solution with concurrent displacement of ferrous ions from the preloaded resin, the concentration of nickel ion in solution decreased while the ferrous ion concentration slightly increased. Furthermore, according to the results of resin stripping for ferrous, it was proven that the amount of ferrous ions that was stripped off the resin was negligible relative to the ferrous ions already in the background. Since the nickel loading behavior could only be determined based on solution assay, 2 mL samples were

taken at approximately 3, 15, 30, 60, and 90 minutes and 2, 3, 4, 6, and 20 hours for the duration of each experiment. Thus the nickel loading with time could be calculated by tracking the volume and concentration of solution with time.

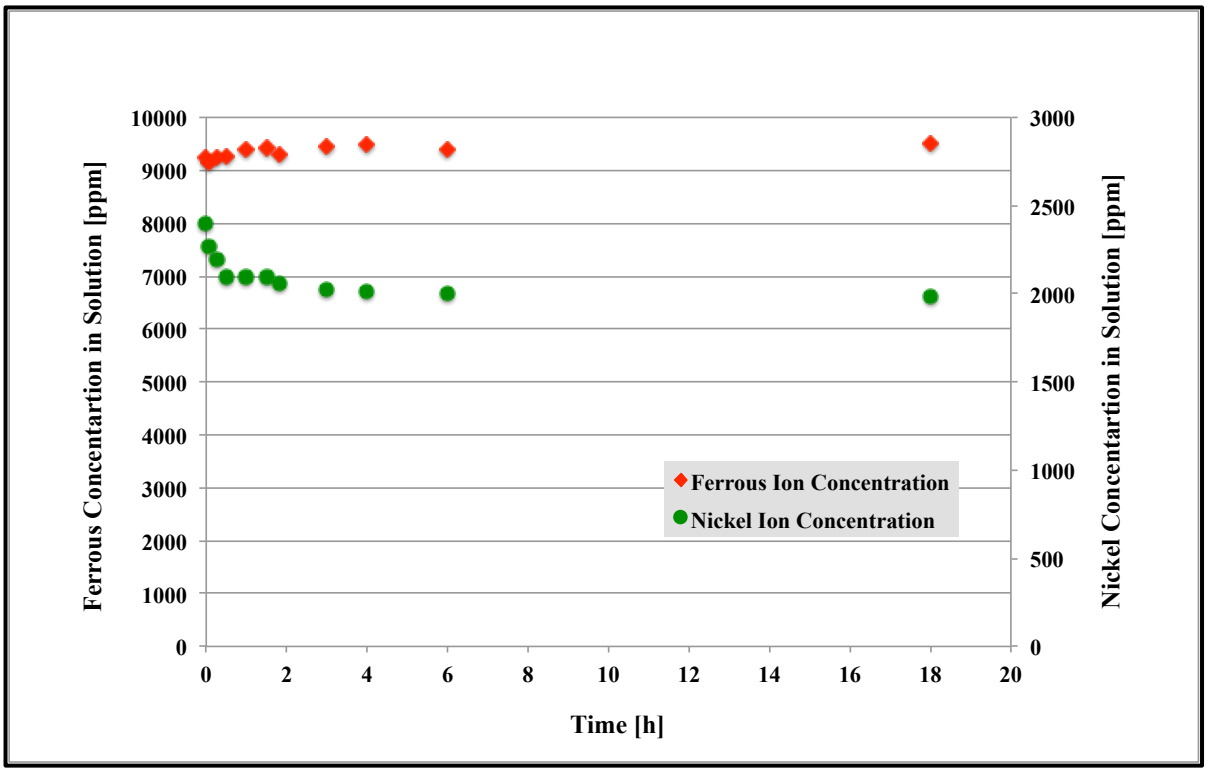

Figure 3.3: Nickel and Ferrous Ions Sample Concentrations During Displacement Experiment *(2,500 ppm Initial Nickel and 10,000 ppm Ferrous in Solution, pH 4, 30^0)*

3.3.2 Elution Procedure

Equilibration tests were completed after about 20 hours, which typically provided adequate time for the ion exchange reaction to reach equilibrium. After equilibration, resins and test solution were separated by filtration. The elution and resin stripping procedure is identical for both ferrous loading and the nickel-ferrous displacement experiments. The photograph of the elution equipment is illustrated in Figure 3.4.

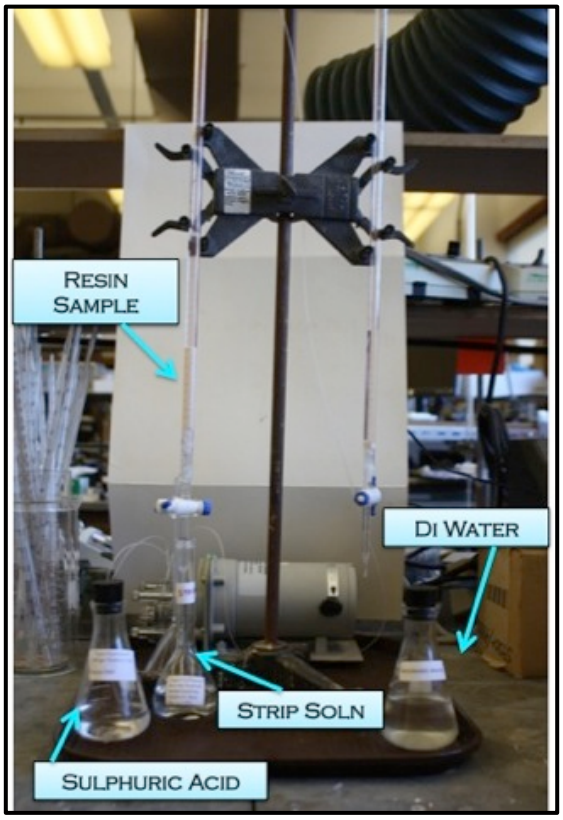

Figure 3.4 : Elution Experimental Apparatus

The loaded resin sample was transferred into the elution column and first washed with five bed volumes (BV) deionized water and stripped afterwards with 5BV of 100-g/L sulphuric

acid using 10BV/hr flowrate. Note that the bed volume is defined as volume of solution per volume of resin [24]. After the acid wash, resin was held for 20 hours in the elution column and again washed by 10 BV deionized water. At the end of the stripping cycle, both the strip and strip wash solutions were collected in a 100 mL volumetric flask. In order to analyze the concentration of ferrous ions in the samples taken during the ferrous or nickel loading test and the strip solution, the atomic absorption (AA) method was used.

4 Ferrous Batch Loading and Application of the Hybrid Correlation

McKevitt [24] previously investigated the application of the hybrid correlation for nickel, cobalt and copper loading onto TP207MP and TP207XL by fitting the model to several experimental datasets. According to McKevitt, the model adequately described all the datasets. In this work, the applicability of the hybrid correlation model was investigated to predict the loading rate of ferrous ions onto TP207XL for the whole range of ferrous concentrations in solution varying between 90 to 9,000 ppm. The initial part of this chapter focuses on generating an equilibrium loading isotherm model for ferrous loading. Afterward, the second part explains how the hybrid correlation was fitted to a series of ferrous loading experimental datasets.

4.1 Equilibrium Loading Isotherm for Ferrous Loading onto TP207XL

In order to apply the hybrid correlation model to ferrous loading experimental datasets, initially an equilibrium loading isotherm must be generated. This approach is similar to most engineering models developed based on following the fractional approach to equilibrium, As mentioned, the loading isotherm illustrates the equilibrium relationship between an ion concentration in the solution phase and one loaded onto resin. In the study of ferrous loading, the Mass Action Law was applied to explain the equilibrium loading behavior of ferrous ions under assumed infinite solution volume conditions.

For the system studied here the corresponding ion exchange reaction as well as the Mass Action Law can be expressed as follows:

$$2R - H + Fe^{2+} \rightarrow R - Fe + 2H^{+} \quad [4.1]$$

$$K = \frac{[H]^2[\overline{Fe}]}{[Fe][\overline{H}]^2} \quad [4.2]$$

Figure 4.2 shows the isotherm graphs for ferrous loading onto TP207XL based on the Mass Action Law. In this plot, the concentration of ferrous (g_{Fe}/L) in the solution is on the X- axis and the concentration of ferrous on the resin (g_{Fe}/L_{Resin}) is on the Y-axis. Since two ferrous concentrations on the resin (measuring the consumption of sodium hydroxide and striping of the resin samples) were applied to monitor and measure the loading rate of ferrous onto resin, two final ferrous loading values based on the load and strip values of each experiment were generated (Table 4.1).

Table 4.1: Load and Strip Data Applied in Mass Action Law

Test Concentration (g Fe/L)	**Stripped Ferrous** (g Fe/L_{resin})	**Loaded Ferrous Based on NaOH Consumption** (g Fe/L_{resin})
0.09	33.9	33.8
0.25	41.2	41.5
0.4	45.7	43.3
0.8	47	44.2
2.0	49	46.1
9	52	51.6

The "load isotherm" was generated based on the final loading values of ferrous described as load value and calculated based on sodium hydroxide (NaOH) consumption during each experiment.

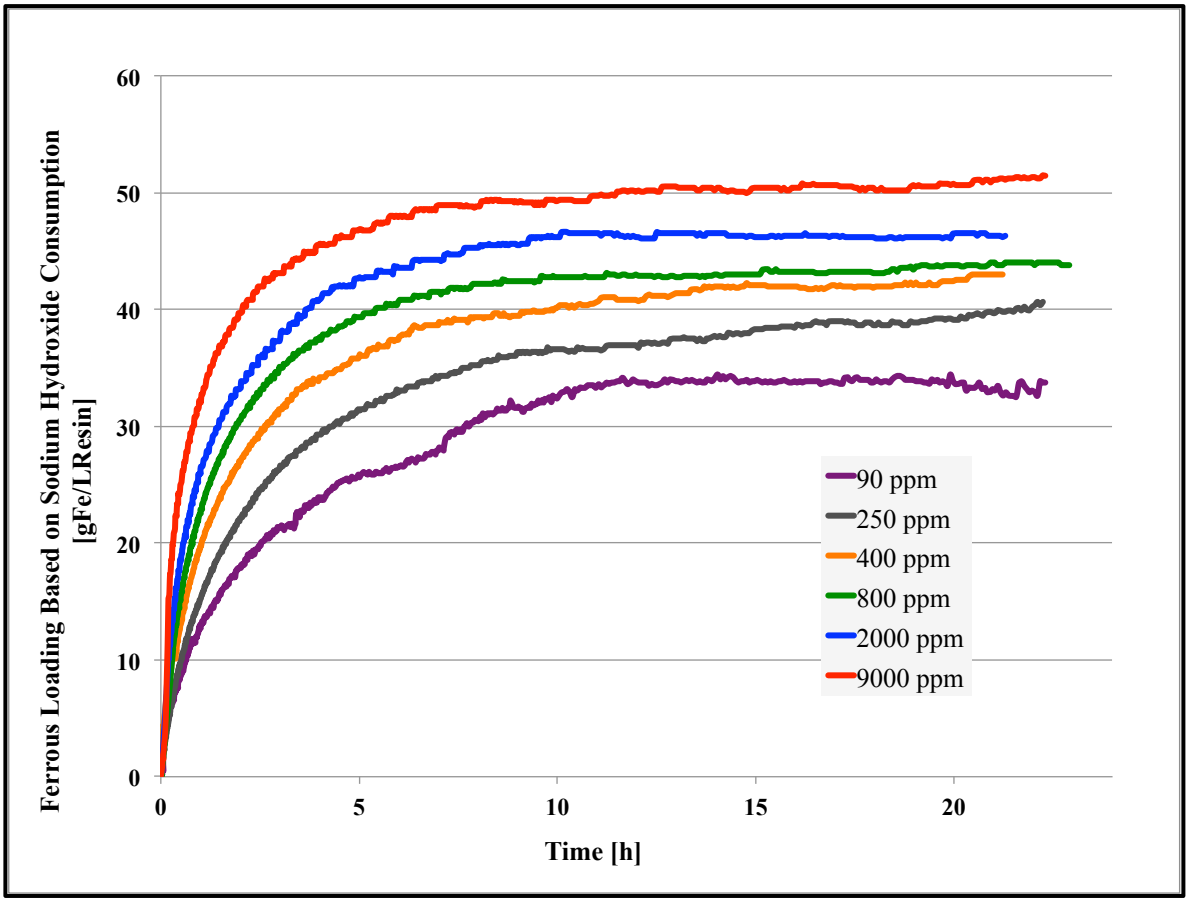

Figure 4.1: Ferrous Loading onto TP207 XL Based on Sodium Hydroxide Consumption *(pH 4, 30^{0}C, Constant Ferrous Concentration)*

NaOH was consumed as base in order to maintain a constant pH by neutralizing the hydrogen ions released from the resins into solution while the metals loaded onto the resin. As a result, one can measure the loading rate of ferrous ions by following the rate of base addition into solution. Figure 4.1 illustrates how the loading rate of ferrous based on sodium

hydroxide consumption varied for several ferrous concentrations in solution. As a result, the final loading value of each graph was used to generate the load isotherm. Furthermore, the plot named "strip isotherm" was developed using the concentration of ferrous ions measured from stripping the resin sample after each experiment and described as strip values in Figure 4.2.

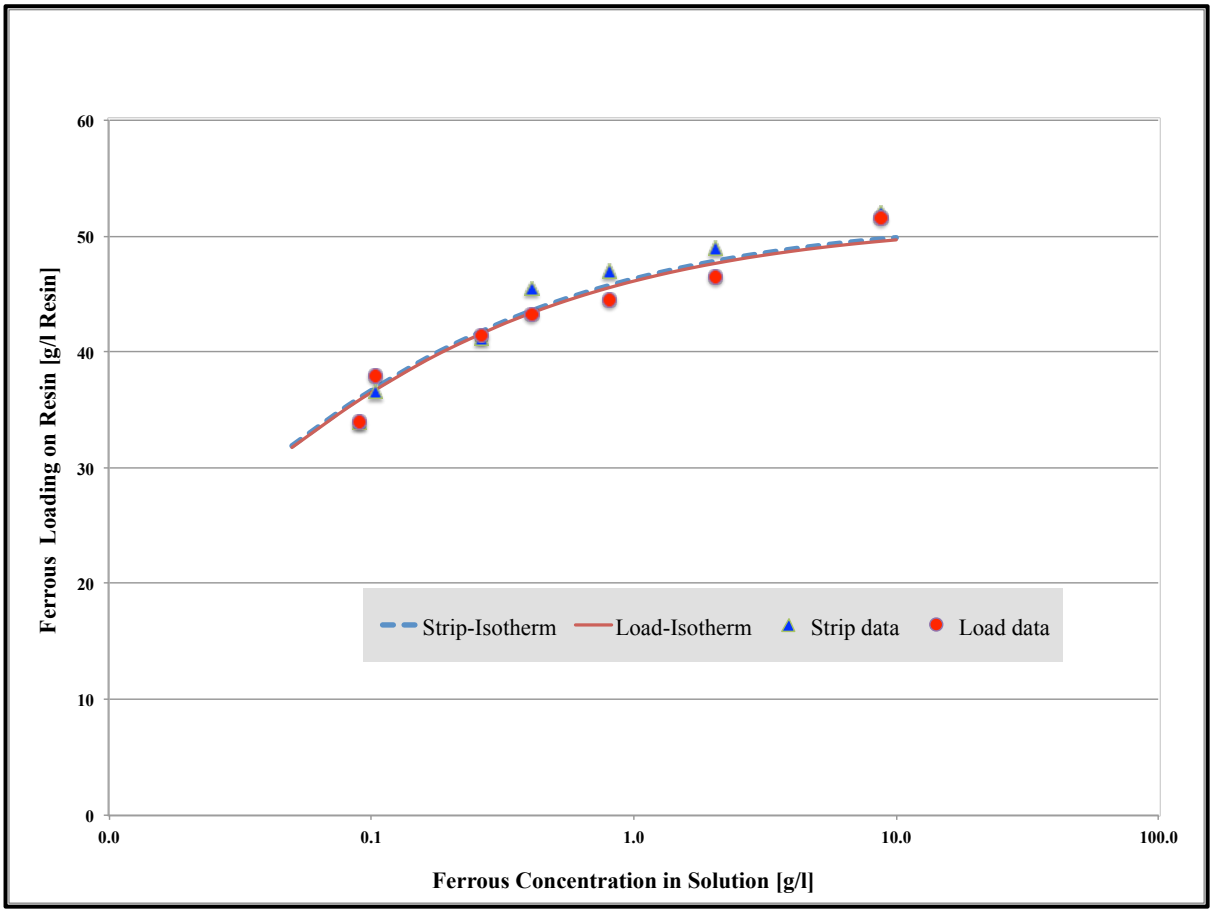

Figure 4.2: Equilibrium Isotherm for Ferrous Loading onto TP207XL *(pH 4, 30^{0}C, Constant Ferrous Concentration)*

The ferrous loading isotherm profile is categorized as one of the favorable isotherms that are always concave downwards. Additionally, the graph indicates that the final loading values increases from approximately 30 to 50 g Fe/L_{Resin} when the solution concentration varies between 90 to 9,000 ppm ferrous under infinite solution volume conditions. In addition, according to the loading isotherm, the graph has more curvature to it compared to the similar isotherm plots generated for nickel, cobalt and copper loading onto TPT07XL [49]. The isotherm graphs generated for loading of those metal ions particularly copper were mostly flat shape isotherms as illustrated in Figure 4.3.

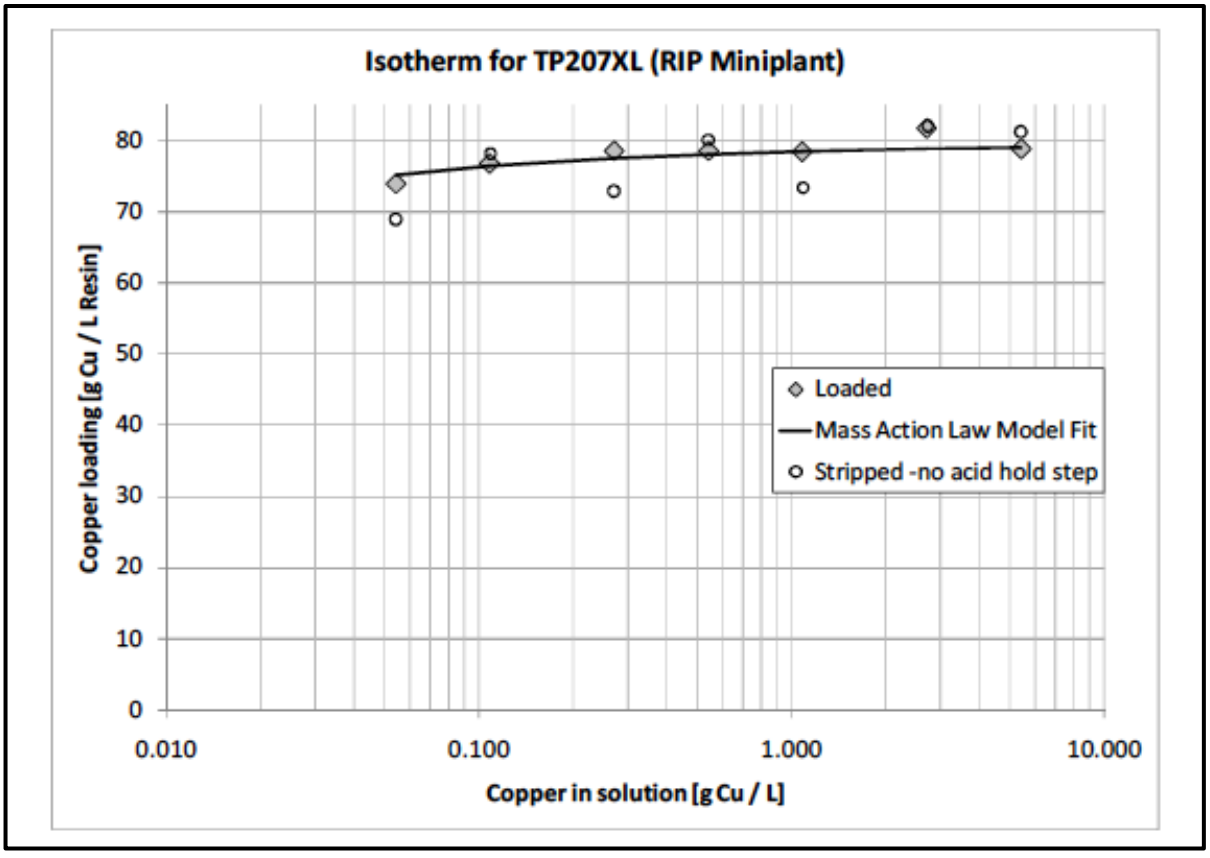

Figure 4.3: Equilibrium Copper Loading onto TP207XL [24]

On the other hand, observing a more concave type of isotherm graph for ferrous loading was expected since the iminodiacetic ion exchange resin has less affinity for ferrous loading in contrast to the nickel, cobalt and mainly copper loading. Note that the ferrous isotherm graph becomes more flat as the concentration of ferrous in solution test increases.

Repeatability of the ferrous loading experiments was also examined by running three tests at a specific concentration of ferrous in solution. Figure 4.4 displays three experiments performed at 400-ppm ferrous concentration in the test solution. Results indicate adequate repeatability with an experimental error of approximately +/- 3 g Fe / L Resin.

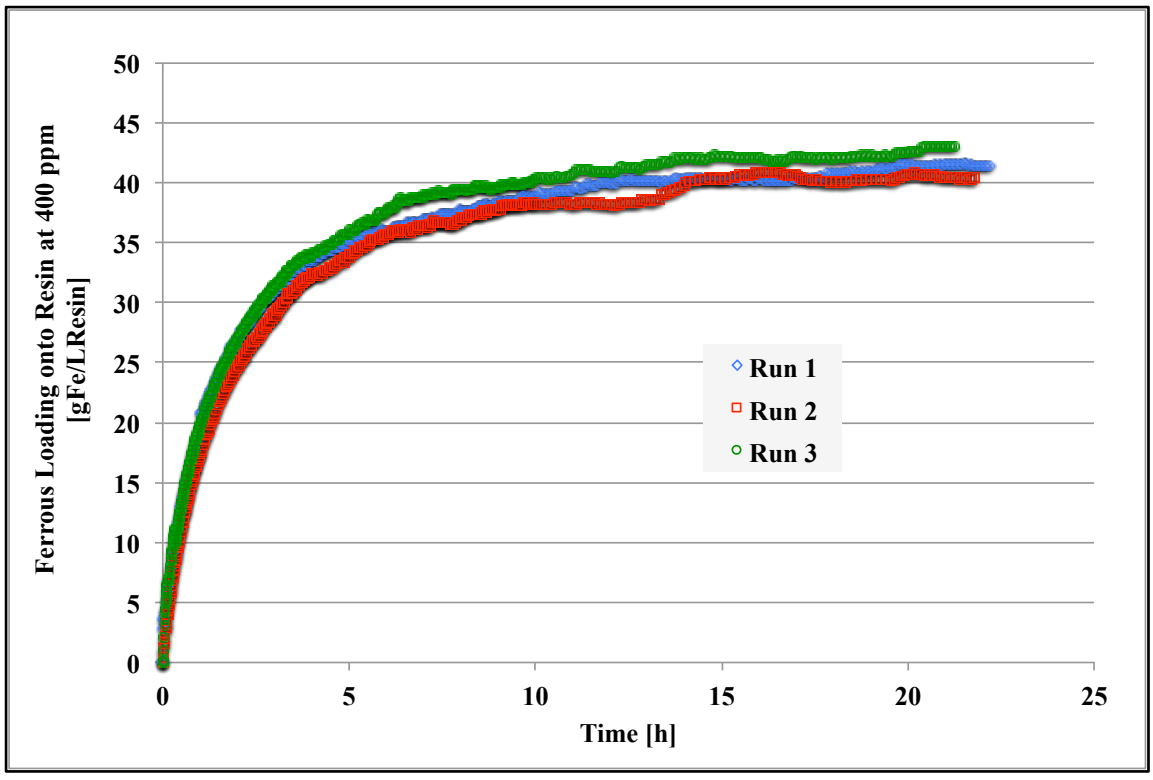

Figure 4.4: Repeatability at 400 ppm Ferrous *(TP207XL, Constant Ferrous Concentration, pH 4, 30^0C)*

4.1.1 Isotherm Fit Parameters

The isotherm was modeled using the data in Table 4.1 using the Mass Action Law [4.2] so that the resin capacity (C) and the selectivity coefficient (K) were taken as fitting parameters. Figure 4.2 shows that the strip and load data are reasonably fitted to the isotherm curves and the values of K = 1.3 $\times 10^{-5}$ and equilibrium capacity = 1.84 (eq/L) were obtained accordingly.

The equilibrium capacity calculated in this study is clearly lower than the theoretical capacity of the resin published by resins manufacturers. Note that the resin capacity calculated based on Equation 4.3 is the total number of moles of hydrogen and ferrous ions loaded onto resin.

$$\text{Capacity} = \frac{\text{molH}}{\text{L}_{\text{Resin}}} + 2\frac{\text{molFe}}{\text{L}_{\text{Resin}}} \qquad [4.3]$$

Isotherm model parameters from previous studies for a series of experiments for the loading of nickel, cobalt, and copper onto an iminodiacetic chelating resin (TP207MP and TP207XL) in the hydrogen form are summarized in Table 4.2 [24]. Comparing those previous results for both types of TP207 with the results obtained in this study on the ferrous loading expresses the fact that, resin selectivity follows this order: Cu >> Ni > Co > Fe. These results indicates that the copper loading rate onto TP207XL (Lot CHE 50019) and TP207MP (Lot CHT 5007) was much higher than nickel, cobalt and ferrous.

The selectivity order of the Lewatit MonoPlus TP207XL (700-800 micron diameter range) for resin-in-pulp applications was also verified by Littlejohn and Vaughan as follows [89] :

$Cr^{3+} > In^{3+} > Fe^{3+} > Al^{3+} > Hg^{2+} > UO^{2+} > Cu^{2+} > Pb^{2+} > Ni^{2+} > Cd^{2+} > Zn^{2+} > Co^{2+} > Fe^{2+} > Mn^{2+} > Ca^{2+} > Mg^{2+}$

Their study also confirmed the exact order of selectivity achieved previously by McKevitt and Dreisinger [49] in terms of copper, nickel loading onto TP207XL. Most importantly, the fact that the selectivity of TP207XL for ferrous listed after copper and nickel in the Littlejohn and Vaughan study is also in agreement with the outcome of ferrous loading behavior onto TP207XL in this study.

Table 4.2: Isotherm Fit Parameters [24]

Resin	TP207MP*	TP207XL*	TP207MP*	TP207XL*	TP207MP*	TP207XL
Metal	Copper		Nickel		Cobalt	Ferrous
Selectivity Coefficient (K)	7.5×10-4		9.8×10-5		5.0×10-5	1.1×10-5
Capacity (eq/L)	2.11	2.5	1.97	2.36	1.91	1.81

***** Data are obtained from reference [24].

McKevitt and Dreisinger [49] stated that the selectivity of the resin depends on how the selectivity experiment is conducted, the pH, and the ion concentration. In terms of pH effect, the selectivity constant can be related to the complex formation of the ion with the resin structure affected by the decomplexing pH for metal ions. Decomplexing pH is the pH at which metal ion starts to strip from the resin functional group. One of the resin manufacturers (Bayer) has released estimated values for decomplexing pH for copper,

nickel, cobalt and ferrous for Lewatit TP207 [90]. This information is illustrated graphically in Figure 4.5.

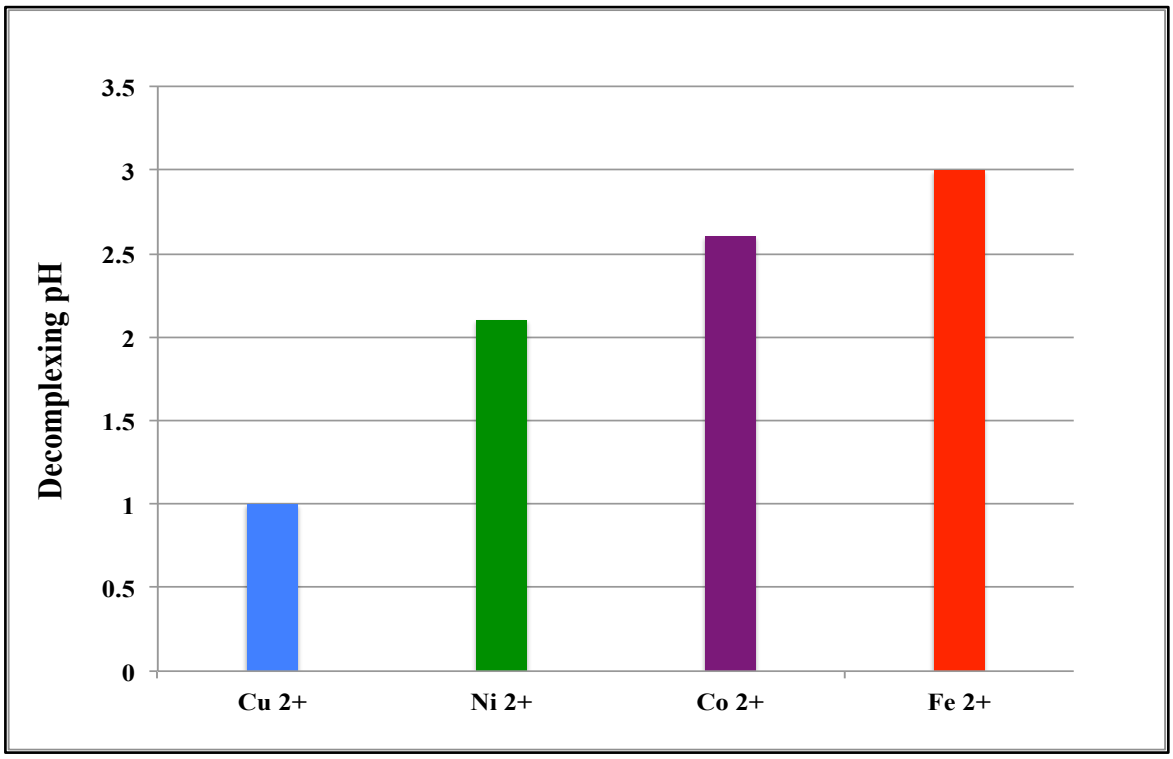

Figure 4.5: Iminodiacetic Resin Decomplexing pH for Divalent Ions [24, 90]

The effect of decomplexing pH can be explained in a way that when the metal ion is loaded on the resin, hydrogen ion is released resulting in decreasing of pH in the area around the resin bead. This drop in localized pH can stop further metal ion loading and also causes stripping of some other loaded ions. For example, decomplexing pH value of ferrous ions is pH=3, and that explains that the ferrous ions start losing their attachment to the resin functional groups and are eluted once the localized pH reaches 3. The pH of the bulk solution was maintained at 4 in these experiments. When ferrous was loaded, hydrogen ions were released to solution, decreasing the local pH in the resin. It is believed that as the

decomplexing pH for ferrous is ~ 3, this local decreases in pH inhibits further ferrous loading. In contrast considering the copper loading behavior studied by McKevitt, the decomplexing pH for copper is ~ 1 and hence the local change in pH is unlikely to reach such a low level. Consequently, this effect of pH drop may explain why the loading rate of ferrous ions on the resin is slower compared to the loading rate of copper, nickel, and cobalt ions [83].

In terms of resin equilibrium capacity, the capacity is also decreasing in the same manner as selectivity coefficient (Cu > Ni > Co > Fe). However, the variation between capacity results is very significant particularly between ferrous (1.84 (eq/L)) and copper (2.56 (eq/L)). Note that selectivity and equilibrium capacity of the resin can be affected by the amount of sodium co-loaded onto resin during the contact time since the pH of the solution was controlled by the addition of sodium hydroxide. This sodium co-loading effect was expected to be even higher in the ferrous loading experiments compared to nickel and copper due to lower affinity of a resin for ferrous ions. However, in order to calculate the equilibrium capacity the available exchangeable sites occupied by sodium were ignored.

4.2 Fitting the Hybrid Correlation to Ferrous Loading Data Sets

Kinetics study of ferrous loading involved engineering modeling of the loading rate process applying the hybrid correlation model [24]. The model and its related equations have been already described in Section 2.5 of the thesis.

To fit the hybrid correlation model for several ferrous loading experimental results, the equilibrium isotherm was initially generated by applying the Mass Action Law. Subsequently, the predicted equilibrium load values, $[\overline{M}]_{eqb}$, along with related selectivity coefficient and resin capacity (K = 1.3 $\times 10^{-5}$ and equilibrium capacity = 1.84 (eq/L)) were used with the hybrid correlation.

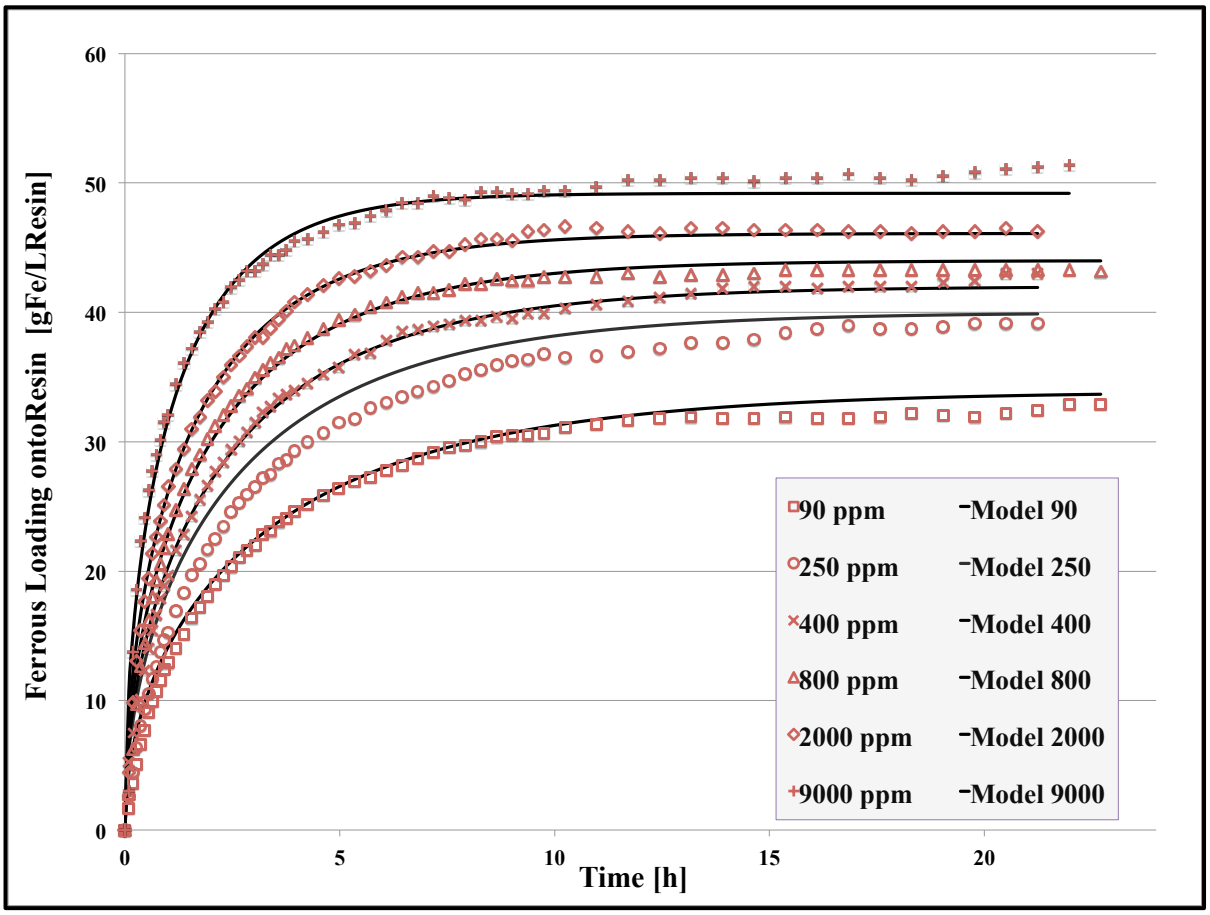

Figure 4.6: Hybrid Correlation Fit to Ferrous Loading onto TP207 XL *(pH 4, 30^{0}C, Constant Ferrous Concentration)*

Figure 4.6 shows a series of ferrous loading tests that were carried out on the +710 – 850 micron-sized fraction of the TP207XL resin. In the figure, the final load values were

obtained from the loading isotherm presented in Figure 4.2. The hybrid correlation then was fitted properly to the set of curves in by adjusting alpha (α) and apparent diffusivity (D_{app}) as fitting parameters.

According to Figure 4.6, or the higher ferrous concentration in solution (800, 2,000, and 9,000 ppm), approximately 90% final loading value is approached after about the first 5 hours of each experiment. The actual loading values after 5 hours of each experiment for some datasets are described in Table 4.3. Furthermore, as the concentration of ferrous in solution increases, the equilibrium loading will be achieved faster. For example, for 9,000 ppm ferrous in solution, equilibrium loading is approached about after 5 hours whereas in the case of 90 ppm ferrous in solution the equilibrium loading will be approached towards the end of the test. As a result, in an actual resin-in-pulp process for nickel recovery depending on the concentration of ferrous in the system and the residence time of the resin in the slurry, the amount of ferrous being loaded onto the resin will vary.

Table 4.3: Ferrous Loading Values Based on Base Consumption After 5 Hours of Test and at Equilibrium Point

Test concentration (gFe/L)	**Load after 5 hours** (g/L)	**Final Loading Value** (g/L)
0.09	28.4	33.8
0.25	34.5	41.4
0.4	37.8	43.3
0.8	40.5	45
2	42.7	46.1
9	47	51.6

Figure 4.6 suggests that the hybrid correlation is able to adequately describe the set of curves for various datasets. The best-fit parameters for ferrous loading onto TP207XL were $\alpha = 0.22$, and $D_{app} = 2.7 \times 10^{-12}$ m^2/s. Table 4.5 describes the empirical fit parameters for the previous study for copper, nickel and cobalt [24]. According to **Table 4.4**, diffusivity coefficient (D_{app}) follows the same trend as equilibrium loading capacity. Regarding the previous studies and experimental results for these metals, the rate of loading can be stated as follows:

TP207XL Cu > TP207XL Ni > TP207MP Co > TP207XL Fe

This confirms the magnitudes of the D_{app} values. The second empirical fit parameter alpha indicates whether a sharp boundary exists between the loaded and unloaded section of the ion exchanger. If the alpha value is high, which can be seen for copper ($\alpha = 0.62$), one can predict existence of the sharper and more obvious boundary within the resin bead. The resin beads loaded with copper, cobalt and nickel were examined for existence of the sharp boundary within the resin in previous studies [83]. The same experimental methodology was applied for ferrous loading onto the resin as well. The details regarding these experiments will be discussed in the next chapter of the thesis. As a result, no distinct boundary was determined within the loaded and unloaded portion within the resin for nickel, cobalt, and ferrous whereas for copper loading the boundary was quite sharp and clear. This outcome clearly confirms the fact that for ferrous, nickel and cobalt as the value of alpha becoming smaller, no boundary would be expected.

Table 4.4: Summary of Hybrid Fit Parameters [24]

Resin	Metal	D_{app} [m^2/s]	Alpha
TP207XL (Lot CHE 50019)	Ferrous	2.7×10^{-12}	0.22
TP207MP (Lot CHT 5007)*	Cobalt	4.2×10^{-12}	0.25
TP207MP (Lot CHT 5007)*	Nickel	3.9×10^{-12}	0.28
TP207XL (Lot CHC 5034)*	Nickel	4.5×10^{-12}	0.32
TP207XL (Lot CHE 50019)*	Nickel	4.4×10^{-12}	0.36
TP207MP (Lot CHT 5007)*	Copper	37×10^{-12}	0.62
TP207XL (Lot CHE 50019)*	Copper	28×10^{-12}	0.62

* The data are extracted from reference [24].

Figure 4.7 illustrates the relationship between alpha values and decomplexing pH for copper, nickel, cobalt and ferrous for both TP207XL and TP207MP. One can explain this relationship in a way that, in the case of ferrous ($\alpha \rightarrow 0$), when one ion loads onto the resin bead, the localized pH in that area drops and it could be below the decomplexing pH. As a result, even if the next exchange site is available, the ferrous ion may have to diffuse further into the bead to get to the zone where the localized pH favors ferrous loading. However, in the case of copper ion loading onto resin with $\alpha \rightarrow 1$, the localized pH drop may not be below the decomplexing pH. As a result, the next copper ion is able to load on the next available resin site. Therefore, for copper loading onto resin, the sharp boundary between loaded and unloaded region on the resin bead can be expected.

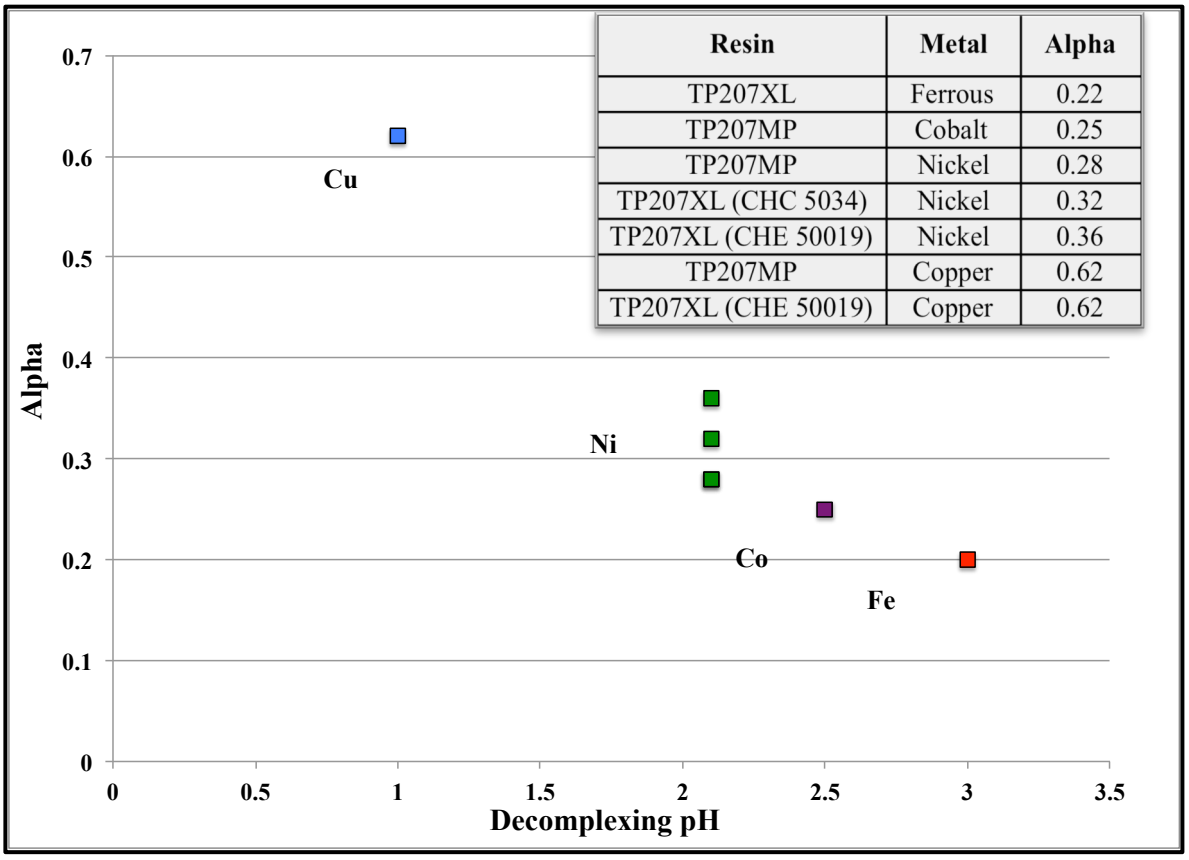

Figure 4.7: Decomplexing pH Versus Alpha Values

The fact that the obtained alpha values appeared to trend fairly well with the decomplexing pH suggests that the empirical fit parameter of hybrid correlation model, alpha, can be related to some known chemical property as opposed to be just an unspecified empirical fit. Further investigation with other impurities to see if this trend holds would be a future recommendation.

4.3 Summary of Ferrous Loading Experimental Results

Since ferrous along with other impurities can be a major concern in the RIP process for nickel recovery, the loading behavior of ferrous onto the iminodiacetic ion exchange resin can be an interesting topic to study. Therefore, to examine the loading rate of ferrous, several experiments were performed to achieve a near-continuous set of loading rate data assuming infinite solution volume conditions. To perform the kinetic study, a hybrid correlation model previously developed was applied. The experimental data for the full range of feed concentrations were fitted quite well with the hybrid correlation. According to the two empirical fit parameters used in the correlation, the observed final loading value of ferrous was smaller than systems previously studied such as copper, nickel and cobalt. This was confirmed by the fact that fitted diffusivity coefficient was smaller for ferrous as well. In terms of alpha value for ferrous loading (0.22), since alpha value was low no distinct boundary for the loaded and unloaded area within the resin bead was observed. In addition, it was concluded that resin loads in more of an intraparticle diffusion manner. The strong loading of ferrous ion at pH 4 indicates that when resin-in-pulp recovery of nickel from a nickel-ferrous solution occurs, it is likely that toward the last stages of adsorption (where nickel in solution is negligible) that ferrous will load on the resin to significant concentrations. The next topic for investigation will be the displacement of ferrous from the resin by nickel, to simulate the chemistry of nickel loading onto a preloaded ferrous containing resin.

5 Application of the Hybrid Correlation for Nickel Loading onto TP207XL Resin in the Presence of Ferrous Ions in the Batch System

The first experimental work reported in this thesis focused on the ion exchange system in which the ferrous ions are loaded onto the resin in hydrogen form under infinite solution volume condition. Hence, the loading behavior of ferrous onto TP207XL was closely examined by applying the hybrid correlation model to several experimental datasets. However, the principal objective of this work was to study the loading rate of nickel ion in the presence of ferrous ion (nickel-ferrous displacement experiments) under finite solution volume conditions (i.e. the concentration of nickel and ferrous ions were not maintained constant over the course of the test). To perform a nickel loading experiment onto a ferrous loaded resin, the same experimental method as applied for the ferrous loading study was used. As a result, the nickel loading equilibrium isotherms initially were developed followed by determination of the hybrid correlation fit parameters for the nickel-ferrous experimental results through the application of the finite difference model.

5.1 Equilibrium Isotherms Development for the Displacement Loading Experiments

In order to develop an equilibrium isotherm, a series of loading tests onto TP207XL resin were carried out at approximately 100, 250, 500, 1,000, 2,500, and 5,000 ppm nickel along with 10,000 ppm ferrous ions in solution under finite solution volume conditions. The 5 mL

resin samples used in each experiment were previously preloaded with approximately 10,000 ppm ferrous under infinite solution volume condition. It was expected that nickel ions mostly loaded onto resin by displacing the ferrous ions previously loaded onto the resin. It is also possible that nickel will displace residual acid protons from the preloaded resin.

To generate the isotherm for the nickel-ferrous displacement experiments, the final nickel loading values were obtained using three separate approaches. One approach was based on the observation of the nickel solution composition for the duration of each experiment. Each displacement experiment started with an initial concentration of nickel in solution, and decreases seen in the concentration can be associated with the movement of nickel ions from the test solution onto the resin. As a result, one can determine the final loaded nickel concentration for each experiment. In addition, another way to calculate how much nickel loaded onto the resin was by determining the amounts of ferrous and hydrogen ions displaced by nickel ions through each experiment. This was accomplished by assaying the ferrous solution concentration and monitoring the sodium hydroxide consumption throughout the experiment (added to maintain a constant pH). The final approach was applied to validate the other two approaches, as it was the most reliable method. Thus, resin samples obtained at the end of the test were stripped using 100 g/L sulphuric acid solution. The strip solutions were analyzed to close the mass balance for nickel and ferrous to determine the final nickel and ferrous recovery and loading values.

For the nickel-ferrous loading ion exchange reaction, the quaternary system of Ni-Fe-H-Na was utilized. Although, ideally it was expected that all the available resin exchangeable sites were fully occupied by ferrous ions before being introduced to the nickel solution, the

sodium hydroxide consumption was still observed for the course of each displacement experiment. This result showed that some hydrogen ions were available on the resin to be displaced by nickel ions. In addition, sodium co-loading was expected as it was in the ferrous loading experiments. Subsequently, the Mass Action Law was not applied to describe the isotherm of such a quaternary system due to not having enough data regarding all the elements present in such a system and not being able to solve the complex mathematical terms. In addition, for the experiments performed using real pulps, the Mass Action Law is never applied for such a complex system since as more and more impurities get involved in the system, the resin loading becomes more and more complicated and cannot be modeled by application of the Mass Action Law [11, 83]. As a result, several assumptions have been considered in this study to simplify the desired ion exchange system. In the system, the solution pH and ferrous ions were maintained to be constant for the course of each experiment in addition to ignoring the effect of sodium co-loading in order to generate an empirical equilibrium isotherm.

The two conventional isotherm models, Freundlich and Langmuir, were initially generated for the nickel-ferrous displacement experiments based on the final loading achieved via assaying the strip solution for the nickel concentration on the resin samples. The Freundlich equation [5.1] was applied to the experimental results of several nickel-ferrous loading experiments (approximately 100 ppm to 5000 ppm nickel in solution) for TP20TXL in the presence of 10,000 ppm ferrous in the test solution. As illustrated in Figure 5.1, the Freundlich model does not adequately fit to the whole range of datasets. As mentioned in section 2.1.3.1, the Freundlich isotherm prediction at both extremes of the isotherm has been

questioned and as illustrated in this figure, at very low and very high equilibrium concentration of nickel in solution, the model overpredicted the loading values.

$$[\overline{M}]_{eqb} = a_2[M]^b_{eqb} \quad [5.1]$$

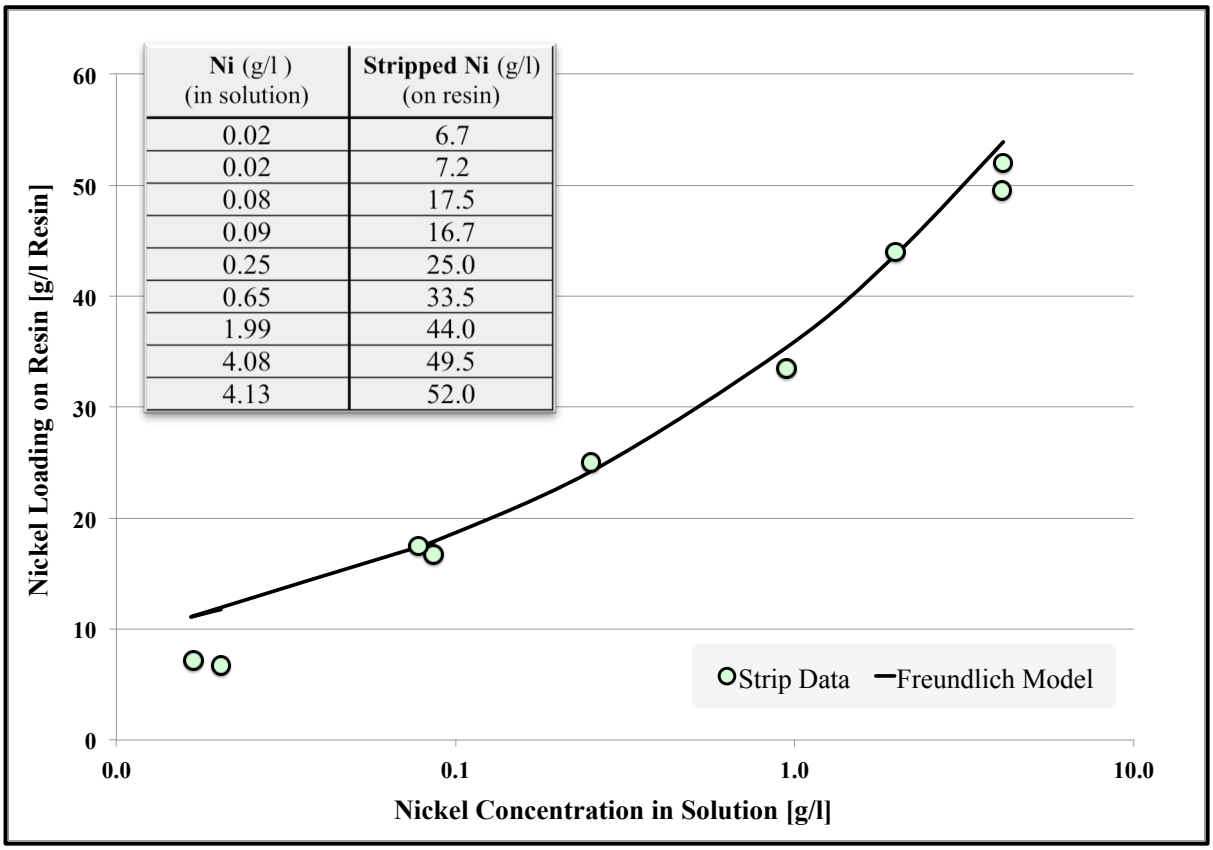

Figure 5.1: Freundlich Isotherm for Nickel Loading onto TP207XL under Finite Solution Volume Conditions *(pH 4, 30^{0}C, 10,000 ppm Ferrous Background in Solution)*

The Langmuir isotherm equation [5.2] was also applied to fit the experimental results of nickel loading under finite solution concentration and 10,000 ppm ferrous sulphate in solution. As illustrated in Figure 5.2, the Langmuir model could not provide an adequate fit to the experimental results.

$$[\overline{M}]_{eqb} = \frac{L[\overline{M}]_{max}[M]_{eqb}}{1 + L[M]_{eqb}} \qquad [5.2]$$

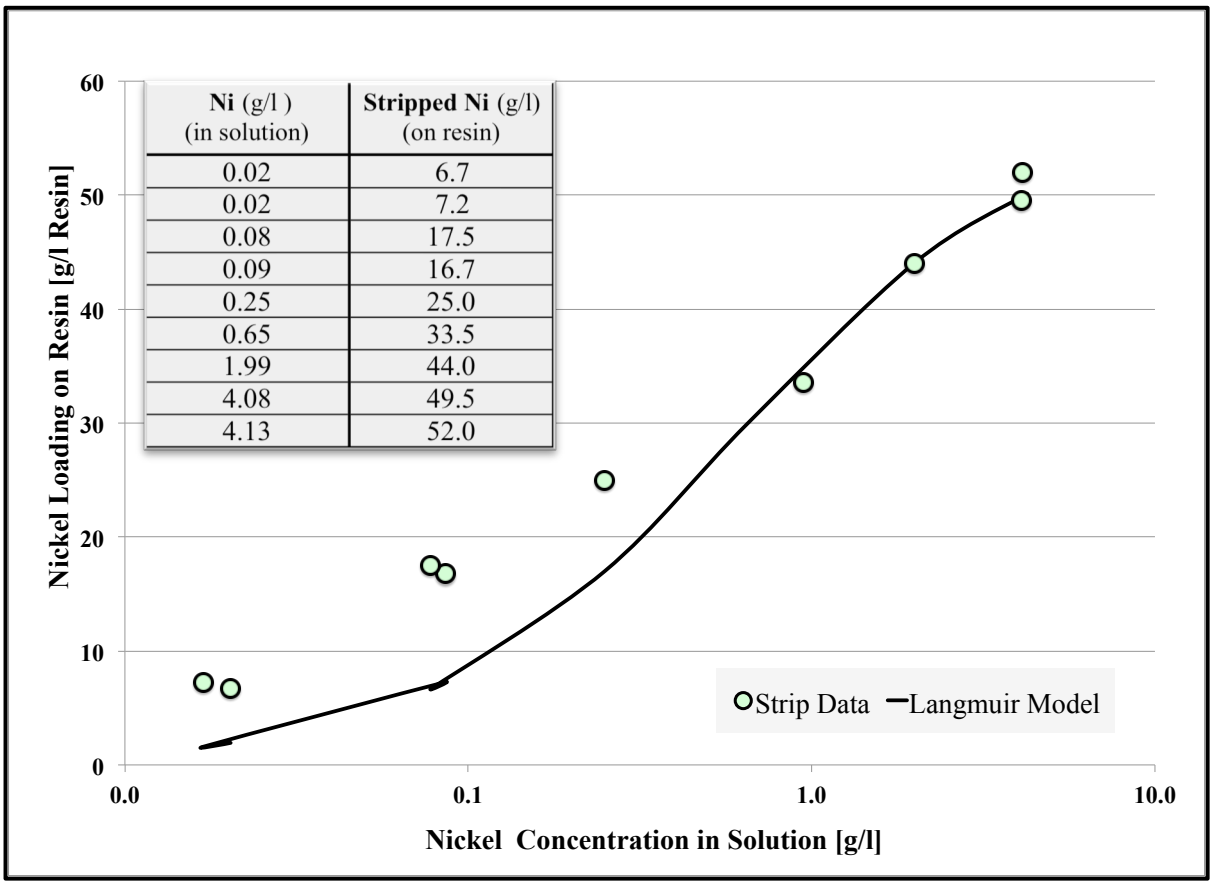

Figure 5.2: Langmuir Isotherm for Nickel Loading onto TP207XL under Finite Solution Volume Conditions (pH 4, 30^0C, 10,000 ppm Ferrous in Solution)

Consequently, the two conventional isotherms, Freundlich and Langmuir, did not provide a proper fit to the whole range of displacement experimental datasets results. However, for such a system, as demonstrated in Figure 5.3, a straight line provides an excellent empirical fit of the nickel isotherm that would allow for good modeling of the kinetic data within this range. Frequently, there is absolutely no theoretical basis for using a Freundlich or Langmuir isotherm to model a quaternary system –they are simply convenient and, therefore, are

frequently used in several engineering applications. For the system studied here, their prediction would not be completely trustworthy for anything extrapolated beyond the range tested, but within this range it is apparent that the linear empirical fit provides the best fitted isotherm for the system.

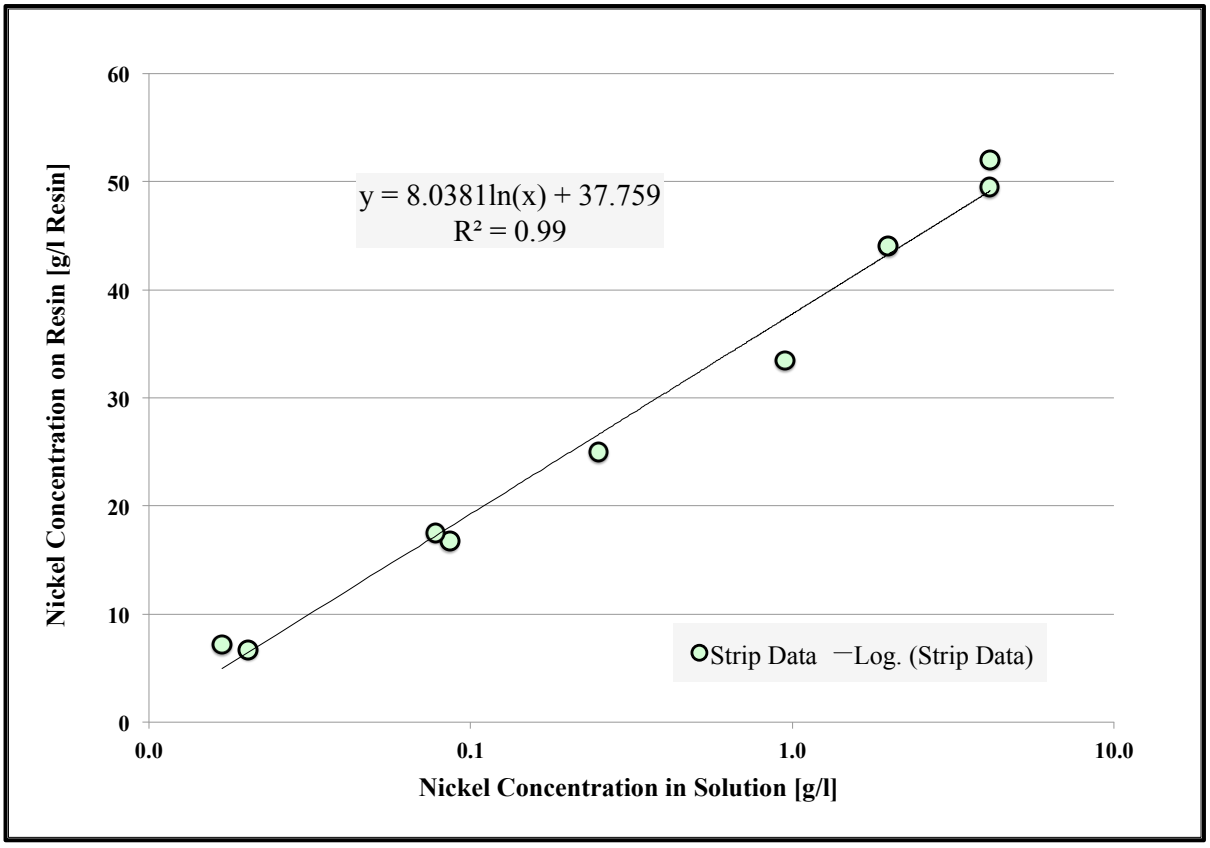

Figure 5.3: Empirical Fit Isotherm for Nickel Loading onto TP207XL under Finite Solution Volume Conditions *(pH 4, 30^{0}C, 10,000 ppm Ferrous Background in Solution)*

The empirical isotherm presented a suitable fit to the final loading datasets based on stripped solution assay analysis; therefore, the same isotherms were developed using the final loading based on observed solution assay (load isotherm) and the hydrogen plus ferrous ions displacements (displacement isotherm). Figure 5.4 indicates that the linear isotherm provided

a good fit to all three sets of loading data. However, as expected, among those isotherms, the strip isotherm generated the best fit to the data. As a result, the corresponding equation [5.3] for the strip isotherm was applied for modeling the kinetic data within the range of experimental datasets.

$$[\overline{M}]_{eqb} = 8.04\,Ln[M]_{eqb} + 37.76 \qquad [5.3]$$

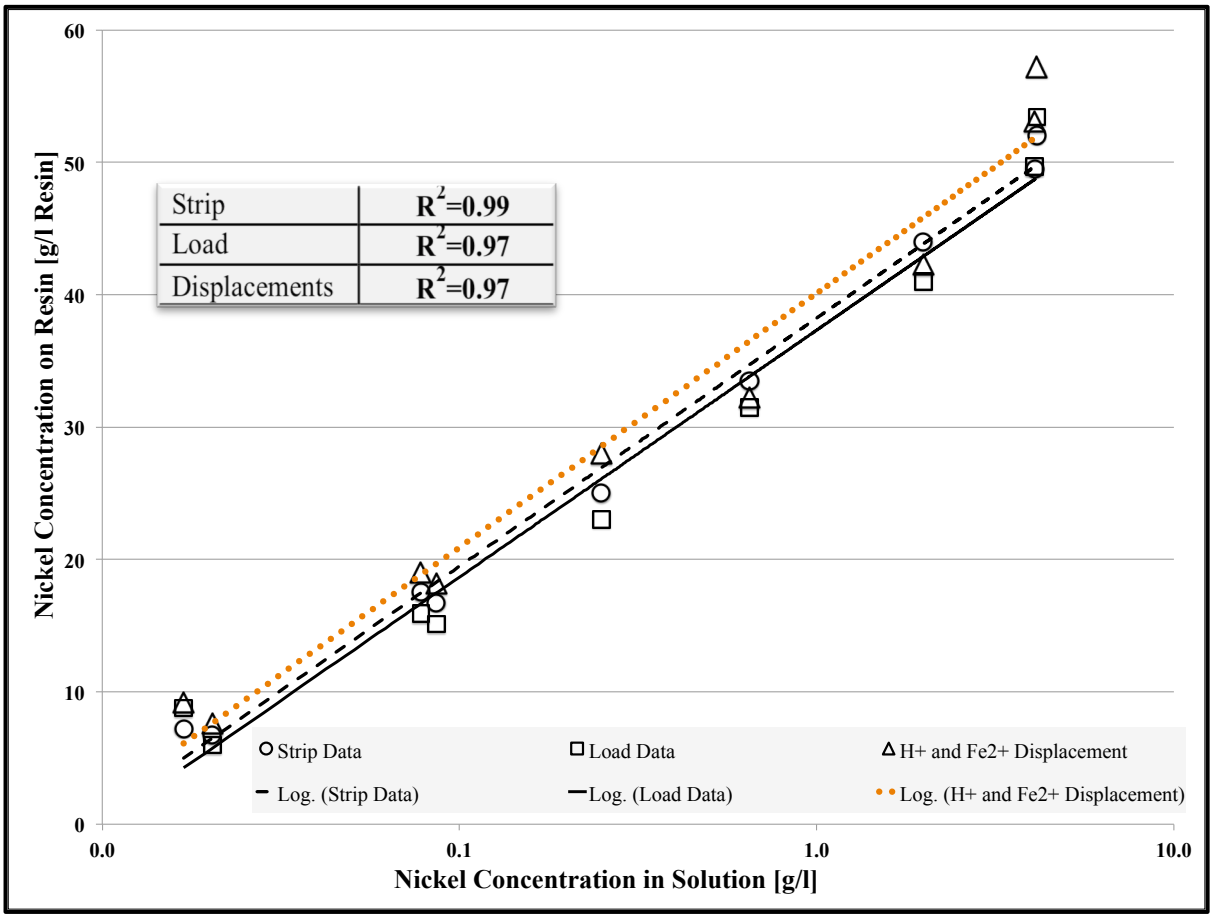

Figure 5.4: Empirical Fit Isotherms for Nickel Loading onto TP207XL under Finite Solution Volume Conditions *(pH 4, 30^{0}C, 10,000 ppm Ferrous in Solution)*

5.2 Separation Factor for Displacement Experiments

The nickel-ferrous displacement loading isotherm was quantified by the calculation of the separation factor, as experimental conditions were varied. As mentioned, the separation factor shows the preference of the ion exchange system for one species over another one regardless of how many different species might exist in the system. The separation factor regarding the ion exchange reaction of nickel displacing ferrous ion [5.4] was estimated by Equation 5.5 using the data summarized in Table 5.1.

$$R_2\text{-}Fe + Ni^{2+} \rightarrow R_2\text{-}Ni + Fe^{2+} \qquad [5.4]$$

$$S_{Fe}^{Ni} = \frac{[\overline{Ni}][Fe]}{[\overline{Fe}][Ni]} \qquad [5.5]$$

Table 5.1: Experimental Data Used to Calculate the Separation Factor for Series of Nickel-Ferrous Displacement Tests onto TP207XL

Ni (in soln) [g/L]	**Fe (in soln)** [g/L]	**Ni (on resin)** [g/L]	**Fe (on resin)** [g/L]	**Ni (in soln)** [mol/L]	**Fe (in soln)** [mol/L]	**Ni (on resin)** [mol/L]	**Fe (on resin)** [mol/L]
0.02	9.50	3.20	49.40	0.0003	0.17	0.05	0.885
0.08	9.64	12.00	41.40	0.0013	0.17	0.20	0.741
0.25	9.53	17.80	34.60	0.0043	0.17	0.30	0.620
0.65	9.75	24.70	24.00	0.0111	0.17	0.42	0.430
1.99	9.55	34.80	23.40	0.0338	0.17	0.59	0.419
4.08	9.48	37.20	13.60	0.0695	0.17	0.63	0.244

Table 5.2: Separation Factor for Series of Nickel-Ferrous Displacement Tests

Initial Ni (in soln) [g/L]	**Sodium Hydroxide Consumption** [mol/L_{resin}]	**Separation Factor**
0.1	0.12	30.31
0.25	0.14	35.87
0.5	0.25	19.61
1	0.29	15.44
2.5	0.31	7.15
5	0.42	6.36

Theoretically, the separation factor is not constant and depends on the solution concentration of the desired species. As illustrated in Table 5.2, the separation factor is higher than unity for all the various nickel concentration in solutions. In the loading experiments that resulted in S > 1, nickel ions were loaded onto resin selectively rather than ferrous ions. However, as the concentration of nickel in solution increased, the separation factor became smaller although it was still higher than one.

One can explain the decrease seen in the separation factor by the effect of sodium co-loading. Due to the reaction of nickel displacing hydrogen in these experiments, sodium hydroxide was consumed to maintain the pH 4 for the system. As a result, the chance of sodium co-loading onto resin was relatively high especially in the case of higher nickel composition in solution where the consumption of sodium hydroxide shown to be higher as well. Furthermore, according to the results summarized in Table 5.1, the overall ratio of $[\overline{Ni}]/[Ni]$ decreases as nickel concentration in solution [Ni] increases. Helfferich explains this decrease in the separation factor value by describing the effect of the "counter-

ionvalences" or "electroselectivity" [52]. Accordingly, as the total ionic strength of the solution increases for nickel ions, subsequently, the selectivity of nickel ions over ferrous ions decreases. Further investigation of the effect of ionic strength on separation factor for such a system with several species involved would be a recommendation for future work.

5.3 Determining the Hybrid Correlation Fit Parameters for Nickel-Ferrous Displacement Tests in a Finite Solution Volume Batch System

In Chapter 4, the hybrid correlation was applied under conditions where the concentration of ferrous was held constant for the duration of each test. However, for the ion exchange system investigated in this part of the thesis, resin bead samples were exposed to the test solution in which the concentration of nickel ions were not held constant for the entire test which is reflective to the real resin-in-pulp operational environment. For the purpose of this study, in order to evaluate the nickel loading behavior under non-infinite solution volume conditions the hybrid correlation fit parameters were estimated by using the finite difference model. McKevitt previously performed a finite model for several experiments on TP207XL resins where the solution concentration of nickel varied for the duration of each test [24].

5.3.1 Defining the Rate-Limiting Step by Applying Modified Helfferich Number

In order to apply the finite difference model, the rate-limiting step was required to be determined for the displacement experiments. Similar to most ion exchange reactions, the rate is controlled by the film diffusion regime at the beginning of the process and then become mostly limited by some combination of intraparticle diffusion and/or the exchange process. Linking the two rate-limiting regimes into a single equation with a combined constant could result in the highly complex mathematical terms since the film diffusion equation is derived based on a linear approach while the intraparticle diffusion derivation is based on non-linear approach [1]. Subsequently, Mckevitt developed a modified Hellfferich number calculation that determines whether the process is limited by film or intraparticle diffusion at any given time for the course of each experiment.

The Helfferich number was formerly developed to determine whether the ion exchange process is limited by film diffusion or intraparticle diffusion. The number is defined as the ratio of the predicted time to reach 50% loading under film diffusion control to the predicted time to attain 50% loading under intraparticle diffusion control.

However, the problem with the original Helfferich number was that the Helfferich number only can explain the rate-limiting step at the time that resins reached to 50% loading capacity. As a result, a modified Helfferich number was developed which could estimate the rate-limiting regime at any time during the resin loading process. The modified Helfferich number (summarized in equations 5.6 – 5.8) is defined as the ratio of the time it would take

to load a resin to any given fraction of loading (F) under the film diffusion regime (t_f) over the time to reach the equivalent loading applying the hybrid correlation (t_h).

Film Diffusion Control: $$t_f = \frac{-1}{k_f}\ln(1-F) \quad [5.6]$$

Hybrid Correlation: $$t_h = \frac{-1}{4k_h}\ln(1-F^2) \quad [5.7]$$

Modified Helfferich Number: $$\frac{4k_h\ln(1-F)}{k_f\ln(1-F^2)} \quad [5.8]$$

To determine the rate-limiting step, the criteria of modified Helfferich number is the same criteria applied for the original Helfferich number and described as follows:

film diffusion control if >>1,

mixed control if~1

intraparticle diffusion control if << 1.

Consequently, for modeling the overall loading rate of this ion exchange system, for modified Helfferich values >1 film diffusion control was applied, and for modified Helfferich values <1, the hybrid correlation was applied. According to the Helfferich criteria, for Helfferich number near one, the ion exchange process goes through a zone of mixed control (i.e. both film diffusion and intraparticle diffusion/exchange process). To determine whether or not there was a significant error in the nickel iron displacement model during mixed control, the modified Helfferich number was used to identify the approximate center of the mixed control zone.

5.3.2 Finite Model Development for Batch Experiments with Changing Solution Concentration

Nickel-ferrous displacement experiments were carried out under the finite solution volume conditions, therefore, there was no longer a simple analytical solution to the model's differential equations. As a result, to model the continually-changing nickel solution concentration over the course of each experiment a finite difference model was applied by using a numerical analysis method, the first order Runge-Kutta (Euler's method) method. The mathematical explanation of the finite difference model and the related Excel sheet for solving the model are outlined in Appendix D.

The results of a series of displacement experiments onto TP207XL were used in the finite model applied to describe the rate of the reaction. The model predicted the nickel loading rate with the assumption that the resin was moved to a fresh solution every Δt seconds. The time increment Δt was varied test-to-test (i.e. Δt = 1, 1.5, 3, 10, 15, and 30 seconds) depending on the initial composition of each test solution. For each experiment, an extra modeling run with a smaller time step was performed in order to confirm that the step size was adequately small enough. For example, as illustrated in Figure 5.5, for the experiment with an initial nickel concentration of 250 ppm in solution, to ensure that the time step of 1 second is small enough, another run was conducted with a time step 1/10 smaller (0.1 seconds). Thus, as indicated in the figure, both time intervals (1 and 0.1 seconds) gave an identical predicted solution concentration versus time model results.

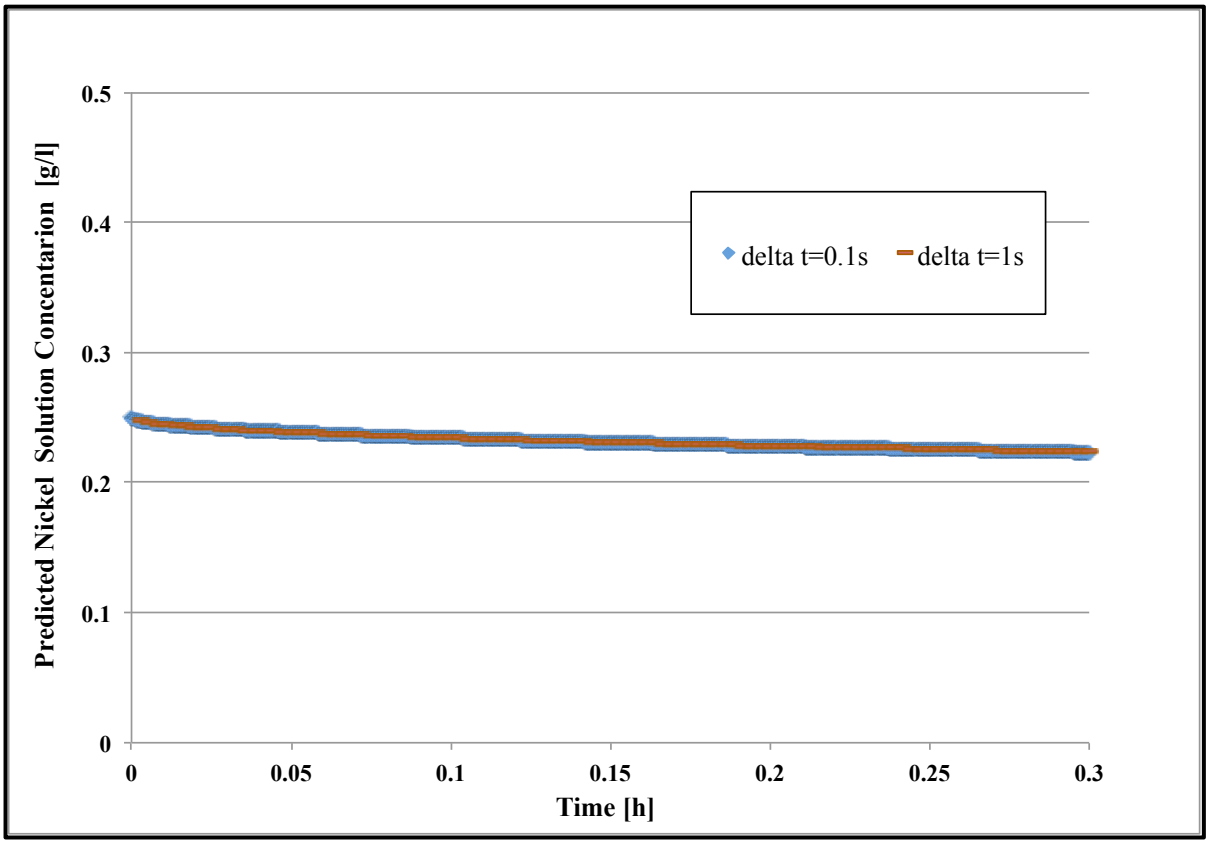

Figure 5.5: Model Step Size Confirmation Results for 250 ppm Nickel in solution *(pH 4, 30^0C, 10,000 ppm Ferrous in Solution)*

The model predicted the loading rate based on the Euler's method and therefore, the numerical solution to the loading rate problem developed an initial value problem. The very first mathematical solution was generated based on the initial nickel solution concentration for each test, the initial nickel loading onto resin (0 g Ni/L_{Resin}), and the initial solution volume added to the test vessel (~ 495 mL). The solution concentration of nickel [Ni] and nickel loading $[\overline{Ni}]$ at any given time of the experiment were calculated from the previous time step calculation. The model then computed the equilibrium resin loading $[\overline{Ni}]_{eqb}$, using the equilibrium isotherm (linear fit) described in Equation 5.3. Afterward, in order to determine the modified Helfferich number, the fractional attainment of equilibrium F along

with two rate constant of the film diffusion model and the hybrid correlation (k_f, k_h) were obtained. The obtained values then were applied in Equations 5.9 and 5.10 to calculate the equivalent time required to reach the current resin loading t_r for the modified Helfferich numbers >1 and ≤1.

Film Diffusion Control: $$t_r = \frac{-1}{k_f}\ln(1-F) \qquad [5.9]$$

Hybrid Correlation: $$t_r = \frac{-1}{4k_h}\ln(1-F^2) \qquad [5.10]$$

As a result, regarding the Helfferich number outcome, the predicted resin loading at time $t + \Delta t$, could be calculated. The model predicted exactly the same loading results as if the loading would have been obtained under infinite solution condition after a time $t_r + \Delta t$ (t_r is the time required under current conditions for resin to achieve the initial loading value). For modified Helfferich numbers larger than unity, the film diffusion equation [5.11] (a modified variation on film diffusion equation reviewed in Table 2.4) was applied to predict the resin loading. In addition, for modified Helfferich numbers less than or equivalent to one the hybrid correlation model equation [5.12], a slightly different version of Equation 2.21 was used.

For Film Diffusion: $$[\overline{M}]_{t+\Delta t} = [\overline{M}]_{eqb}[1-\exp[-k_f(t_r+\Delta t)]] \qquad [5.11]$$

Hybrid Correlation: $$[\overline{M}]_{t+\Delta t} = [\overline{M}]_{eqb}\sqrt{[1-\exp[-4k_h(t_r+\Delta t)]]} \qquad [5.12]$$

Results for the displacement test run at 250 ppm nickel are displayed in Figure 5.6. The model prediction and the observed experimental results can be compared in the figure. Hence, the model fit to the observed data quite well. The loading value obtained from the assay of the resin strip solution is also plotted in the same figure as a reference, which confirms that the model adequately predicted the rate of loading for the system.

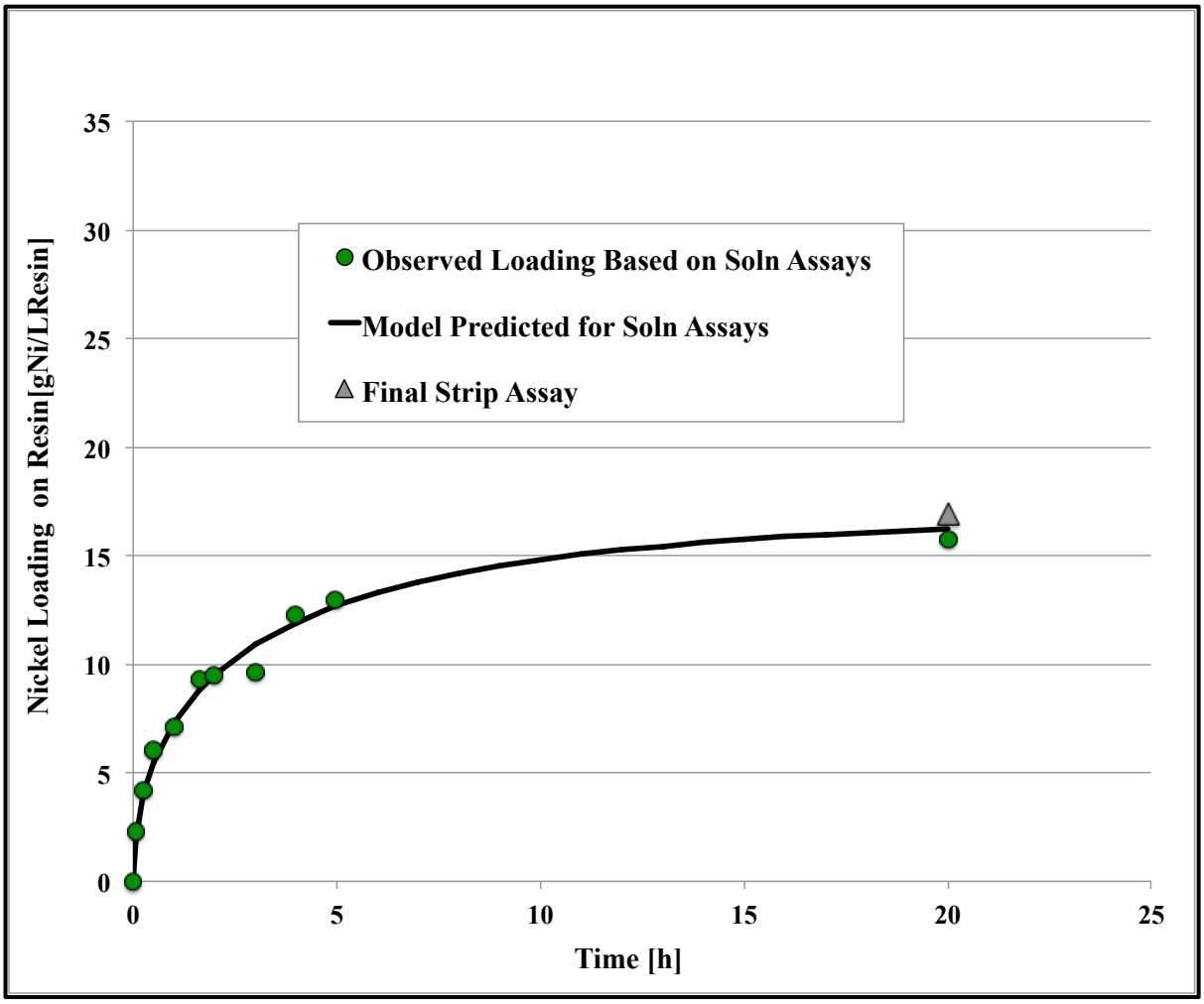

Figure 5.6: Resin Loading onto TP207XL under Finite Volume Solution Conditions

(pH 4, 30^{0}C, 250 ppm, 10,000 ppm Ferrous at t=0)

To get a better understanding of the rate-limiting step for the duration of the test, the modified Helfferich number is plotted in Figure 5.7, along with the observed loading based on the solution assays for the test with 250 ppm nickel in solution.

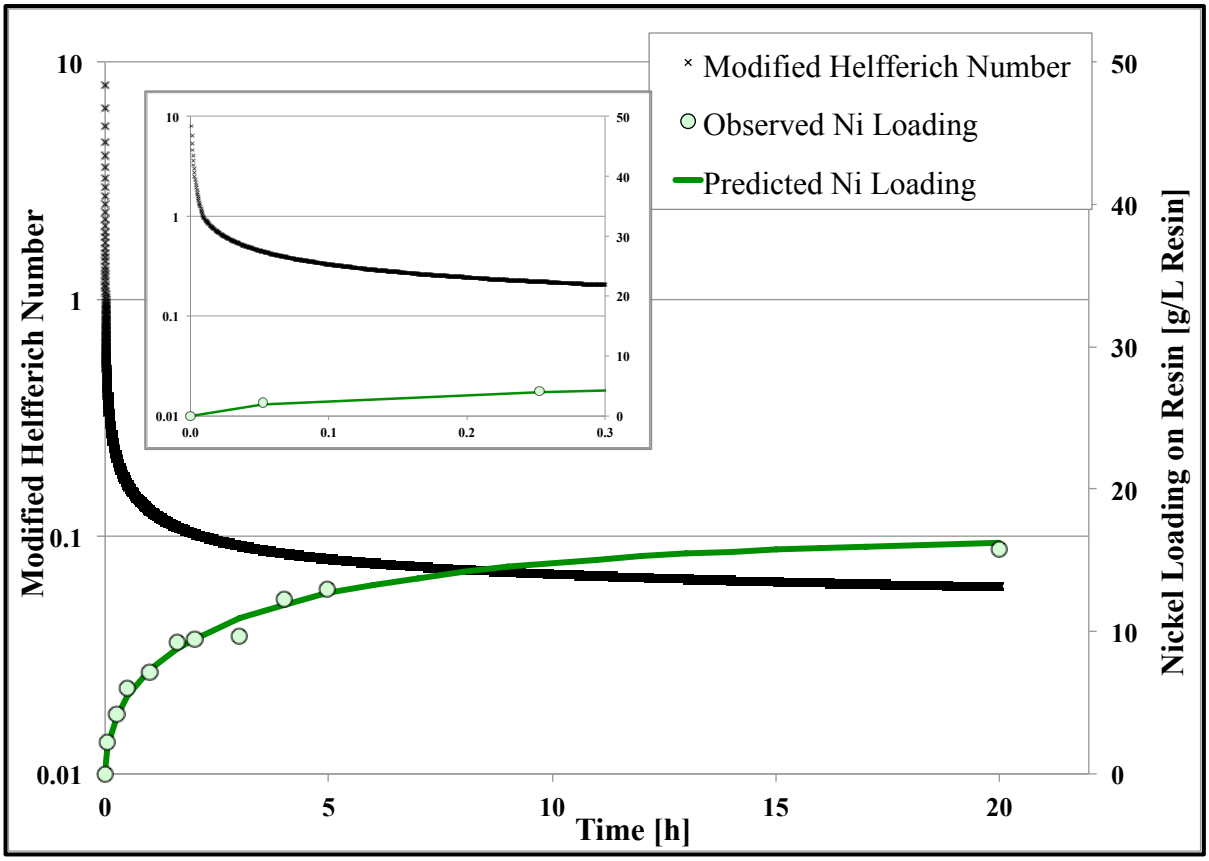

Figure 5.7: Nickel Loading onto TP207XL Resin under Finite Solution Volume Conditions *(pH 4, 30^{0}C, 250 ppm Ni, 10,000 ppm Ferrous at t=0)*

The test started with a Helfferich number higher than one, suggesting film diffusion control. Then, right after the film diffusion controlled zone where the Helfferich number is around one, the mixed control zone existed. To confirm that the model was adequate to describe the mixed control zone, it was required to compare whether or not the predicted and obtained

experimental data where the Helfferich number is around one were close. As indicated in the part of the graph zoomed around Helfferich number 1, the model does not diverge significantly more than for the rest of test in that region. Apparently, looking at the overall loading curve, the model fit adequately in this zone although there were not enough assay points to completely support this fact. As a result, it was not clear where the mixed control zone starts or ends.

As the resin bead loads, the modified Helfferich number decreased to a value of 0.06. Thus, the rate of the nickel loading in the presence of ferrous is predominately limited by combination of intraparticle diffusion/ion exchange reaction control as the modified Helfferich number is <<1 for most of the experiment.

Table 5.3: Film Diffusion Control Duration for Several Experiments

Test Concentration (ppm Ni)	**Film Diffusion Control Period** (s)
100	120
250	33
500	13
1000	5
2500	1.2
5000	0.4

Table 5.3 illustrates the time duration in which the loading rate of each experiment was under film diffusion control (Helfferich number greater than 1). As shown, the time period for the rate of loading to be limited by the film diffusion regime became smaller as the

concentration of the test solution increased. This phenomenon was expected since as the nickel concentration increased in the test solution the driving force was large enough that the liquid film existing around the resin particle would not limit the diffusion process. This also indicates that the nickel-loading rate was mainly under the intraparticle diffusion/ion exchange reaction limited regime for the various nickel concentrations in solution ranging from 100 to 5,000 ppm in solution.

5.3.2.1 Application of the Finite Model for Several Nickel- Ferrous Displacement Experimental Results

The finite difference model was then used to predict resin loadings onto TP207XL over the course of several displacement experiments. The best fit of the kinetic parameters, D_{app}=9.95 x 10^{-12} m^2/s, and α=0.65, were determined by minimizing the total errors between predicted and observed loading values for all the experiments. According to Figure 5.8, the model was found to predict the observed values quite well for all the experimental results.

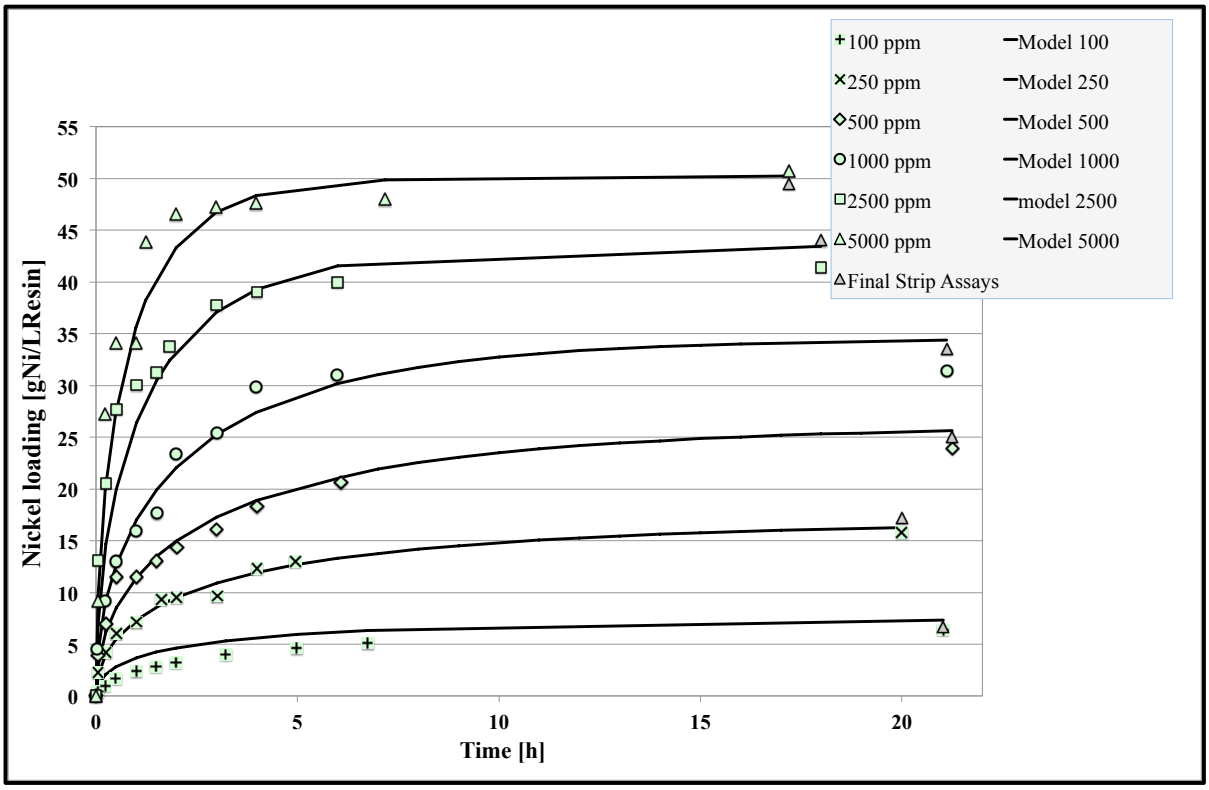

Figure 5.8: Nickel Loading onto TP207XL Resin under Finite Solution Volume Conditions *(pH 4, 30^{0}C, 10,000 ppm Ferrous in Solution)*

The principal objective of this work was to see if the overall loading model can be employed for conditions reflective of a counter current resin-in-pulp system where several impurities could co-load onto the resin. As described in the literature review, in the RIP counter current circuit typically (Figure 5.9) fresh resin is added to the circuit in the last RIP stage and transferred towards the feed entry end of the circuit with the higher nickel concentration. McKevitt studied the nickel-loading rate onto TP207XL in such a system in which there were no impurities (Figure 5.10) and nickel was mainly displacing hydrogen ions on the resin.

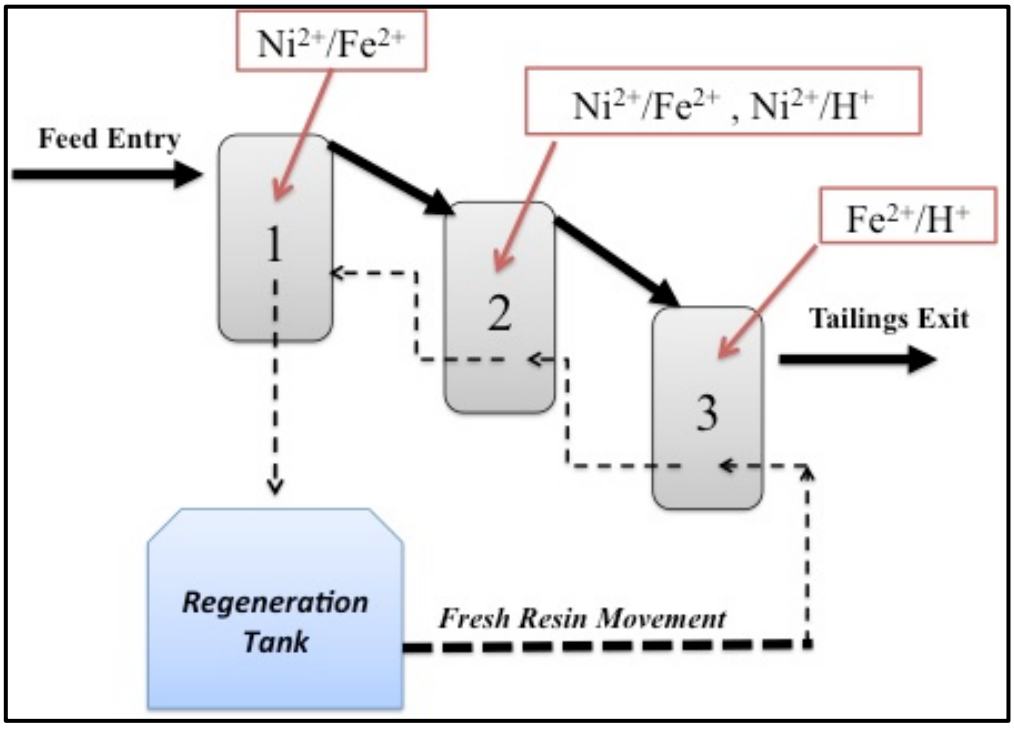

Figure 5.9: Three-Stage Counter Current RIP Circuit for Nickel Recovery in the Presence of Ferrous as an Impurity in the System

The first part of the thesis investigated the system representative of tank 3 in Figure 5.9 where the fresh resins are introduced to the solution with high concentration of impurities such as ferrous. In such a system ferrous ions would load onto the resin. Additionally, the study of the nickel-ferrous displacement experiments under finite solution volume conditions can describe the reaction that may occur mainly in tank 2 and 1. In those tanks, the resins preloaded with ferrous (from tank 3) are introduced to the solution with higher nickel concentration. Under this condition, we should expect that nickel would load onto the resin by displacing ferrous ions (Figure 5.10).

According to Figure 5.8, the maximum resin loading is outlined after about the first 5 hours of each experiment. In addition, as the concentration of nickel in solution increases the

loading rate increases as well. For example, for the 5,000 ppm nickel in solution the maximum loading is approached around 2.5 hours into the experiment whereas for 100 ppm nickel in solution the system approached the maximum loading value after about 5 hours of the test. Most importantly, even in the case of very low concentration of nickel in solution (100 ppm), it was observed that nickel could still load onto the resin even in small amounts. This is likely reflective of the fact that even in tank 3 where the majority of the resin capacity will be occupied by ferrous, a small quantity of nickel can still be recovered. This is of course the reason that the last stage of RIP is so important to maximize the overall recovery of nickel from solution.

5.3.3 Hybrid Fit Parameters for Nickel - Ferrous Loading Experiments

The hybrid correlation fit parameters for nickel loading under finite solution volume condition (FSV) are summarized in Table 5.4 along with the parameters taken from previous study of nickel loading under infinite solution volume condition (ISV).

Table 5.4: Summary of Hybrid Fit Parameters for Nickel Loading

Main Reaction	D_{app} (m^2/s)	Alpha
Ni/Fe (FSV)	9.8×10^{-12}	0.65
Ni/H (ISV)*	4.4×10^{-12}	0.36

* Data are extracted from reference [24].

According to the table, the apparent diffusivity obtained with the hybrid correlation for nickel loading in the presence of ferrous appear to be of the same order of magnitude as the one obtained for nickel-hydrogen ion exchange system. In addition, the apparent diffusivity obtained for the nickel-ferrous loading experiments is higher than the other one.

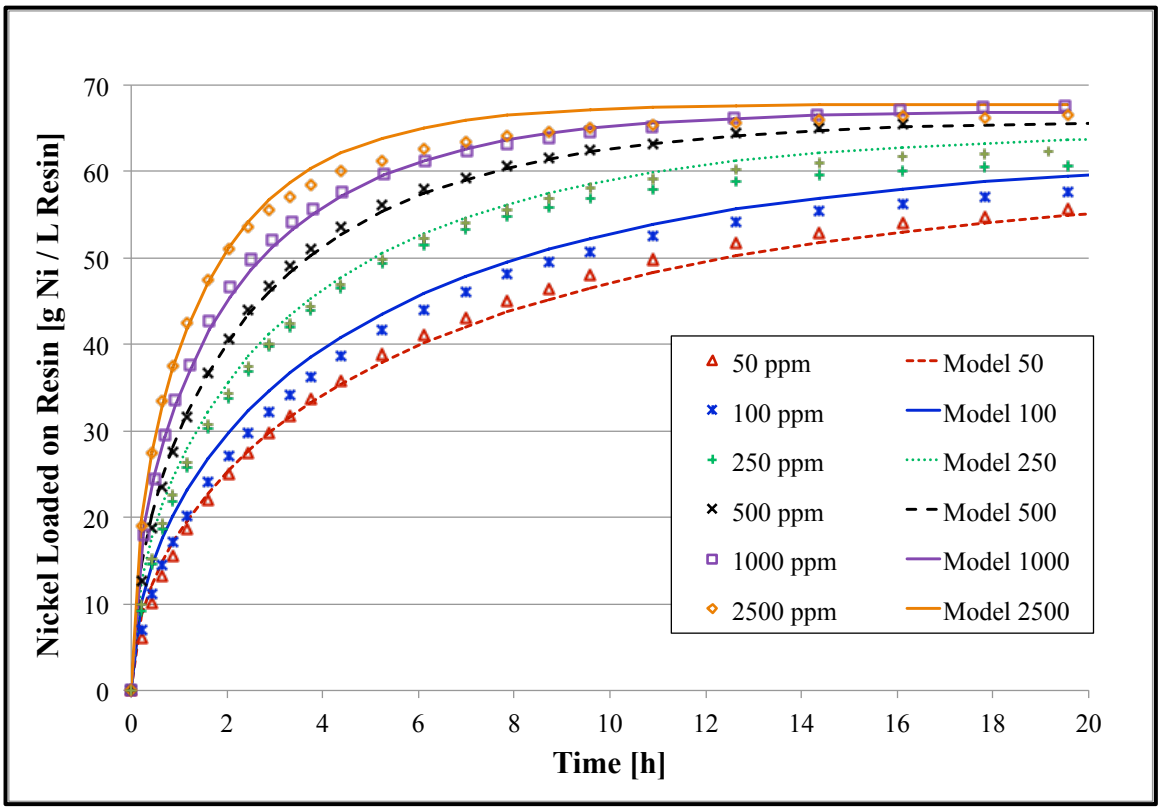

Figure 5.10: Hybrid Correlation Fit to Nickel Loading onto TP207XL *(Constant Nickel in Solution, pH 4, 300C)* [83]

Comparing Figure 5.8 with Figure 5.10, as shown, in the nickel-ferrous displacement experiments the rate is faster since the maximum loading was achieved much quicker. Whereas in the experiments where nickel is just displacing the hydrogen the maximum loading was approached towards the end of each experiment. As a result, fit parameter, D_{app},

trends well with the rate of loading of nickel in both experimental conditions. Note, the second empirical fit parameter, alpha, will be discussed in details in the next section.

The second empirical fit parameter of the hybrid correlation model, α, can be related to the boundary presented between loaded and unloaded part of the resin bead. Resin would be loading under a shrinking core mechanism if α approaches 1 whereas for α approaches 0, the resin should be loading in a Vermeulen intraparticle diffusion manner. Therefore, for a system with α approaching to 1 a much sharper boundary would be expected to exist. To confirm this hypothesis, McKevitt performed a series of loading tests onto TP207XL resin beads in hydrogen form. The resin beads were loaded to approximately 1eq/L (50% capacity) with about 500 ppm nickel, cobalt and copper in solution. The photographs of those resin beads are illustrated in Figure 5.11.

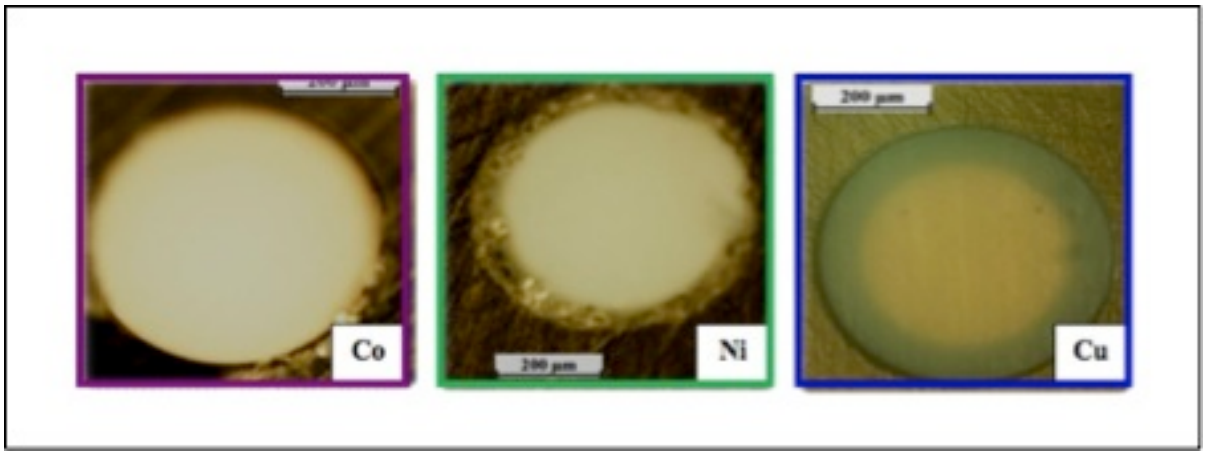

Figure 5.11: **Photographs of Resin Beads Loaded to 1 eq/L** [24]

In this work also TP207XL were loaded to 50% capacity with 500 ppm nickel and 500 ppm ferrous in solution under infinite solution volume conditions. In addition, the same approach was performed for the resin beads loaded with 50 %capacity for nickel under finite solution (nickel-ferrous displacement experiment). Afterwards the results of all three experiments in addition to the ones from previous study of TP207XL were compared and analyzed in terms of alpha parameter. The brief description of the procedure is outlined below:

1. After running all the three types of loading experiments, resin samples of each experiment were removed from the test solution at the time the system reached 50% loading capacity. Time required for 50% loading was obtained from the related metal loading rate graphs.
2. Resin samples were afterward immediately mounted using rapid cold cure epoxy.
3. The polishing of the resin samples consisted of grinding with 1200 SiC emery paper, polishing with 1 micron diamond paste and rinsed with deionized water.
4. The samples then were observed under the optical microscope roughly 16-18 hours after removing the resins from the test solutions (the microscopic observation of the resin beads related to the three sets of loading experiments are illustrated in Figure 5.12 and Figure 5.13.

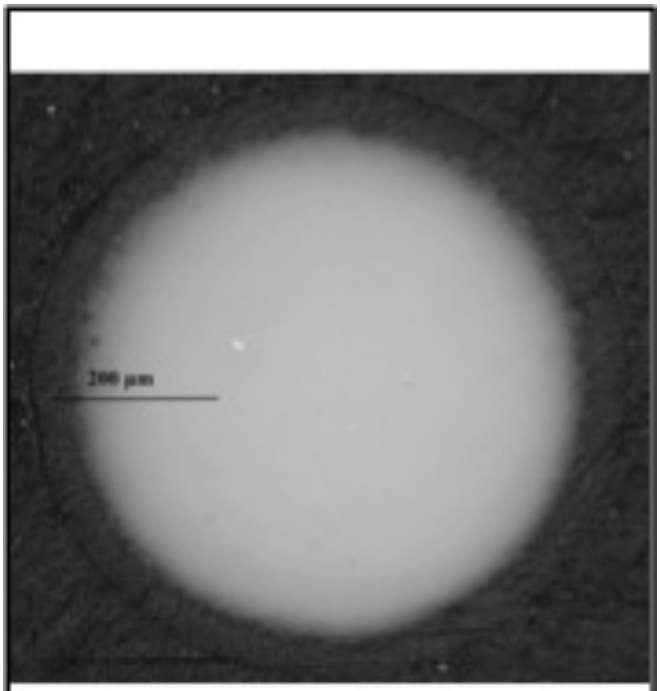

20X magnification

Figure 5.12 :Optical Microscopy Image of resin bead loaded with 500 ppm ferrous

(50% of capacity)

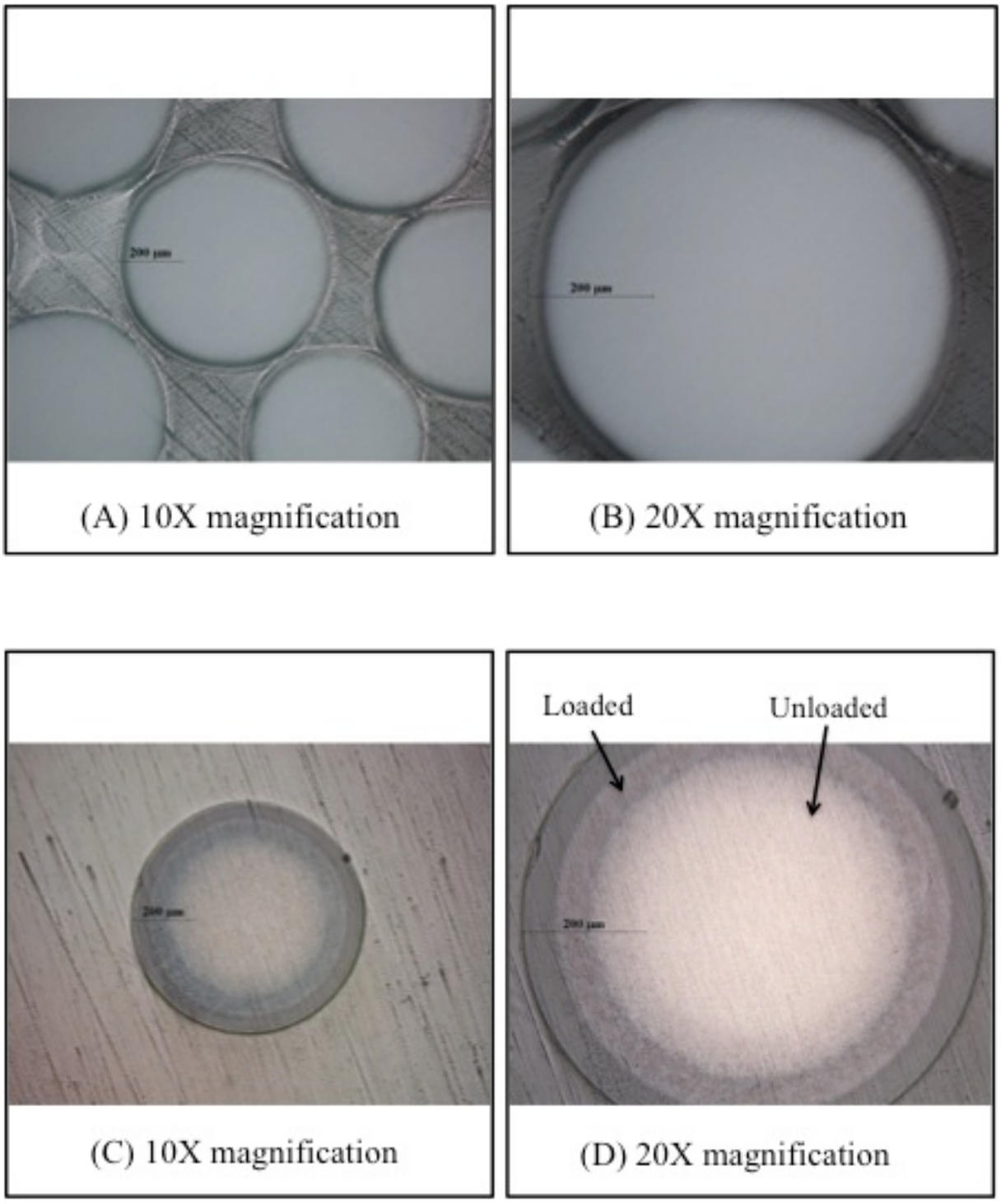

Figure 5.13: Optical Microscopy Image of Resin Bead of Nickel Loading to 50% Capacity onto Resin in Hydrogen Form (A,B) and onto Resin Preloaded with Ferrous (C,D)

According to all optical microscopic images of the resin beads, there is no boundary or gradient between loaded and unloaded portion of resin beads in case of nickel (α=0.36), cobalt (α=0.25) and ferrous (α=0.22) loading under infinite solution volume condition. However, for copper loading (α=0.62), a distinctive boundary (green ring) between loaded and unloaded portion of resin bead was distinguished (Figure 5.11).

The model performed on the nickel-ferrous displacement tests resulting in a high alpha value (α=0.65), suggested that the loading occurred predominantly under a shrinking core mechanism. As a result, for the resin beads loaded in displacement experiments it was expected to see a visible boundary as earlier detected for copper loading. The existence of an obvious gradient between loaded and unloaded regions within the resin bead for the displacement experiments was apparent in the optical microscopic images illustrated in Figure 5.13.

As mentioned earlier in the thesis, the alpha value can be related to a decomplexing pH value. When the resin is in the hydrogen form, the exchange reaction is such that the nickel displaces a hydrogen ion. Therefore, considering one particle at a time, one nickel ion loads onto the resin bead, then the localized pH in that area drops due to the ion exchange reaction. Thus, even if the next site is available on the resin, the nickel ion may have to diffuse further into the bead to get to a zone where the localized pH favors nickel loading. When the resin is preloaded with ferrous, the ion exchange reaction for sites loaded with ferrous may not cause a localized pH drop. As a result, the next nickel ion can load on the next available resin exchangeable site.

5.4 Summary of Nickel-Ferrous Displacement Experimental Results

The hybrid correlation kinetics fit parameters were determined for the nickel-ferrous displacement experiments under the finite solution volume conditions. Initially, the linear equilibrium loading isotherm was selected based on the final nickel loading of several displacement experiments. The finite difference model was applied to predict the loading behavior of nickel in the presence of ferrous in the batch system using the modified Helfferich number and the linear isotherm equation. As confirmed, the ion exchange reaction examined in this study was predominantly controlled under some combination of intraparticle/ion exchange reaction. Regarding the hybrid correlation fit parameter (D_{app} = 9.95 x 10^{-12} m^2/s, α = 0.65), these parameters corelated well with the loading behavior of nickel onto resin. The apparent diffusivity determined for nickel loading in the presence of ferrous was the same order of magnitude as the one previously obtained for nickel loading under infinite solution volume conditions. The alpha value determined for the system approached to 1, which indicated that the resin loaded predominantly under a shrinking core fashion and there was a sharp boundary between the loaded and unloaded portion of the resin bead.

6 Conclusion and Recommendation

The two objectives defined for this research program have been accomplished. The conclusions from this study and how they correspond to the research objectives will be discussed in this chapter. The conclusions will be continued by recommendations for future work.

6.1 Conclusion from Ferrous Batch Loading Experiments

To investigate the ferrous loading rate under infinite solution volume conditions, the pH-stat method developed previously by McKevitt was applied. This method was designed to maintain a near constant concentration of ferrous for the duration of all experiments. For the specific concentration of ferrous in solution, the modified pH-stat method was proven to provide good repeatability with maximum error of +/- 3g Fe/L Resin.

An ion exchange correlation (hybrid) was selected to explain the loading rate of ferrous in the ion exchange reaction which was predominantly limited by the intraparticle diffusion /ion exchange limited regime. The hybrid correlation related the Vermeulen approximation to intraparticle diffusion controlled loading and an approximation to the shrinking core model.

By combining those two models, a new fit parameter alpha was generated to describe the solution concentration dependency of the system. The model predicts shrinking core type intraparticle diffusion for $\alpha \rightarrow 1$ and intraparticle diffusion described by Vermeulen

approximation for $\alpha \rightarrow 0$.

The hybrid correlation was proven to adequately describe the loading rate of ferrous over the range of 100 to10,000 ppm using the following kinetics fit parameters: $D_{app} = 2.2 \times 10^{-12}$ m^2/s, $\alpha = 0.22$. Those two fitting parameters trend well with the loading behavior of ferrous onto TP207XL resin compared to copper, nickel and cobalt metal ions loading rate studied previously. As indicated, the loading rate of ferrous onto the iminodiacetic ion exchange resin was slower than those metals. Furthermore, the alpha parameter could be considered as a measure of how sharp a boundary existed between the reacted and unreacted region with the resin bead during loading process. For ferrous loading experiments, the obtained alpha ($\alpha = 0.22$) was low. As expected and illustrated in the optical microscopic image obtained from a resin bead, no visible gradient was detected within the bead loaded with ferrous ions.

The association of the alpha parameter with the decomplexing pH indicated that, there was a relationship between alpha values and the known decomplexing pH of several metal ions loading onto TP207XL under infinite solution volume condition. As the decomplexing pH decreased (in the case of copper loading), the alpha parameter value approaches 1 and, as expected, a sharp boundary between loaded/unloaded resin within the resin bead was detected. However, in the case of ferrous loading ($\alpha \rightarrow 0$), when one ferrous ion loads onto the resin bead, the localized pH could drop to a pH value approaching or below the decomplexing pH. As a result, even if the next exchange site was free, the ferrous ion may have to diffuse further into the bead to get to the zone where the localized pH favors ferrous loading.

6.2 Conclusion from Nickel Loading in the Presence of Ferrous Ions in the Batch System

Several nickel-ferrous batch loading experiments were conducted in the presence of 10,000 ppm ferrous with non-constant nickel concentrations in solution. The hybrid correlation kinetic fit parameters were determined for the nickel-ferrous displacement experiments through the application of the finite difference model. To perform this fitting, an equilibrium loading isotherm was developed. Since the ion exchange system studied here was a quaternary system due to the complicated mathematical terms, the Mass Action Law was not applied. Consequently, the empirical linear equilibrium loading isotherm was selected based on the final nickel loading of several displacement experiments. As an assessment to the equilibrium isotherm, the separation factor was calculated for nickel displacing ferrous ions for each experiment. Separation factor appeared to vary with the solution composition of each experiment. The separation factor (for nickel over ferrous) was always greater than one. This result confirmed the fact that nickel was always selected over ferrous by iminodiacetic ion exchange resin studied in this work.

The finite difference model was then applied to predict the loading behavior of nickel in the presence of ferrous. The modified Helfferich number was used to determine the rate-limiting step as the resin bead loaded over the course of each experiment. The initial part of loading was modeled using the film diffusion model where the Helfferich number was greater than one and the latter portion of loading was modeled using the hybrid correlation for Helfferich values less than one. Results established that the two models delivered a reasonable fit to the experimental data. The mixed control regime portion of the loading curve was always a

minor component of the overall loading behavior of the resin. Therefore no additional mixed control model was required. As confirmed, the ion exchange reaction examined in this study was predominantly controlled under some combination of intraparticle/ion exchange reaction and the film diffusion controlled zone was too short and even negligible specifically where the concentration of nickel was very high in the solution test. Furthermore, the nickel loading rate was faster as the concentration of nickel increased in the solution. Remarkably, even when the [Ni]/[Fe] ratio in the solution is small, nickel loading values of a few grams of nickel per liter of resin were still obtained.

The finite model fitted fairly well to all nickel-ferrous displacement experimental results by using the hybrid correlation fit parameters D_{app} = 9.95 x 10^{-12} m^2/s and α = 0.65. The apparent diffusivity calculated for nickel loading in the presence of ferrous was the same order of magnitude as the one previously obtained for nickel loading under infinite solution volume condition with slightly lower value. In terms of a second fit parameter, the alpha value determined for the system approached to 1, which indicated that the resin predominantly loaded under a shrinking core fashion. It was expected to see the visible boundary (as detected for copper loading) between the Ni-loaded and Fe-unloaded regions within the resin bead loaded with nickel from a nickel-ferrous solution. The optical microscopic analysis of the resin bead loaded in the nickel-ferrous displacement loading experiments confirmed the presence of the sharp boundary between the reacted and unreacted core.

The overall results from displacement loading experiments suggest that in the presence of high levels of impurities as one would expect in an actual RIP process slurry, the impurities

such as ferrous primarily load onto the resin and are then displaced by nickel. This emphasizes the importance of the outcomes of the loading experiments under condition reflective of its actual anticipated operating condition. It is reasonable to expect a different loading behavior related to the nickel-ferrous displacement process compared to the rates of nickel when loaded directly onto a resin in the hydrogen form. The displacement test outcomes highlight the fact that resin loaded noticeably faster when ferrous was displaced by nickel rather than hydrogen being displaced. However, as expected, TP207XL was shown to load to a higher capacity when nickel displaced hydrogen under the infinite solution volume condition. That is, ferrous ion present in the system speeds the rate of exchange of nickel onto the resin, but limits the ultimate loading value.

6.2.1 Recommendations for Future Work

Based on the results of this research study, several suggestions and recommendations can be proposed and discussed in point form below:

- In this study, in order to generate an equilibrium loading isotherm for nickel loading under the finite solution condition, the empirical linear model was selected. As a result, the ion exchange system was simplified and several assumptions were considered accordingly. Therefore, one logical extension of this research is to study the actual quaternary (Ni-Fe-H-Na) ion exchange system. Knowing the mechanism of the ion exchange process and generating enough data under various conditions for all the four elements (Ni-Fe-H-Na) in the system, it may be possible to develop the loading isotherm using the Mass Action Law model.

- One can also try to study how the other impurities such as calcium, magnesium, manganese, aluminum, and chromium (III), will affect the loading rate in an RIP circuit. The objective would be to see how the loading rate of nickel and cobalt would be affected when the resin is preloaded by several impurities. This can be performed by performing several loading experiments for the impurities under infinite solution volume conditions and obtaining related hybrid model kinetics fit parameters. Subsequently, nickel-impurity displacement loading experiments can be conducted followed by generating an equilibrium isotherm and determining the hybrid correlation fit parameters.

- Physical characteristics of the second hybrid correlation fit parameter can be further investigated regarding the loading behavior of metal ions (Fe, Co, Cu, and Ni) onto sodium form of TP207XL under finite solution volume conditions. The purpose is to detect partially loaded resin beads under various conditions to see whether alpha accurately matches the observed metal loading distribution within the resin bead. From a practical point of view, depending on the primary form of the resin, if a distinct difference in the loading pattern of metal ion within the resin bead exists, this could help answer the question as to whether or not conditioning the resin has any effect in an actual RIP operation. This objective can be achieved by obtaining the hybrid correlation fit parameters via generating the loading isotherm graph from the related experimental datasets. Finally, investigation of partially loaded resin beads with Fe, Co, Ni, and Cu onto resin in H-form and Na-form can be obtained using an optical microscope to observe the presence or absence of visible gradients between the reacted and unreacted portion of the resin beads. Note, Scanning Electron

Microscope (SEM) and Energy Dispersive X-ray Spectroscopy (EDX) can be used in order to quantify the metal loading profile across the resin bead cross section.

References

[1] S. Sudol, The thunder from down under-everything you wanted to know about nickel laterites but were afraid to ask, Can. Min. J., vol. 126, pp. 8-12, 2005.

[2] R. McDonald and B. Whittington, Atmospheric acid leaching of nickel laterites review: Part I. Sulphuric acid technologies, Hydrometallurgy, vol. 91, pp. 35-55, 2008.

[3] A. D. Dalvi, W. G. Bacon and R. Osborne, The past and the future of nickel laterites, in PDAC 2004 International Convention, Trade show & Investors Exchange, 2004, pp. 1-27.

[4] Y. Zhai, W. Mu, Y. Liu and Q. Xu, A green process for recovering nickel from nickeliferous laterite ores, Transactions of Nonferrous Metals Society of China, vol. 20, pp. s65-s70, 2010.

[5] C. Fan, X. Zhai, Y. Fu, Y. Chang, B. Li and T. Zhang, Extraction of nickel and cobalt from reduced limonitic laterite using a selective chlorination–water leaching process, Hydrometallurgy, vol. 105, pp. 191-194, 2010.

[6] O. Coto, F. Galizia, I. Hernández, J. Marrero and E. Donati, Cobalt and nickel recoveries from laterite tailings by organic and inorganic bio-acids, Hydrometallurgy, vol. 94, pp. 18-22, 2008.

[7] D. Georgiou and V. Papangelakis, Sulphuric acid pressure leaching of a limonitic laterite: chemistry and kinetics, Hydrometallurgy, vol. 49, pp. 23-46, 1998.

[8] B. Ma, C. Wang, W. Yang, F. Yin and Y. Chen, Screening and reduction roasting of limonitic laterite and ammonia-carbonate leaching of nickel–cobalt to produce a high-grade iron concentrate, Minerals Eng, vol. 50, pp. 106-113, 2013.

[9] M. Valix and W. Cheung, Study of phase transformation of laterite ores at high temperature, Minerals Eng, vol. 15, pp. 607-612, 2002.

[10] B. Whittington and D. Muir, Pressure acid leaching of nickel laterites: a review, Mineral Processing and Extractive Metullargy Review, vol. 21, pp. 527-599, 2000.

[11] Z. Zainol, The development of a resin-in-pulp process for the recovery of nickel and cobalt from laterite leach slurries, Murdoch University PhD Thesis, School of Mineral Science, 2005.

[12] C. Köse and Y. Topkaya, Hydrometallurgical processing of nontronite type lateritic nickel ores by MHP process, Minerals Eng, vol. 24, pp. 396-415, 2011.

[13] X. Guo, D. Li, K. Park, Q. Tian and Z. Wu, Leaching behavior of metals from a limonitic nickel laterite using a sulfation–roasting–leaching process, Hydrometallurgy, vol. 99, pp. 144-150, 2009.

[14] A. Oxley and N. Barcza, Hydro–pyro integration in the processing of nickel laterites, Minerals Eng,vol 53, pp. 2-13, 2013.

[15] J. E. De Graaf, The treatment of lateritic nickel ores — a further study of the Caron process and other possible improvements. Part I. Effect of reduction conditions, Hydrometallurgy, vol. 5, pp. 47-65, 10, 1979.

[16] Ş. Kaya and Y. Topkaya, High pressure acid leaching of a refractory lateritic nickel ore, Minerals Eng, vol. 24, pp. 1188-1197, 2011.

[17] B. Ma, C. Wang, W. Yang, B. Yang and Y. Zhang, Selective pressure leaching of Fe (II)-rich limonitic laterite ores from Indonesia using nitric acid, Minerals Eng, vol. 45, pp. 151-158, 5, 2013.

[18] Z. Zainol and M. J. Nicol, Comparative study of chelating ion exchange resins for the recovery of nickel and cobalt from laterite leach tailings, Hydrometallurgy, vol. 96, pp. 283-287, 5, 2009.

[19] F. Mendes and A. Martins, Selective nickel and cobalt uptake from pressure sulfuric acid leach solutions using column resin sorption, Int. J. Miner. Process., vol. 77, pp. 53-63, 2005.

[20] P. Littlejohn and J. Vaughan, Selective elution of nickel and cobalt from iminodiacetic acid cation exchange resin using ammoniacal solutions, Hydrometallurgy, vol. 141, pp. 24-30, 2014.

[21] M. Adams, Towards a virtual metallurgical plant: CCD vs RIP case study, LTA Ni/Co Conference Proceedings 2006, ALTA Metallurgical Services, Melbourne, p.17 2006.

[22] Z. Zainol and M. J. Nicol, Comparative study of chelating ion exchange resins for the recovery of nickel and cobalt from laterite leach tailings, Hydrometallurgy, vol. 96, pp. 283-287, 2009.

[23] B. Wassink, M. Neufeld, D. Dreisinger and G. Freeman, Towards a resin-in-pulp process for recovery of nickel and cobalt from laterite leach tailings: An iminodiacetic acid ion exchange resin as a prospective resin, in Official Proceedings-International Water Conference, 2006.

[24] B. R. McKevitt, An ion exchange loading correlation for the simulation of base metal resin-in-pulp circuits, University of British Columbia PhD thesis, Department of Material Engineering 2012

[25] F. Mendes and A. Martins, Recovery of nickel and cobalt from acid leach pulp by ion exchange using chelating resin, Minerals Eng, vol. 18, pp. 945-954, 2005.

[26] B. McKevitt, P. Abbasi and D. Dreisinger, A comparison of large bead ion exchange resins for the recovery of base metals in a resin-in-pulp (RIP) circuit, in Proceedings of the 6th Southern African Base Metals Conference, SAIMM, 2011, pp. 337-352.

[27] P. Littlejohn and J. Vaughan, Selectivity of commercial and novel mixed functionality cation exchange resins in mildly acidic sulfate and mixed sulfate–chloride solution, Hydrometallurgy, vol. 121, pp. 90-99, 2012.

[28] Z. Zainol and M. J. Nicol, Ion-exchange equilibria of Ni^{2+}, Co^{2+}, Mn^{2+} and Mg^{2+} with iminodiacetic acid chelating resin Amberlite IRC 748, Hydrometallurgy, vol. 99, pp. 175-180, 11, 2009.

[29] M. Luqman, Ion-Exchange Technology I: Theory and Materials. Springer, 2012.

[30] M. Streat, Applications of ion exchange in hydrometallurgy, in Ion Exchange Science and Technology Anonymous Springer, vol 107, pp. 449-461, 1986.

[31] K. Dorfner, Ion Exchangers. Walter de Gruyter Berlin, 1991.

[32] V. J. Inglezakis and A. Zorpas, Fundamentals of ion exchange fixed-bed operations, in Ion Exchange Technology I, Anonymous Springer, 2012, pp. 121-161.

[33] P. C. Hayes, Process principles in minerals and materials production, Hayes Publishing: Brisbane, Australia 2003.

[34] D. Dang, W. Ding, A. Cheng, S. Liu and X. Zhang, Isotherm equation study of F adsorbed from water solution by $Fe_2SO_4^{3-}$ modified granular activated alumina, Chin. J. Chem. Eng., vol. 19, pp. 581-585, 2011.

[35] G. P. O'Malley, Recovery of gold from thiosulfate solutions and pulps with anion-Exchange Resins, Murdoch University PhD thesis, 2002.

[36] T. R. Makhubela, base metal recovery by resin-in-pulp (RIP) technology, Tshwane University of Technology PhD thesis, 2006.

[37] D. G. Kinniburgh, General purpose adsorption isotherms, Environ. Sci. Technol., vol. 20, pp. 895-904, 1986.

[38] N. Z. Misak, Langmuir isotherm and its application in ion-exchange reactions, Reactive Polymers, vol. 21, pp. 53-64, 1993.

[39] A. Deepatana, J. Tang and M. Valix, Comparative study of chelating ion exchange resins for metal recovery from bioleaching of nickel laterite ores, Minerals Eng, vol. 19, pp. 1280-1289, 2006.

[40] H. Freundlich, Over the adsorption in solution, J. Phys. Chem., vol. 57, pp. 292, 1906.

[41] X. Song, Y. Zhang, C. Yan, W. Jiang and C. Chang, The Langmuir monolayer adsorption model of organic matter into effective pores in activated carbon, J. Colloid Interface Sci, vol 389, pp 213-219, 2012.

[42] A. Deepatana and M. Valix, Comparative adsorption isotherms and modeling of nickel and cobalt citrate complexes onto chelating resins, Desalination, vol. 218, pp. 334-342, 2008.

[43] I. Langmuir, The constitution and fundamental properties of solids and liquids, part I. solids, J. Am. Chem. Soc., vol. 38, pp. 2221-2295, 1916.

[44] A. Wołowicz and Z. Hubicki, Selective adsorption of palladium (II) complexes onto the chelating ion exchange resin Dowex M 4195–kinetic studies, Solvent Extraction and Ion Exchange, vol. 28, pp. 124-159, 2010.

[45] L. Lin, J. Li and R. Juang, Removal of Cu (II) and Ni (II) from aqueous solutions using batch and fixed-bed ion exchange processes, Desalination, vol. 225, pp. 249-259, 2008.

[46] I. Langmuir, The adsorption of gases on plane surfaces of glass, mica and platinum. J. Am. Chem. Soc., vol. 40, pp. 1361-1403, 1918.

[47] A. P. Vanselow, Equilibria of the base-exchange reactions of bentonites, permutites, soil colloids, and zeolites, Soil Sci., vol. 33, pp. 95-114, 1932.

[48] J. G. Reynolds, A Multiresponse method for fitting solid-phase activity coefficient models to ternary ion-exchange data, Geoderma, vol. 151, pp. 264-269, 2009.

[49] B. McKevitt and D. Dreisinger, Development of an engineering model for nickel loading onto an iminodiacetic resin for resin-in-pulp applications: Part I—Method development and discussion of rate limiting factors, Hydrometallurgy, vol. 121, pp. 35-44, 2012.

[50] H. Walton, Ion exchange in analytical chemistry J. Chem. Educ., vol. 42, pp. 111, 1965.

[51] F. G. Helfferich, Ion Exchange. Courier Dover Publications, 1995.

[52] G. Myasoedova, S. Savvin and E. Blasius, Chelating sorbents in analytical chemistry, 1986.

[53] A. Wołowicz and Z. Hubicki, The use of the chelating resin of a new generation Lewatit MonoPlus TP-220 with the bis-picolylamine functional groups in the removal of selected metal ions from acidic solutions, Chem. Eng. J., vol. 197, pp. 493-508, 2012.

[54] G. Myasoedova, I. Antokol'skaya and S. Savvin, New chelating sorbents for noble metals, Talanta, vol. 32, pp. 1105-1112, 1985.

[55] M. Diaz and F. Mijangos, Metal recovery from hydrometallurgical wastes, JOM, vol. 39, pp. 42-44, 1987.

[56] F. Gode and E. Pehlivan, A comparative study of two chelating ion-exchange resins for the removal of chromium (III) from aqueous solution, J. Hazard. Mater., vol. 100, pp. 231-243, 2003.

[57] H. Leinonen and J. Lehto, Ion-exchange of nickel by iminodiacetic acid chelating resin Chelex 100, React Funct Polym, vol. 43, pp. 1-6, 2000.

[58] L. Lin and R. Juang, Ion-exchange equilibria of Cu (II) and Zn (II) from aqueous solutions with Chelex 100 and Amberlite IRC 748 resins, Chem. Eng. J., vol. 112, pp. 211-218, 2005.

[59] E. Korngold, S. Belfer and C. Urtizberea, Removal of heavy metals from tap water by a cation exchanger, Desalination, vol. 104, pp. 197-201, 1996.

[60] A. Dabrowski, Z. Hubicki, P. Podkościelny and E. Robens, Selective removal of the heavy metal ions from waters and industrial wastewaters by ion-exchange method, Chemosphere, vol. 56, pp. 91-106, 2004.

[61] E. Korngold, N. Belayev, L. Aronov and S. Titelman, Influence of complexing agents on the removal of metals from water by a cation exchanger, Desalination, vol. 133, pp. 83-88, 2001.

[62] B. Laskorin, V. Mamilov, Y. A. Koreisho, D. Skorovarov, L. Vodolazov, I. Smirnov, O. Kedrovskii, V. Shulika, B. Nevskii and V. Mosinets, Extraction and processing of uranium ore in the USSR, Atomic Energy, vol. 54, pp. 301-309, 1983.

[63] V. Yahorava, J. Scheepers, M. Kotze and D. Auerswald, Evaluation of various durability tests to assess resins for in-pulp applications, in Proceedings of the Fifth Southern African Base Metals Conference, Kasane, Botswanna, 2009, pp. 341-358.

[64] W. P. Duyvesteyn, D. A. Neudorf and E. M. Weenink, Resin-in-Pulp Method for Recovery of Nickel and Cobalt, U.S. Patent No. 6,350,420, 2002.

[65] N. Zontov, Potential benefits of resin-in-pulp for PAL plants, ALTA 2001 Nickel/Cobalt-7, 2001.

[66] J. Wyethe, M. Kotze, I. Greager and A. Swarts, Cobalt, nickel, and copper recovery with resin-in-pulp, in Proceedings of ALTA, vol 2002, 2002.

[67] M. J. Nicol and Z. Zainol, The development of a resin-in-pulp process for the recovery of nickel and cobalt from laterite leach slurries, Int. J. Miner. Process., vol. 72, pp. 407-415, 2003.

[68] B. McKevitt and D. Dreisinger, Lessons from the past: a literature review of the resin-in-pulp process for the uranium industry, Proceedings of the 3rd International Conference on Uranium, vol. II, pp. 3-14, 2010.

[69] S. K. Pondugula, Mixed Bed Ion-Exchange Modeling for Divalent Ions in a Ternary System, Oklahoma State University, 1995.

[70] C. Fleming and M. Nicol, A comparative study of kinetic models for the extraction of uranium by strong-base anion-exchange resins, J. S. Afr. Inst. Min. Metall., vol. 80, pp. 89-99, 1980.

[71] E. E. Graham and J. S. Dranoff, Application of the Stefan-Maxwell equations to diffusion in ion exchangers. 1. Theory, Industrial & Engineering Chemistry Fundamentals, vol. 21, pp. 360-365, 1982.

[72] F. Mijangos, N. Tikhonov, M. Ortueta and A. Dautov, Modeling ion-exchange kinetics in bimetallic systems, Ind Eng Chem Res, vol. 41, pp. 1357-1363, 2002.

[73] F. Helfferich, Ion-exchange kinetics. 1 III. Experimental test of the theory of particle-diffusion controlled ion exchange, J. Phys. Chem., vol. 66, pp. 39-44, 1962.

[74] O. O. Omatete, R. N. Clazie and T. Vermeulen, Column Dynamics of Ternary Ion Exchange Part I: Diffusional and Mass Transfer Relations, The Chemical Engineering Journal, vol. 19, pp. 229-240, 1980.

[75] T. Smith and J. Dranoff, Film diffusion-controlled kinetics in binary ion exchange, Industrial & Engineering Chemistry Fundamentals, vol. 3, pp. 195-200, 1964.

[76] H. Yoshida, T. Kataoka and S. Fujikawa, Kinetics in a chelate ion exchanger—II. Experimental, Chemical Engineering Science, vol. 41, pp. 2525-2530, 1986.

[77] H. Yoshida, T. Kataoka and S. Fujikawa, Kinetics in a chelate ion exchanger—I. Theoretical analysis, Chemical Engineering Science, vol. 41, pp. 2517-2524, 1986.

[78] A. Fernandez, M. Diaz and A. Rodrigues, Kinetic mechanisms in ion exchange processes, The Chemical Engineering Journal and the Biochemical Engineering Journal, vol. 57, pp. 17-25, 1995.

[79] E. Glueckauf and J. Coates, Theory of chromatography. Part IV. The influence of incomplete equilibrium on the front boundary of chromatograms and on the effectiveness of separation, Journal of the Chemical Society, pp. 1315-1321, 1947.

[80] H. C. Thomas, Heterogeneous ion exchange in a flowing system, J. Am. Chem. Soc., vol. 66, pp. 1664-1666, 1944.

[81] M. Trgo, J. Perić and N. V. Medvidović, A comparative study of ion exchange kinetics in zinc/lead—modified zeolite-clinoptilolite systems, J. Hazard. Mater., vol. 136, pp. 938-945, 2006.

[82] A. Dyer and K. J. White, "Cation diffusion in the natural zeolite clinoptilolite, Thermochimica Acta, vol. 340, pp. 341-348, 1999

[83] B. McKevitt and D. Dreisinger, Development of an engineering model for nickel loading onto an iminodiacetic resin for resin-in-pulp applications: Part II—Evaluation of existing models and their extension into a hybrid correlation, Hydrometallurgy, vol. 125, pp. 1-7, 2012.

[84] T. Vermeulen, Theory for irreversible and constant-pattern solid diffusion, Industrial & Engineering Chemistry, vol. 45, pp. 1664-1670, 1953.

[85] M. Pritzker, Shrinking core model for multispecies uptake onto an ion exchange resin involving distinct reaction fronts, Separation and Purification Technology, vol. 42, pp. 15-24, 3, 2005.

[86] G. W. Dicinoski, L. R. Gahan, P. J. Lawson and J. A. Rideout, Application of the shrinking core model to the kinetics of extraction of gold (I), silver (I) and nickel (II) cyanide complexes by novel anion exchange resins, Hydrometallurgy, vol. 56, pp. 323-336, 2000.

[87] F. Helfferich, Ion-exchange kinetics. V. Ion exchange accompanied by reactions, J. Phys. Chem., vol. 69, pp. 1178-1187, 1965.

[88] B. McKevitt and D. Dreisinger, Development of an engineering model for nickel loading onto an iminodiacetic resin for resin-in-pulp applications: Part III—Verification of hybrid correlation, Hydrometallurgy, vol. 121, pp. 45-53, 2012.

[89] P. Littlejohn and J. Vaughan, Selective ammoniacal elution of nickel and cobalt from iminodiacetate cation exchange resin, in ALTA 2010 Nickel-Cobalt-Copper, Uranium and Gold Conference, pp. 1-14, 2010.

[90] O. Halle, D. Rossoni, A new (monodisperse) chelating resin designed for mining application: Lewatit MonoPlus TP207, in Proceedings of ALTA 200*5,* ALTA Metallurgical Services, Melbourne, 2005.

Appendices

Appendix A: Blank Batch Test Check Sheet for Loading Experiments

TP207XL, +710-850 **Metal Tested:** Ferrous **M2+ Conc:** **951.3** **Date:**

LOADING RATE TEST with NITROGEN SPARGING

- ☐ Turn on power and scales. Place 50 mL DI water into stock flask and dearate at 1 LPM for 20 mins
- ☐ Use beaker sparger to deaerate (1 LPM for 20 mins) >100 mL water to make up stock NaOH solution
- ☐ Calibrate pH probe and check resin addition water is truly at pH 4
- ☐ Prep 5 mL resin in H+ form with 15 mL water. Initial resin pH: _____ final resin pH: _____
- ☐ Add : 1.874 g MSO4 into the 50 mL stock flask containing dearated water g added: _____
- ☐ Prep NaOH Stock solution. Dearate resin with beaker sparger for 15 mins _____
- ☐ Flush stock solution addition lines. Measure gross weight. MSO4: _____ NaOH: _____
- ☐ Prep reaction vessel -use vacuum grease on connections
- ☐ Add all but ~10mL of 500 mL water to vessel and dearate 30 mins at 300 RPM. Bring waterbath to 30C
- ☐ Add target g of MSO4 via pH port. Flush with saved H2O: 2.416 actual g MSO4 added: _____
- ☐ Measure SG NaOH to three decimal places by pipetting excess into flask on scale.

SG of NaOH:							Calc SG	#DIV/0!

- ☐ pH adjust test solution via sample/N2 exit port initial pH: _____ final pH: _____
- ☐ Take sample #1, and record volume. Dilute 2mL into 25 mL flask with 5mL 100gpL acid
- ☐ Turn on computer with USB cable removed. When booted, plug in USB cable, then start windmill logger
- ☐ Record initial weight of scale tracking NaOH: _____ Scale tracking MSO4: _____
- ☐ Start Windmill logger. Record file names: _____ _____
- ☐ Turn stock pump to OFF. Add resin via sample port as fast as possible. Start Time: _____
- ☐ Turn stock pump to auto. Record lowest pH attained: _____ pH controlling well at: _____
- ☐ After 30 mins, turn down N2. Test bkr 0.2 LPM, stock __0.1__LPM. Time turned down: _____
- ☐ Solution Sampling: Record sample volume taken. Dilute 2mL sample and 5mL 100gpL H2SO4 into 25mL

Time of Samples:	0:00:00						
Total volume of sample taken:							

- ☐ **End Test**. Shut off stock addition pump. Turn off logger. Stop Mixer.

Record final volumes on scales: Scale tracking NaOH: _____ Scale tracking MSO4: _____

Turn off N2 addition to beaker and to stock solution.

Record final volumes of individual flasks NaOH: _____ MSO4: _____

Measure SG MSO4:							Calc SG	#DIV/0!

Nickel-Iron Displcement Test

TP207XL, +710-850 **Metal Tested** **Ni Conc.** 1000 **M2+ Conc:** **9511.2** **Date:**

LOADING RATE TEST with NITROGEN SPARGING

Use beaker sparger to deaerate (1 LPM for 20 mins) >100 mL water to make up stock NaOH solution

Calibrate pH probe and check resin addition water is truly at pH 4

Prep 5 mL resin in H+ form with 15 mL water. Initial resin pH: _____ final resin pH: _____

Prep NaOH Stock solution. Dearate resin with beaker sparger for 15 mins

Flush stock solution addition lines. Measure gross weight. NaOH: _____

Prep reaction vessel -use vacuum grease on connections

Add all but ~10mL of 500 mL water to vessel and dearate 30 mins at 300 RPM. Bring waterbath to 30C

Add target g of FeSO4 via pH port. Flush with saved H2O: 24.159 actual g MSO4 added: _____

Add target g of NiSO4 via pH port. Flush with saved H2O: 2.241 actual g MSO4 added: _____

Measure SG NaOH to three decimal places by pipetting excess into flask on scale.

SG of NaOH:							Calc SG	#DIV/0!

pH adjust test solution via sample/N2 exit port initial pH: _____ final pH: _____

Take sample #1 (Fe), and record volume. Dilute 2mL into 25 mL flask with 5mL 100gpL H2So4 acid

Take sample #1 (Ni), and record volume. Dilute 2mL into 50 mL flask with 5mL 3M HCl acid

Turn on computer with USB cable removed. When booted, plug in USB cable, then start windmill logger

Record initial weight of scale tracking NaOH: _____

Start Windmill logger. Record file names: _____ _____

Turn stock pump to OFF. Add resin via sample port as fast as possible. Start Time: _____

Turn stock pump to auto. Record lowest pH attained: _____ pH controlling well at: _____

After 30 mins, turn down N2. Test bkr 0.2 LPM, stock __0.1__LPM. Time turned down: _____

Solution Sampling: Record sample volume taken. Dilute 2mL sample and 5mL 100gpL H2SO4 into 25mL

Time of Samples:

Time	0:00:00									
Volume										

time										
volume										

End Test. Shut off stock addition pump. Turn off logger. Stop Mixer.

Record final volumes on scales: Scale tracking NaOH: _____

Turn off N2 addition to beaker and to stock solution.

Record final volumes of individual flasks NaOH:

Appendix B: Photos of Experimental Setup

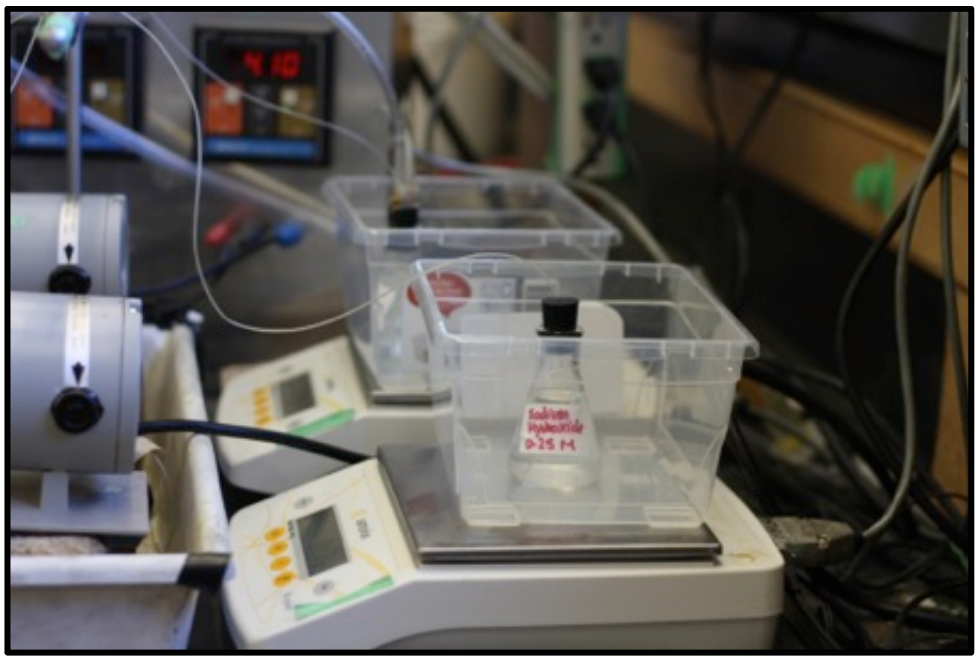


StableTemp

Appendix C: Derivation of Hybrid Correlation

The hybrid correlation model was generated based on the Shrinking Core model and the Vermeulen approximation. The correlation minimized the errors between the two models when k_v=0.677 k_c which resulted in an approximation of the Shrinking Core model by a Vermeulen expression. To combine the Vermeulen model and the Vermeulen approximation to the Shrinking Core model into a single hybrid correlation, a second empirical fit parameter, α, beside the apparent diffusivity (D_{app}) was defined for the system. The hybrid model derivation is summarized below:

Equation for the Rate of Reaction Based on Vermeulen Approximation:

$$\frac{d}{dt}[\overline{M}] = \frac{2k_V([\overline{M}]_{eq\bar{b}}^2[\overline{M}]^2)}{[\overline{\overline{M}}]} \qquad [C\text{-}1]$$

Rate Constant for Vermeulen Model:

$$k_v = \frac{\pi^2 D_p}{d_p^2} \qquad [C\text{-}2]$$

Rate Constant for Shrinking Core Model:

$$k_c = \frac{24 D_s[M]}{d_p^2[\overline{M}]_{max}} \qquad [C\text{-}3]$$

Hybrid Model Generated When $k_v \approx 2/3\ k_c$:

$$k_v = \frac{16 D_s[M]}{d^2 p[\overline{\overline{M}}]_{max}} \qquad [C\text{-}4]$$

The analytical solution to the Vermeulen model, using k_h in lieu of k_v:

$$F = \sqrt{1 - \exp(-4 k_v t)} \qquad [C\text{-}5]$$

$$F = \sqrt{1 - \exp\left(-4\left(\frac{16 D_s [M]}{d_p^2 [\overline{M}]_{max}}\right) t\right)} \qquad [C\text{-}6]$$

Taking all constants and pulling out $4\pi^2$:

$$F = \sqrt{1 - \exp\left(-\left(\frac{4 * \frac{\pi^2}{\pi^2} * 16 D_s [M]}{d_p^2 [\overline{M}]_{max}}\right) t\right)} \qquad [C\text{-}7]$$

Fractional attainment of equilibrium:

$$F = \sqrt{1 - \exp\left(-\frac{4\pi^2 * D_{app}\left(\frac{16}{\pi^2} * \frac{[M]}{[\overline{M}]_{max}}\right)^{\alpha}}{d_p^2} t\right)} \qquad [C\text{-}8]$$

Hybrid Correlation Model:

$$\boxed{F = \sqrt{1 - \exp(-4 k_h t)}} \qquad [C\text{-}9]$$

Hybrid Correlation Rate Constant:

$$\boxed{k_h = \frac{\pi^2 D_{app}}{d_p^2}\left(\frac{16[M]}{\pi^2 [\overline{M}]_{max}}\right)^{\alpha}} \qquad [C\text{-}10]$$

Appendix D: Derivation of Modified Helfferich Number

The following section outlines the main steps McKevitt applied in developing the modified Helfferich number. In terms of developing this number, instead of considering equal valence and mobility ions for film diffusion control, the simpler type of isotopic exchange generally used in engineering models was applied.

The loading process is expected to be film diffusion controlled at the initial stages followed by the intraparticle diffusion mechanism as the loading proceeds. Thus, in this work a hybrid correlation model was chose instead of the exact solution of the differential equation for the intraparticle diffusion. Based on that, the original Helfferich number was modified to be a function of the fraction load at any given time. This shows how the mechanism transforms from initial film diffusion control to finally being intraparticle diffusion controlled.

Ion exchange reaction of nickel-ferrous displacement loading:

$$R_2\text{-}Fe + Ni^{2+} \rightarrow R_2\text{-}Ni + Fe^{2+} \qquad \text{[C-11]}$$

$$F = \frac{[\overline{Ni}]}{[\overline{Ni}]_{eqb}} \qquad \text{[C-12]}$$

Fractional attainment of equilibrium for isotopic exchange under infinite solution volume are calculated for both cases of diffusion controls:

For Film Diffusion Control:

$$F = 1 - \exp(-k_f t) \qquad \text{[C-13]}$$

For Intraparticle Diffusion Control:

$$F = \sqrt{1 - \exp(-4 k_h t)} \qquad \text{[C-14]}$$

Time required to achieve fractional loading of F:

Film Diffusion Control:

$$t_f = \frac{-1}{k_f} \ln(1 - F) \qquad \text{[C-15]}$$

Intraparticle Diffusion Control:

$$t_p = \frac{-1}{4 k_h} \ln(1 - F^2) \qquad \text{[C-16}$$

Both two diffusion constant (k_f and k_h) are calculated as follows:

Film Diffusion Control:

$$k_f = \frac{6 D_f [Ni]}{d_p \delta [\overline{Ni}]_{eqb}} \qquad \text{[C-17]}$$

Intraparticle Diffusion Control:

$$k_h = \frac{\pi^2 D_{app} \left(\frac{16}{\pi^2} \frac{[Ni]}{[\overline{Ni}]_{eqb}} \right)^a}{d_p^2} \qquad \text{[C-18]}$$

Modified Helfferich Number

$$\frac{t_f}{t_p} = \frac{4k_h \ln(1-F)}{k_f \ln(1-F^2)} \qquad \text{[C-19]}$$

$$\left(\frac{4}{6}\right)\left(\pi^2\right)(1.622)^{\alpha}\left(\frac{\ln(1-F)}{\ln(1-F^2)}\right)\left(\frac{\frac{D_{app}}{d_p^2}}{\frac{D_f}{d_p\,\delta}}\right)\left(\frac{\left(\frac{[Ni]}{[\overline{Ni}]_{eqb}}\right)^{\alpha}}{\frac{[Ni]}{[\overline{Ni}]_{eqb}}}\right)$$

[C-20]

$$\boxed{\left(\frac{2}{3}\right)\left(\pi^2\right)(1.622)^{\alpha}\left(\frac{\ln(1-F)}{\ln(1-F^2)}\right)\left(\frac{D_{app}\,\delta}{d_p D_f}\right)\left\langle\frac{[Ni]}{[Ni]_{eqb}}\right\rangle^{\alpha-1}}$$

Appendix E: Finite Model Applied in Nickel-Ferrous Displacement Experiments

The excel sheet regarding a single run of the finite difference model extends more than one thousand pages long. As a result, only the results of the few minutes of the 1000 ppm nickel-ferrous loading experiment have been printed out for inclusion in this section. The sample calculation of final load values predicted by the finite difference model is reviewed at the end of this section.

The model starts at t = 0 with initial nickel concentration [M] and 0 g Ni/L Resin loading $[\overline{M}] = 0$. Then, all resin and solution values calculated subsequently at time t + Δt from previous values using the Euler's method Equation D-1. Resin loading value in each time step, $[\overline{M}]_{(t+\Delta t)}$, is calculated based on the equilibrium resin loading value, $[\overline{M}]_{eqb}$, and the equivalent resin loading times, t_r for both the film diffusion model and hybrid correlation determined from the previous resin loading, $[\overline{M}]_t$, and the previous solution concentration, $[M]_t$ Subsequently, at time t + Δt, the resin loading value is determined by both the film diffusion model and the hybrid correlation. Then, for the resin loading, $[\overline{M}]_{(t+\Delta t)}$, the lower of these two values is used.

Euler's Method: $$[M]_{t+\Delta t} = [M] + \Delta t \frac{d}{dt}[M] \qquad [D\text{-}1]$$

Resin Isotherm Properties

Capacity	1.97	eq/L
	57.8	g Ni/L Resin
Nickel AMU	58.71	

Resin Kinetic Properties

Df/delta	2.7E-05	m/s
Dapp	1.0E-11	m2/s
alpha	0.6478926	
dp	7.36E-04	m

Volume Balance

Initial solution vol	495	mL
Initial resin volume	5	mL
Evaporation rate	1.2	mL/h

Base Stock Conc 0.25 M NaOH

Finite Difference Step Size 5 s

Time [h]	Time [s]	[M]	[M]	[Mbar]	[Mbar]	[Mbar]eqb	[Mbar]eqb	F	kf	kh	eqv t film	eqv t hybrid	Mod He	model	F	g Ni / L R	mol Ni load
[h]	[s]	gpL	molar	g Ni / L Resin	molar	g Ni / L Resin	molar		1/s	1/s							
0.0000	0.0000	1.0000	0.0170	0.0000	0.0000	37.7600	0.6432	0.0000	0.0038	0.0000	0.0000	0.0000	1000000.0000	FILM	0.0189	0.7118	0.0121
0.0014	5.0000	0.9918	0.0169	0.7118	0.0121	37.6941	0.6420	0.0189	0.0038	0.0000	5.0500	5.0069	1.0086	FILM	0.0372	1.4033	0.0118
0.0028	10.0000	0.9839	0.0168	1.4033	0.0239	37.6298	0.6409	0.0373	0.0037	0.0000	10.1485	19.6390	0.5168	HYBRID	0.0418	1.5717	0.0029
0.0042	15.0000	0.9820	0.0167	1.5717	0.0268	37.6140	0.6407	0.0418	0.0037	0.0000	11.4197	24.6909	0.4625	HYBRID	0.0458	1.7234	0.0026
0.0056	20.0000	0.9803	0.0167	1.7234	0.0294	37.5999	0.6404	0.0458	0.0037	0.0000	12.5748	29.7473	0.4227	HYBRID	0.0495	1.8624	0.0024
0.0069	25.0000	0.9787	0.0167	1.8624	0.0317	37.5869	0.6402	0.0495	0.0037	0.0000	13.6424	34.8078	0.3919	HYBRID	0.0530	1.9915	0.0022
0.0083	30.0000	0.9772	0.0166	1.9915	0.0339	37.5748	0.6400	0.0530	0.0037	0.0000	14.6412	39.8723	0.3672	HYBRID	0.0562	2.1125	0.0021
0.0097	35.0000	0.9758	0.0166	2.1125	0.0360	37.5634	0.6398	0.0562	0.0037	0.0000	15.5837	44.9405	0.3468	HYBRID	0.0593	2.2267	0.0019
0.0111	40.0000	0.9745	0.0166	2.2267	0.0379	37.5527	0.6396	0.0593	0.0037	0.0000	16.4794	50.0122	0.3295	HYBRID	0.0622	2.3352	0.0018
0.0125	45.0000	0.9733	0.0166	2.3352	0.0398	37.5425	0.6395	0.0622	0.0037	0.0000	17.3351	55.0873	0.3147	HYBRID	0.0650	2.4386	0.0018
0.0139	50.0000	0.9721	0.0166	2.4386	0.0415	37.5328	0.6393	0.0650	0.0037	0.0000	18.1563	60.1657	0.3018	HYBRID	0.0676	2.5377	0.0017
0.0153	55.0000	0.9710	0.0165	2.5377	0.0432	37.5235	0.6391	0.0676	0.0037	0.0000	18.9473	65.2471	0.2904	HYBRID	0.0702	2.6329	0.0016
0.0167	60.0000	0.9699	0.0165	2.6329	0.0448	37.5145	0.6390	0.0702	0.0037	0.0000	19.7115	70.3315	0.2803	HYBRID	0.0726	2.7247	0.0016
0.0181	65.0000	0.9689	0.0165	2.7247	0.0464	37.5059	0.6388	0.0726	0.0037	0.0000	20.4517	75.4189	0.2712	HYBRID	0.0750	2.8133	0.0015
0.0194	70.0000	0.9679	0.0165	2.8133	0.0479	37.4975	0.6387	0.0750	0.0037	0.0000	21.1704	80.5090	0.2630	HYBRID	0.0773	2.8991	0.0015
0.0208	75.0000	0.9669	0.0165	2.8991	0.0494	37.4894	0.6386	0.0773	0.0037	0.0000	21.8696	85.6018	0.2555	HYBRID	0.0796	2.9823	0.0014
0.0222	80.0000	0.9660	0.0165	2.9823	0.0508	37.4816	0.6384	0.0796	0.0037	0.0000	22.5509	90.6973	0.2486	HYBRID	0.0817	3.0631	0.0014
0.0236	85.0000	0.9650	0.0164	3.0631	0.0522	37.4739	0.6383	0.0817	0.0037	0.0000	23.2159	95.7954	0.2423	HYBRID	0.0838	3.1418	0.0013
0.0250	90.0000	0.9642	0.0164	3.1418	0.0535	37.4665	0.6382	0.0839	0.0037	0.0000	23.8659	100.8959	0.2365	HYBRID	0.0859	3.2184	0.0013
0.0264	95.0000	0.9633	0.0164	3.2184	0.0548	37.4593	0.6380	0.0859	0.0037	0.0000	24.5019	105.9989	0.2312	HYBRID	0.0879	3.2932	0.0013
0.0278	100.0000	0.9624	0.0164	3.2932	0.0561	37.4522	0.6379	0.0879	0.0037	0.0000	25.1250	111.1043	0.2261	HYBRID	0.0899	3.3661	0.0012
0.0292	105.0000	0.9616	0.0164	3.3661	0.0573	37.4453	0.6378	0.0899	0.0037	0.0000	25.7360	116.2121	0.2215	HYBRID	0.0918	3.4375	0.0012
0.0306	110.0000	0.9608	0.0164	3.4375	0.0586	37.4385	0.6377	0.0918	0.0037	0.0000	26.3358	121.3221	0.2171	HYBRID	0.0937	3.5073	0.0012
0.0319	115.0000	0.9600	0.0164	3.5073	0.0597	37.4319	0.6376	0.0937	0.0037	0.0000	26.9250	126.4344	0.2130	HYBRID	0.0955	3.5757	0.0012
0.0333	120.0000	0.9592	0.0163	3.5757	0.0609	37.4254	0.6375	0.0955	0.0037	0.0000	27.5042	131.5489	0.2091	HYBRID	0.0973	3.6427	0.0011
0.0347	125.0000	0.9585	0.0163	3.6427	0.0620	37.4191	0.6374	0.0973	0.0036	0.0000	28.0741	136.6655	0.2054	HYBRID	0.0991	3.7084	0.0011
0.0361	130.0000	0.9577	0.0163	3.7084	0.0632	37.4128	0.6372	0.0991	0.0036	0.0000	28.6355	141.7855	0.2020	HYBRID	0.1008	3.7729	0.0011
0.0375	135.0000	0.9570	0.0163	3.7729	0.0643	37.4066	0.6371	0.1009	0.0036	0.0000	29.1885	146.9075	0.1987	HYBRID	0.1026	3.8362	0.0011
0.0389	140.0000	0.9563	0.0163	3.8362	0.0653	37.4005	0.6370	0.1026	0.0036	0.0000	29.7335	152.0317	0.1956	HYBRID	0.1042	3.8985	0.0011
0.0403	145.0000	0.9556	0.0163	3.8985	0.0664	37.3945	0.6369	0.1043	0.0036	0.0000	30.2710	157.1578	0.1926	HYBRID	0.1059	3.9596	0.0010
0.0417	150.0000	0.9549	0.0163	3.9596	0.0674	37.3886	0.6368	0.1059	0.0036	0.0000	30.8013	162.2860	0.1898	HYBRID	0.1075	4.0198	0.0010
0.0431	155.0000	0.9542	0.0163	4.0198	0.0685	37.3828	0.6367	0.1075	0.0036	0.0000	31.3249	167.4162	0.1871	HYBRID	0.1091	4.0791	0.0010
0.0444	160.0000	0.9535	0.0162	4.0791	0.0695	37.3771	0.6366	0.1091	0.0036	0.0000	31.8418	172.5483	0.1845	HYBRID	0.1107	4.1374	0.0010
0.0458	165.0000	0.9528	0.0162	4.1374	0.0705	37.3715	0.6365	0.1107	0.0036	0.0000	32.3526	177.6823	0.1821	HYBRID	0.1122	4.1948	0.0010
0.0472	170.0000	0.9522	0.0162	4.1948	0.0714	37.3660	0.6365	0.1123	0.0036	0.0000	32.8574	182.8182	0.1797	HYBRID	0.1138	4.2514	0.0010
0.0486	175.0000	0.9515	0.0162	4.2514	0.0724	37.3605	0.6364	0.1138	0.0036	0.0000	33.3565	187.9560	0.1775	HYBRID	0.1153	4.3072	0.0010
0.0500	180.0000	0.9509	0.0162	4.3072	0.0734	37.3552	0.6363	0.1153	0.0036	0.0000	33.8501	193.0956	0.1753	HYBRID	0.1168	4.3623	0.0009
0.0514	185.0000	0.9503	0.0162	4.3623	0.0743	37.3499	0.6362	0.1168	0.0036	0.0000	34.3384	198.2370	0.1732	HYBRID	0.1182	4.4166	0.0009
0.0528	190.0000	0.9496	0.0162	4.4166	0.0752	37.3446	0.6361	0.1183	0.0036	0.0000	34.8216	203.3802	0.1712	HYBRID	0.1197	4.4701	0.0009
0.0542	195.0000	0.9490	0.0162	4.4701	0.0761	37.3394	0.6360	0.1197	0.0036	0.0000	35.3000	208.5252	0.1693	HYBRID	0.1211	4.5230	0.0009
0.0556	200.0000	0.9484	0.0162	4.5230	0.0770	37.3343	0.6359	0.1211	0.0036	0.0000	35.7737	213.6719	0.1674	HYBRID	0.1225	4.5752	0.0009

	Resin at t+delta t			Volume Balance -Basis mL					Ni in Soln Balance -Basis: g Ni	
Time [h]	NaOH stock	Sample	Evap	Net Vol	Initial Ni	lost to sample	loaded on resin	net	molar	gpL
[h]	[mL]	[mL]	[mL]	495						
0.0000	0.4850		0.0017	495.4833	0.4950	0.0000	0.0036	0.4914	0.0169	0.9918
0.0014	0.4711		0.0017	495.9528	0.4914	0.0000	0.0035	0.4880	0.0168	0.9839
0.0028	0.1147		0.0017	496.0658	0.4880	0.0000	0.0008	0.4871	0.0167	0.9820
0.0042	0.1033		0.0017	496.1675	0.4871	0.0000	0.0008	0.4864	0.0167	0.9803
0.0056	0.0947		0.0017	496.2606	0.4864	0.0000	0.0007	0.4857	0.0167	0.9787
0.0069	0.0880		0.0017	496.3468	0.4857	0.0000	0.0006	0.4850	0.0166	0.9772
0.0083	0.0824		0.0017	496.4276	0.4850	0.0000	0.0006	0.4844	0.0166	0.9758
0.0097	0.0778		0.0017	496.5038	0.4844	0.0000	0.0006	0.4839	0.0166	0.9745
0.0111	0.0739		0.0017	496.5760	0.4839	0.0000	0.0005	0.4833	0.0166	0.9733
0.0125	0.0705		0.0017	496.6448	0.4833	0.0000	0.0005	0.4828	0.0166	0.9721
0.0139	0.0675		0.0017	496.7107	0.4828	0.0000	0.0005	0.4823	0.0165	0.9710
0.0153	0.0649		0.0017	496.7739	0.4823	0.0000	0.0005	0.4818	0.0165	0.9699
0.0167	0.0625		0.0017	496.8347	0.4818	0.0000	0.0005	0.4814	0.0165	0.9689
0.0181	0.0604		0.0017	496.8934	0.4814	0.0000	0.0004	0.4809	0.0165	0.9679
0.0194	0.0585		0.0017	496.9502	0.4809	0.0000	0.0004	0.4805	0.0165	0.9669
0.0208	0.0567		0.0017	497.0052	0.4805	0.0000	0.0004	0.4801	0.0165	0.9660
0.0222	0.0551		0.0017	497.0586	0.4801	0.0000	0.0004	0.4797	0.0164	0.9650
0.0236	0.0536		0.0017	497.1105	0.4797	0.0000	0.0004	0.4793	0.0164	0.9642
0.0250	0.0522		0.0017	497.1611	0.4793	0.0000	0.0004	0.4789	0.0164	0.9633
0.0264	0.0509		0.0017	497.2103	0.4789	0.0000	0.0004	0.4785	0.0164	0.9624
0.0278	0.0497		0.0017	497.2584	0.4785	0.0000	0.0004	0.4782	0.0164	0.9616
0.0292	0.0486		0.0017	497.3054	0.4782	0.0000	0.0004	0.4778	0.0164	0.9608
0.0306	0.0476		0.0017	497.3513	0.4778	0.0000	0.0003	0.4775	0.0164	0.9600
0.0319	0.0466		0.0017	497.3962	0.4775	0.0000	0.0003	0.4771	0.0163	0.9592
0.0333	0.0457		0.0017	497.4401	0.4771	0.0000	0.0003	0.4768	0.0163	0.9585
0.0347	0.0448	5	0.0017	492.4833	0.4768	0.0048	0.0003	0.4717	0.0163	0.9577
0.0361	0.0439		0.0017	492.5255	0.4717	0.0000	0.0003	0.4713	0.0163	0.9570
0.0375	0.0432		0.0017	492.5670	0.4713	0.0000	0.0003	0.4710	0.0163	0.9563
0.0389	0.0424		0.0017	492.6077	0.4710	0.0000	0.0003	0.4707	0.0163	0.9556
0.0403	0.0417		0.0017	492.6478	0.4707	0.0000	0.0003	0.4704	0.0163	0.9549
0.0417	0.0410		0.0017	492.6871	0.4704	0.0000	0.0003	0.4701	0.0163	0.9542
0.0431	0.0404		0.0017	492.7258	0.4701	0.0000	0.0003	0.4698	0.0162	0.9535
0.0444	0.0397		0.0017	492.7639	0.4698	0.0000	0.0003	0.4695	0.0162	0.9528
0.0458	0.0391		0.0017	492.8013	0.4695	0.0000	0.0003	0.4692	0.0162	0.9522
0.0472	0.0386		0.0017	492.8382	0.4692	0.0000	0.0003	0.4690	0.0162	0.9515
0.0486	0.0380		0.0017	492.8746	0.4690	0.0000	0.0003	0.4687	0.0162	0.9509
0.0500	0.0375		0.0017	492.9104	0.4687	0.0000	0.0003	0.4684	0.0162	0.9503
0.0514	0.0370		0.0017	492.9457	0.4684	0.0000	0.0003	0.4681	0.0162	0.9496
0.0528	0.0365		0.0017	492.9806	0.4681	0.0000	0.0003	0.4679	0.0162	0.9490
0.0542	0.0360		0.0017	493.0149	0.4679	0.0000	0.0003	0.4676	0.0162	0.9484
0.0556	0.0356		0.0017	493.0488	0.4676	0.0000	0.0003	0.4673	0.0161	0.9478

Sample Calculation for the Finite Model:

at time=0

[M]= 1 g/L

[M]= 1/58.71=0.0170 molar

$[\overline{M}]$= 0 g/L $[\overline{M}]$=0 molar

$[\overline{M}]_{eqb}$=8.04ln[M] + 37.76= 37.76 gNi/L resin

$$[\overline{M}]_{eqb}=\frac{37.60}{58.71}=0.6432 \quad \text{molar}$$

$$F=\frac{[\overline{M}]}{[\overline{M}]_{eqb}}=\frac{0}{37.76}=0$$

$$k_f=6\frac{D_f}{\delta}\left(\frac{\frac{[M]}{[\overline{M}]max}}{d_p}\right)=(6)(2.7*10^{-4})\left(\frac{1}{\frac{(58.71*1.971)/2}{(7.36*10^{-4})}}\right)=0.0038 \quad 1/s$$

$$k_h=\frac{\pi^2 D_{app}}{d_p^2}\left(\frac{1.622[M]}{[\overline{M}]_{max}}\right)=\frac{\pi 2(1*10^{-11})}{(7.36*10^{-4})^2}\left(\frac{1.622(1)}{58.71*1.971/2}\right)=0.0000179 \quad 1/s$$

$$t_f=\frac{-1}{k_f}\ln(1-F)=\frac{-1}{0.0038}\ln(1-0)=0$$

$$t_h=\frac{-1}{4k_h}\ln(1-F^2)=\frac{-1}{(4)(0.0000179)}\ln(1-0)=0$$

at time =0 modified Helfferich number = infinite.

if He>1 F= Film Diffusion Model

He<1 F= Hybrid Model

$F=[1-\exp[-k_f(t_r+\Delta t)]$ = 1-exp [-0.0038(0+5)]=0.0189

$[\overline{M}]_{t+\Delta t} = [\overline{M}]_{eqb}[1 - \exp[-k_f(t_r + \Delta t)]]$ =37.60*0.0189=0.7118 gNi/L resin

$$\frac{([\overline{M}]_{(t+\Delta t)} - [\overline{M}])}{58.71} = \underline{\textbf{0.0121 mol Ni load}}$$

Volume Balance:

Net Volume = Initial Volume - NaOH Stock Addition -Sample Volume - Test Evaporation

at $(t+\Delta t)$ **:**

Net volume = (0.495 - 0 - 0.4850 - 0.0017)= 495.5

Mass Balance:

Net Ni in Soln (g) = Initial Ni - Ni lost to sample - Ni loaded onto resin

Initial Ni= $\frac{[M](459)}{1000}$ =(0.459)(1)=0.4590 gNi

Ni Loaded onto resin= $\left([\overline{M}]_{(t+\Delta t)} - [\overline{M}]_t\right)(\frac{5}{1000}) = (0.7118)(.005) = 0.0036$ gNi

Net Ni = (0.459-0-0.0036) =0.4914 gNi

Nickel in the Test Vessel

Net Ni = $\frac{\text{Net(g)}}{\text{Net(V)}} = \frac{0.4914}{0.4955} =$ 0.9918 g/L = **0.0169 molar**